Supporting Information

Configurational ligand isomerism in conjoined-cages†

Hareesha Dasary, ‡[a] Moumita Sarkar‡[a] and Dillip Kumar Chand*[a]

[a] Department of Chemistry, Indian Institute of Technology Madras, Chennai 600036, India,

E-mail: dillip@iitm.ac.in

Table of Contents **Page**

1. Materials and general methods

$PdCl_2$, pyridine-3,5-dicarboxylic acid, nicotinoyl chloride hydrochloride, and 1,2/1,3/1,4-diaminobenzene, were acquired from Aldrich; diphenylphosphorylazide (DPPA), $AgNO_3$, NaN_3, and all common reagents, solvents were obtained from Spectrochem, India and were used as received without further purification. The deuterated solvents were obtained from Aldrich and Cambridge Isotope Laboratories. ^1H and ^{13}C NMR spectral data were obtained using a Bruker 400 MHz or 500 MHz FT NMR spectrometer in DMSO-d_6. The ESI-MS spectra were recorded on an Agilent 6545A Q-TOF, Micromass Q-TOF spectrometer and Impact QTOF HRMS system (Bruker Daltonik GmbH). The crystal structures were obtained using a Bruker X8 Kappa XRD instrument.

The regioisomeric tridentate ligands are new and has been prepared as follows. Pyridine-3-carbonyl azide [1] and pyridine-3,5-dicarbonyl diazide [2] required for the synthesis of ligands were prepared following a reported procedure.

2. Synthesis of the tridentate ligands (L4-L6)

The quantitative synthesis of tridentate ligands, (**L4-L6**) involves multiple steps as follows.

Synthesis of Ligand L4

Pyridine-3,5-dicarbonyl diazide (500 mg, 2.30 mmol) was dissolved in 50 mL of dry CH_3CN and refluxed under nitrogen flow. 1,2-diaminobenzene (630 mg, 5.80 mmol) was added to the reaction mixture and stirred at reflux for 8 h under nitrogen atmosphere to result diamine **A**. The resulting precipitate was collected by filtration and washed with CH_3CN and dried under vacuum.

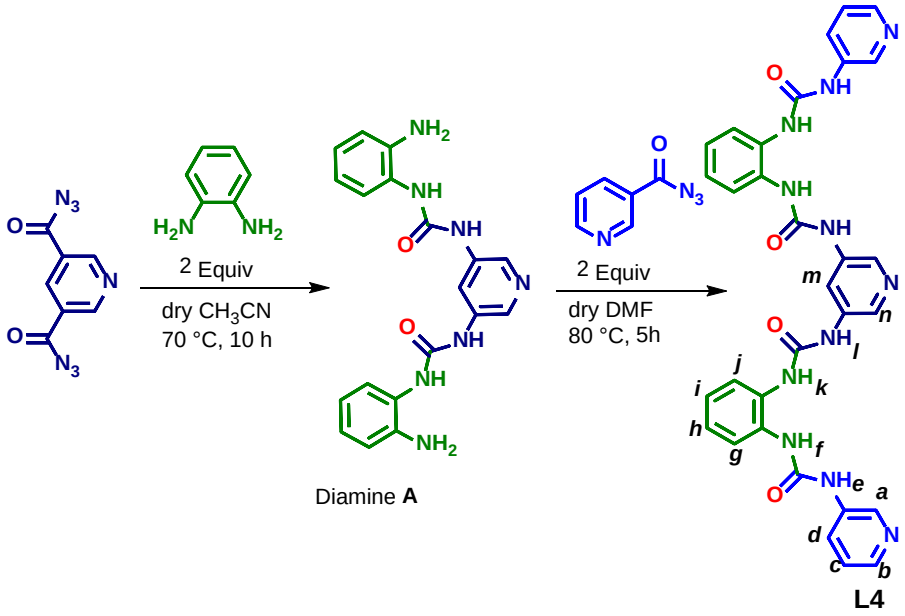

Scheme S1. Schematic representation of the stepwise synthesis of tridentate ligand, **L4**

1,1'-(pyridine-3,5-diyl)bis(3-(2-aminophenyl)urea): Yield: (434.02 mg, 50%). Melting point: 185 °C. ^{1}H NMR (400 MHz, DMSO-d_6) δ = 8.97 (s, 2H, H_g), 8.24 (d, J = 2.3 Hz, 2H, H_i), 8.14 (t, J = 2.3 Hz, 1H, H_h), 7.78 (s, 2H, H_f), 7.32 (dd, J_1 = 7.9 Hz, J_2 = 1.4 Hz, 2H, H_e), 6.84 (td, J_1 = 7.9 Hz, J_2 = 1.5 Hz, 2H, H_c), 6.73 (dd, J_1 = 7.9 Hz, J_2 = 1.4 Hz, 2H, H_b), 6.58 (td, J_1 = 7.8 Hz, J_2 = 1.5 Hz, 2H, H_d), 4.94 (bs, 4H, H_a) *ppm*; ^{13}C NMR (125 MHz, DMSO-d_6): δ = 154.72, 142.63, 137.76, 133.99, 127.11, 126.56, 124.56, 118.68, 116.61 *ppm*. ESI-MS (*m/z*):

calculated for [**A** + H]$^+$ and [**A** + Na]$^+$: 378.1678 and 400.1498. Observed: 378.1676 and 400.1489, respectively.

Diamine A (400 mg, 1.06 mmol) was dissolved in dry DMF (4 mL), pyridine-3-carbonyl azide (349.83 mg, 2.36 mmol) was added. The reaction mixture was stirred at 80 °C for 5 h under nitrogen atmosphere. The white precipitate was isolated by adding excess H_2O to the clear solution so obtained, which was filtered off, washed several times with acetone and dried under vacuum to result **L4**.

1-(pyridin-3-yl)-3-(2-(3-(5-(3-(2-(3-(pyridin-3-yl)ureido)phenyl)ureido)pyridin-3-yl)ureido)phenyl)urea, L4. (Yield: 510 mg, 78%). Melting point: 165 °C. ^{1}H NMR (500 MHz, DMSO-d_6): δ = 9.31 (s, 2H, H_l), 9.24 (s, 2H, H_e), 8.62 (d, J = 1.4 Hz, 2H, H_a), 8.30 (d, J = 1.8 Hz, 2H, H_n), 8.20-8.17 (m, 5H, H_b, H_f, H_m), 8.13 (s, 2H, H_k), 7.95 (ddd, J_1 = 8.3 Hz, J_2 = 2.3 Hz, J_3 = 1.4 Hz, 2H, H_d), 7.63 (m, 2H, H_g), 8.12-7.57 (m, 2H, H_j), 7.31 (dd, J_1 = 8.2 Hz, J_2 = 4.6 Hz, 2H, H_c), 7.12-7.10(m, 4H, H_h and H_i) *ppm*; ^{13}C NMR (125 MHz, DMSO-d_6): δ = 153.32, 153.11, 142.86, 140.03, 136.57, 133.20, 131.49, 130.91, 125.17, 124.47, 124.41, 124.20, 123.97, 123.64, 114.12 *ppm*. ESI-MS (*m/z*): calculated for [**L4** + H]$^+$ and [**L4** + Na]$^+$: 618.2326 and 640.2145. Observed: 618.2301 and 640.2150, respectively.

Synthesis of ligand L5 and L6

The quantitative synthesis of tridentate ligands **L5** and **L6** requires three consecutive steps as Scheme S2 and Scheme S3.

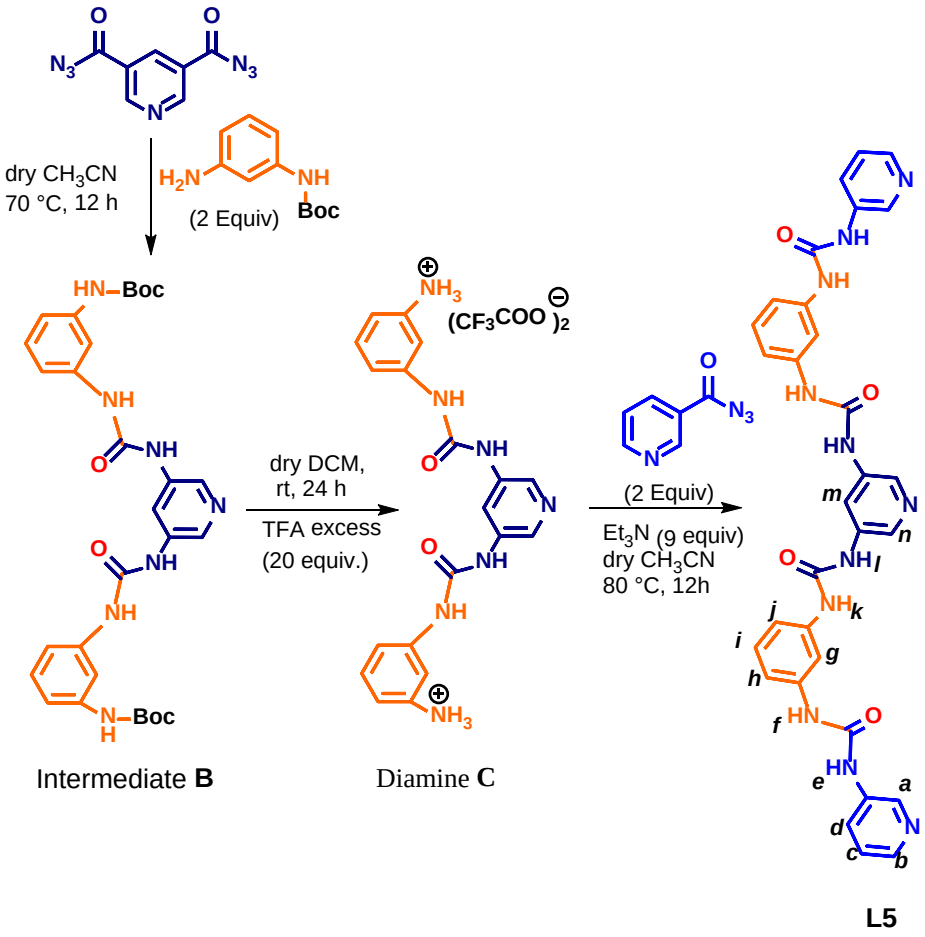

Scheme S2. Schematic representation of the stepwise synthesis of tridentate ligand, **L5**

The *N*-Boc-*m*-phenylenediamine[3] (500 mg, 2.40 mmol) and *N*-Boc-*p*-phenylenediamine[3],[4] (500 mg, 2.40 mmol) was prepared by slight modifications of reported procedure, which were undergone condensation with pyridine-3,5-dicarbonyl diazide (236.97 mg, 1.09 mmol) at 2.2:1 ratio in 60 mL dry acetonitrile at 70 ºC for 12 h. The resulted precipitate was filtered and washed with acetonitrile and dried under vacuum to afford the Boc protected intermediates **B** (465.92 mg, 74%) and **D** (465.92mg, 74%), respectively.

Boc protected intermediates **B** (400 mg, 0.69 mmol) and **D** (400 mg, 0.69 mmol) were treated with trifluoroacetic acid (1573.48 mg, 13.80 mmol) (at 1:20 molar ratio) to obtain a clear yellow solution in 50 mL dry DCM. The reaction mixture was stirred at room temperature for 12 h. The solvent (DCM) was evaporated and the resulting oily solution was washed with toluene and finally dried under vacuum to obtain corresponding diamines **C** (332.82 mg, 82%) and **E** (345 mg, 85%), respectively and utilized in the next step without further purification, isolation, and analysis.

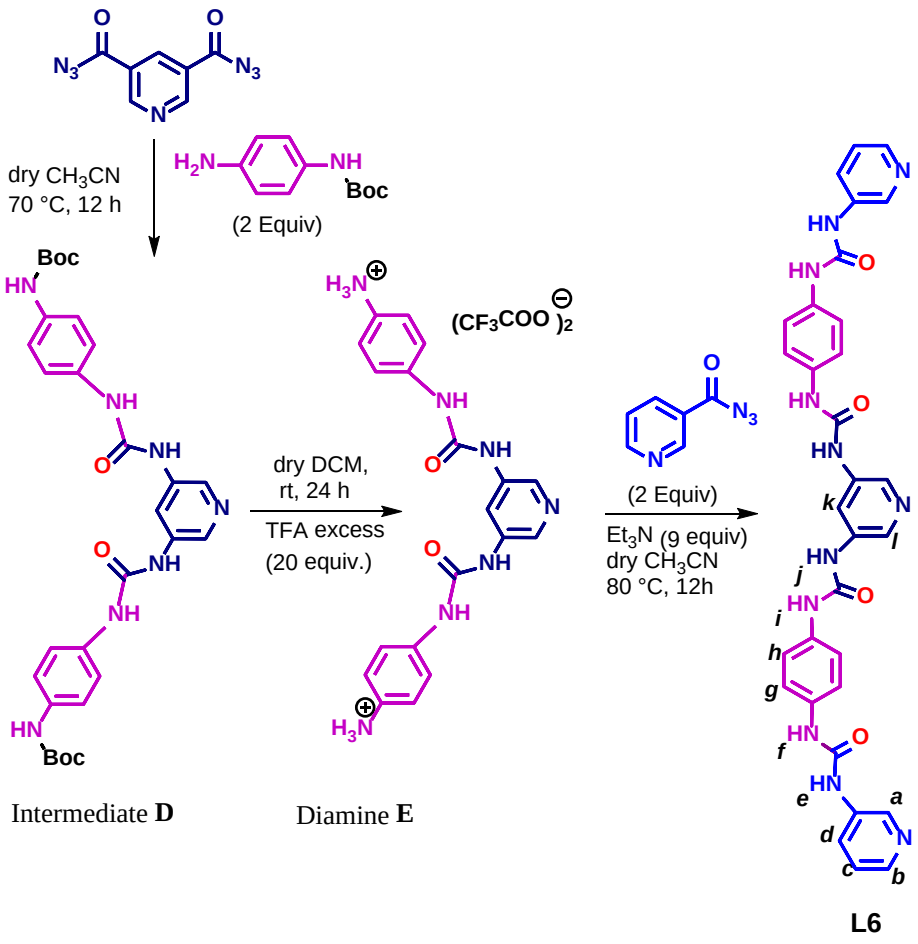

Scheme S3. Schematic representation of the stepwise synthesis of tridentate ligand, **L6**

Diamines **C** (320 mg, 0.54 mmol) and **E** (320 mg, 0.54 mmol) were dissolved in dry acetonitrile and triethylamine (491.78 mg, 4.86 mmol) was added to neutralize the acidic nature of the

compounds. To this pyridine-3-carbonyl azide (159.98 mg, 1.08 mmol) was added at 70 ºC and the reaction solution was stirred for 10 h to afford the targeted precipitates which were filtered and washed with acetonitrile and vacuum dried to result the tridentate ligands **L5** (133.41 mg, 40%) and **L6** (140.08 mg, 42%).

Tert-butyl (3-aminophenyl)carbamate), *N*-Boc-*m*-phenylenediamine[3]**:** (615.78 mg, 32%) ^{1}H NMR (400 MHz, $CDCl_3$) δ = 7.03 (t, J = 8.0 Hz, 1H, H_c), 6.97 (s, 1H, H_f), 6.54 (ddd, J = 8.0, 2.0, 0.8 Hz, 1H, H_b), 6.36 (ddd, J = 8.0, 2.0, 0.8 Hz, 1H, H_e), 3.67 (bs, 2H, H_a), 1.51 (s, 9H) *ppm*; ESI-MS (*m/z*): calculated for $[M + H]^+$ and $[M + Na]^+$: 209.1290 and 231.1190; Observed: 209.1287 and 231.1102, respectively.

di-*tert*-butyl((((pyridine-3,5-diylbis(azanediyl))bis(carbonyl))bis(azanediyl))bis(3,1-phenylene))dicarbamate, Intermediate **B:** Yield: (465.92 mg, 74%) ^{1}H NMR (400 MHz, DMSO-d_6) δ = 9.32 (s, 2H, H_a), 8.75 (s, 2H, H_e), 8.72 (s, 2H, H_i), 8.22 (s, 3H, H_b, H_h), 7.62 (bs, 2H, H_c), 7.14 (m, 4H, H_f, H_g), 7.03 (m, 2H, H_d) *ppm*; ^{13}C NMR (125 MHz, DMSO-d_6): δ = 152.73, 152.29, 139.99, 139.71, 136.42, 128.89, 113.97, 112.17, 112.09, 108.17, 78.94 *ppm*. ESI-MS (*m/z*): calculated for $[M + H]^+$ and $[M + Na]^+$: 578.2727 and 600.2547. Observed: 578.2730 and 600.2550, respectively.

1-(pyridin-3-yl)-3-(3-(3-(5-(3-(3-(3-(pyridin-3-yl)ureido)phenyl)ureido)pyridin-3-yl)ureido)phenyl)urea, L5. (Yield: 133.41, 40%). Melting point: 318 °C. ^{1}H NMR (500 MHz, DMSO-d_6) δ = 8.89-8.79 (m, 4H, urea NH), 8.61 (d, J = 2.7 Hz, 2H, H_a), 8.30 (t, J = 2.3 Hz, 1H, H_m), 8.23 (d, J = 2.3 Hz, 2H, H_n), 8.18 (dd, J_1 = 4.6 Hz, J_2 = 1.5 Hz, 2H, H_b), 7.94 (ddd, J_1 = 8.3 Hz, J_2 = 2.6 Hz, J_3 = 1.5 Hz, 2H, H_d), 7.73 (t, J = 2.1 Hz, 2H, H_g), 7.31 (ddd, J_1 = 8.3 Hz, J_2 = 4.6 Hz, J_3 = 0.7 Hz, 2H, H_c), 7.24-7.15 (m, 2H, H_h), 7.13-7.05 (m, 4H, H_j and H_i), 7.12-7.10 (m, 4H, H_h and H_i) *ppm*; ^{13}C NMR (125 MHz, DMSO-d_6): δ = 152.52, 152.41, 142.88, 140.07, 139.96, 136.48, 133.18, 129.18, 125.14, 123.64, 114.10, 112.12, 108.19 *ppm*.

ESI-MS (*m/z*): calculated for [**L5** + H]$^+$ and [**L5** + Na]$^+$: 618.2326 and 640.2145. Observed: 618.2311 and 640.2111, respectively.

Tert-butyl (4-aminophenyl)carbamate), *N*-Boc-*p*-phenylenediamine[3]**:** (615.78 mg, 32%) ^{1}H NMR (400 MHz, $CDCl_3$) δ = 7.12 (d, J = 8.0 Hz, 2H, H_c), 6.64 (d, J = 8.0 Hz, 2H, H_b), 6.27 (s, 1H, H_d), 3.53 (s, 2H, H_a), 1.50 (s, 9H) *ppm*; ESI-MS (*m/z*): calculated for [M + H]$^+$ and [M + Na]$^+$: 209.1290 and 231.1190; Observed: 209.1286 and 231.1103, respectively.

di-*tert*-butyl((((pyridine-3,5-diylbis(azanediyl))bis(carbonyl))bis(azanediyl))bis(4,1-phenylene))dicarbamate, Intermediate **D:** Yield: (465.92 mg, 74%) ^{1}H NMR (400 MHz, DMSO-d_6) δ = 9.20 (s, 2H, H_a), 8.81 (s, 2H, H_e), 8.57 (s, 2H, H_d), 8.22 (s, 2H, H_f), 8.19 (s, 1H, H_g), 7.35 (m, 4H, H_b, H_c), *ppm*; ^{13}C NMR (125 MHz, DMSO-d_6): δ = 152.87, 152.52, 136.55, 134.17, 133.86, 133.01, 119.00, 118.76, 113.98, 78.77 *ppm*. ESI-MS (*m/z*): calculated for [M + H]$^+$ and [M + Na]$^+$: 578.2727 and 600.2547. Observed: 578.2713 and 600.2528, respectively.

1-(pyridin-3-yl)-3-(4-(3-(5-(3-(4-(3-(pyridin-3-yl)ureido)phenyl)ureido)pyridin-3-yl)ureido)phenyl)urea, L6. (Yield: 140.08, 42%). Melting point: 300 °C. ^{1}H NMR (500 MHz, DMSO-d_6) δ = 8.83 (s, 2H, H_j), 8.79 (s, 2H, H_e), 8.69 (s, 2H, H_i), 8.62 (s, 2H, H_f), 8.59 (d, J = 2.3 Hz, 2H, H_a), 8.23 (d, J = 2.14 Hz, 2H, H_l), 8.20 (d, J = 2.03 Hz, 1H, H_k), 8.17 (dd, J_1 = 4.73 Hz, J_2 = 1.15 Hz, 2H, H_b), 7.92 (ddd, J_1 = 8.4 Hz, J_2 = 2.7 Hz, J_3 = 1.5 Hz, 2H, H_d), 7.38 (m, 8H, H_g and H_h), 7.31 (dd, J_1 = 8.3 Hz, J_2 = 4.6 Hz, 2H, H_c) *ppm*; ^{13}C NMR (125 MHz, DMSO-d_6): δ = 152.68, 152.57, 142.73, 140.02, 136.59, 136.57, 136.52, 134.07, 134.03, 133.08, 125.08, 123.61, 120.96, 119.24, 119.19, 114.13 *ppm*. ESI-MS (*m/z*): calculated for [**L6** + H]$^+$ and [**L6** + Na]$^+$: 618.2326 and 640.2145. Observed: 618.2307 and 640.2116, respectively.

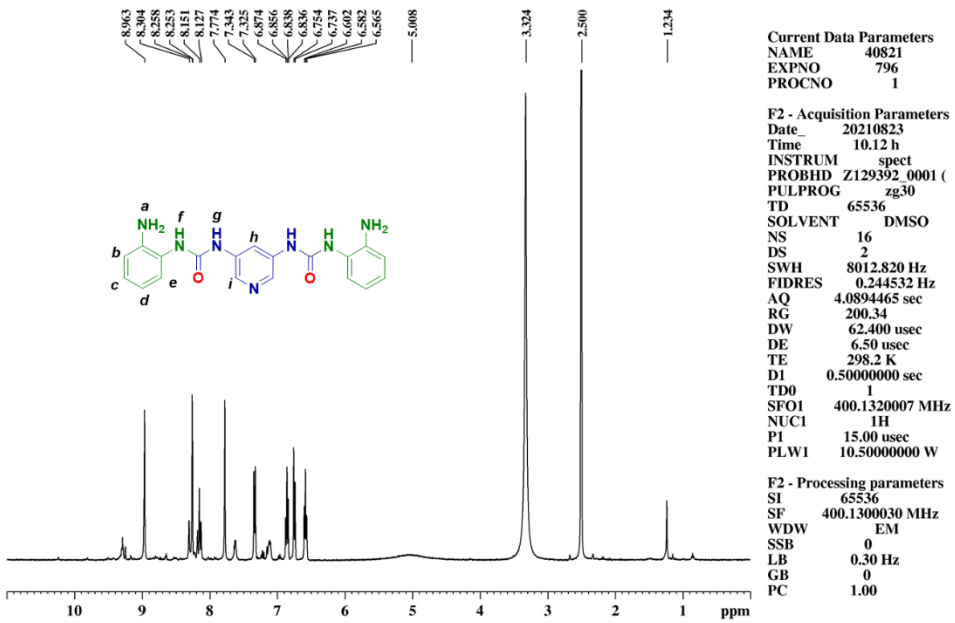

Fig. S1 400 MHz ^{1}H NMR spectrum of diamine **A** in DMSO-d_6.

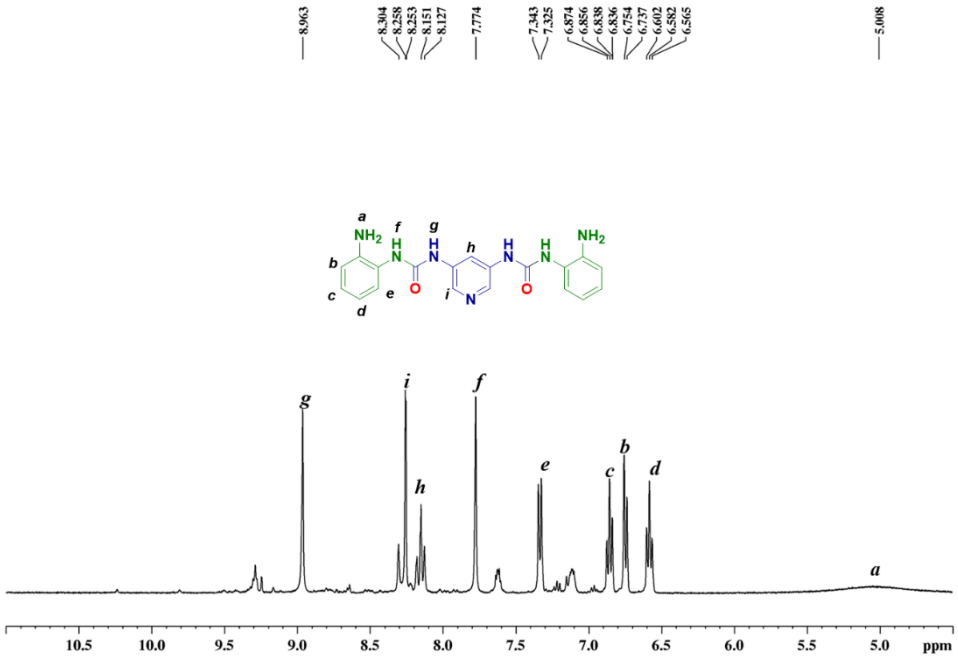

Fig. S2 400 MHz ^{1}H NMR expansion spectrum of diamine **A** in DMSO-d_6.

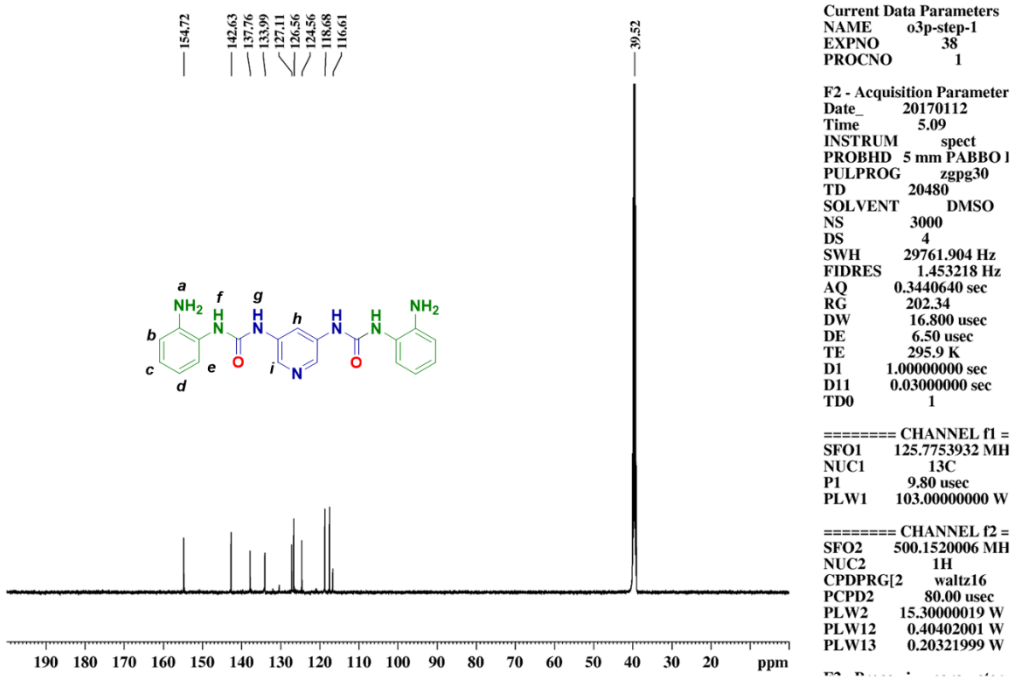

Fig. S3 125 MHz ^{13}C NMR spectrum of diamine **A** in DMSO-d_6.

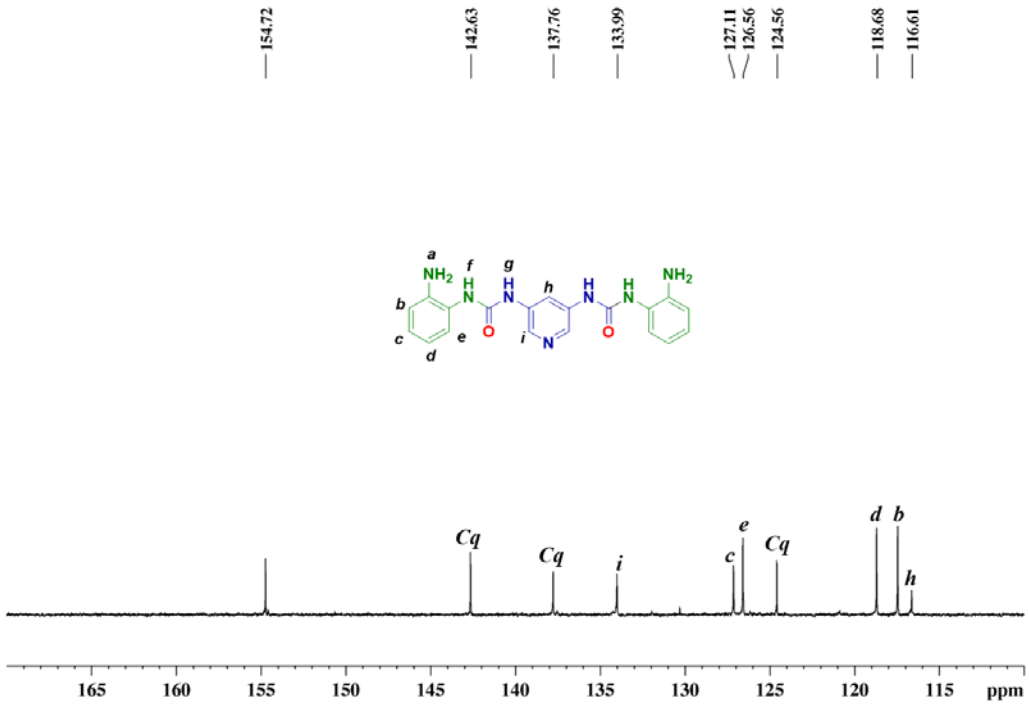

Fig. S4 125 MHz ^{13}C NMR expansion spectrum of diamine **A** in DMSO-d_6.

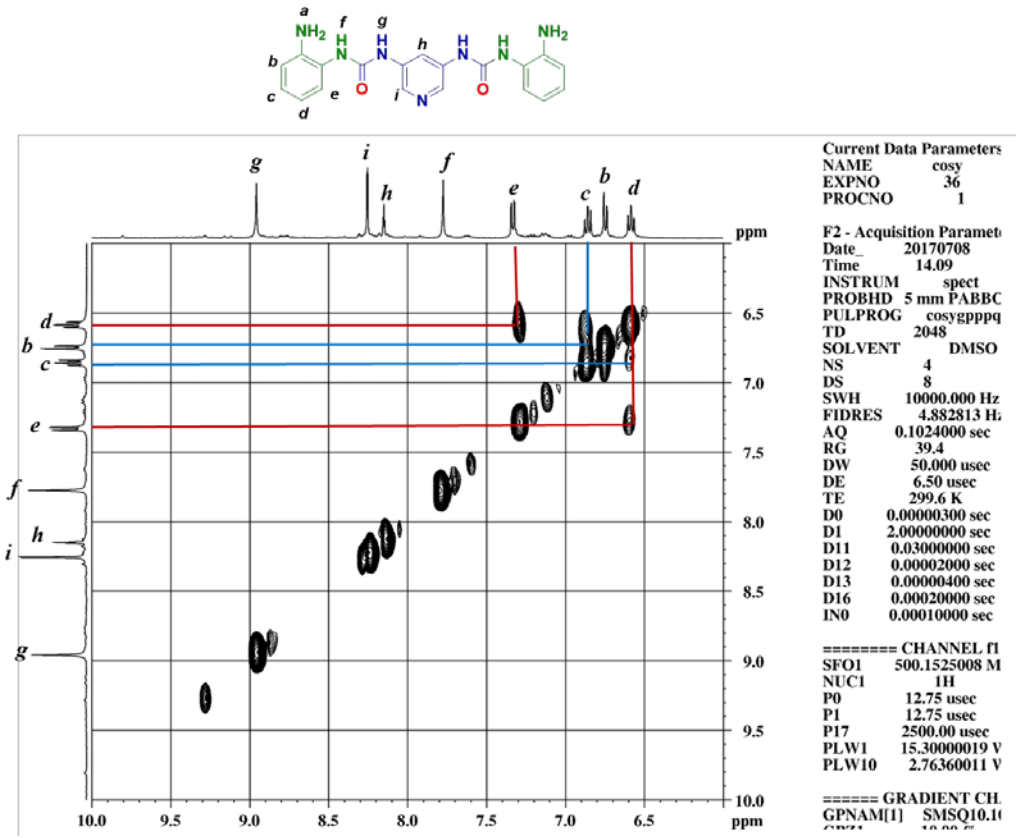

Fig. S5 500 MHz H-H COSY expansion spectrum of diamine **A** in DMSO-d_6.

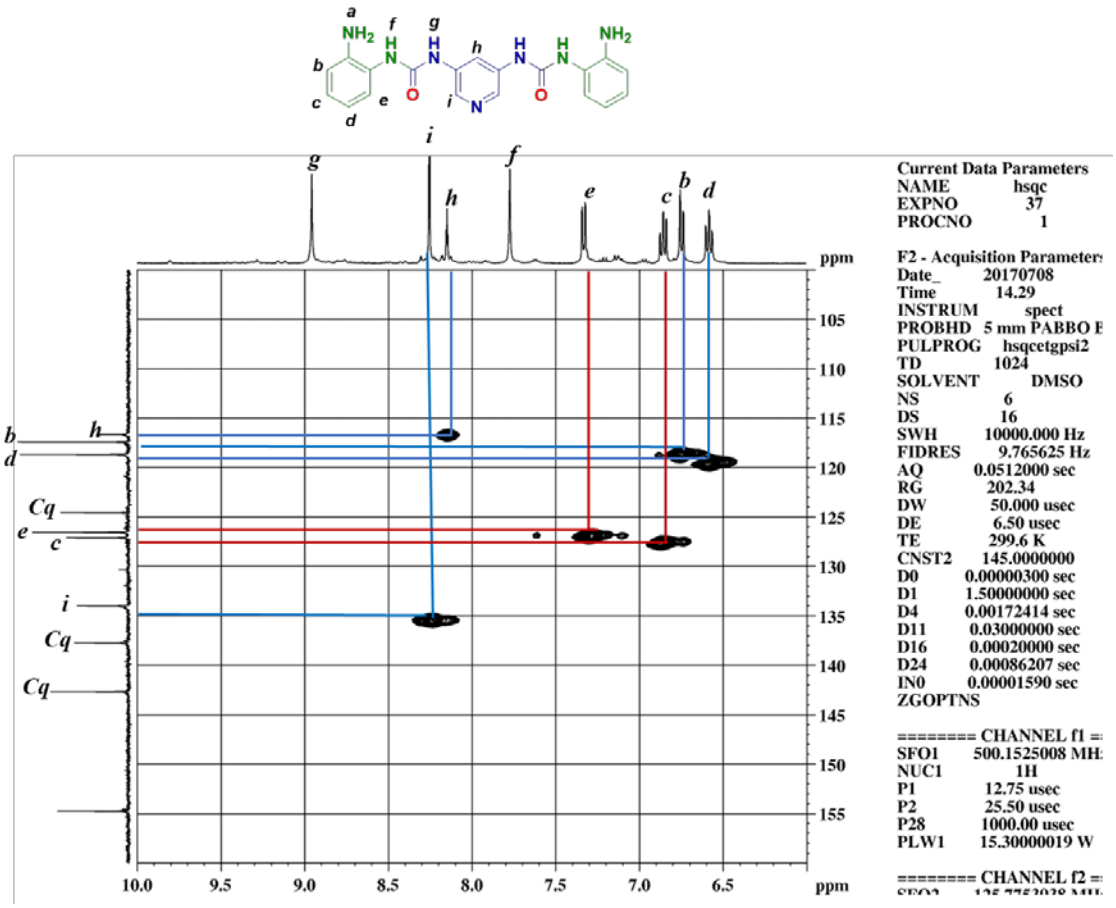

Fig. S6 500 MHz HSQC expansion spectrum of diamine **A** in DMSO-d_6.

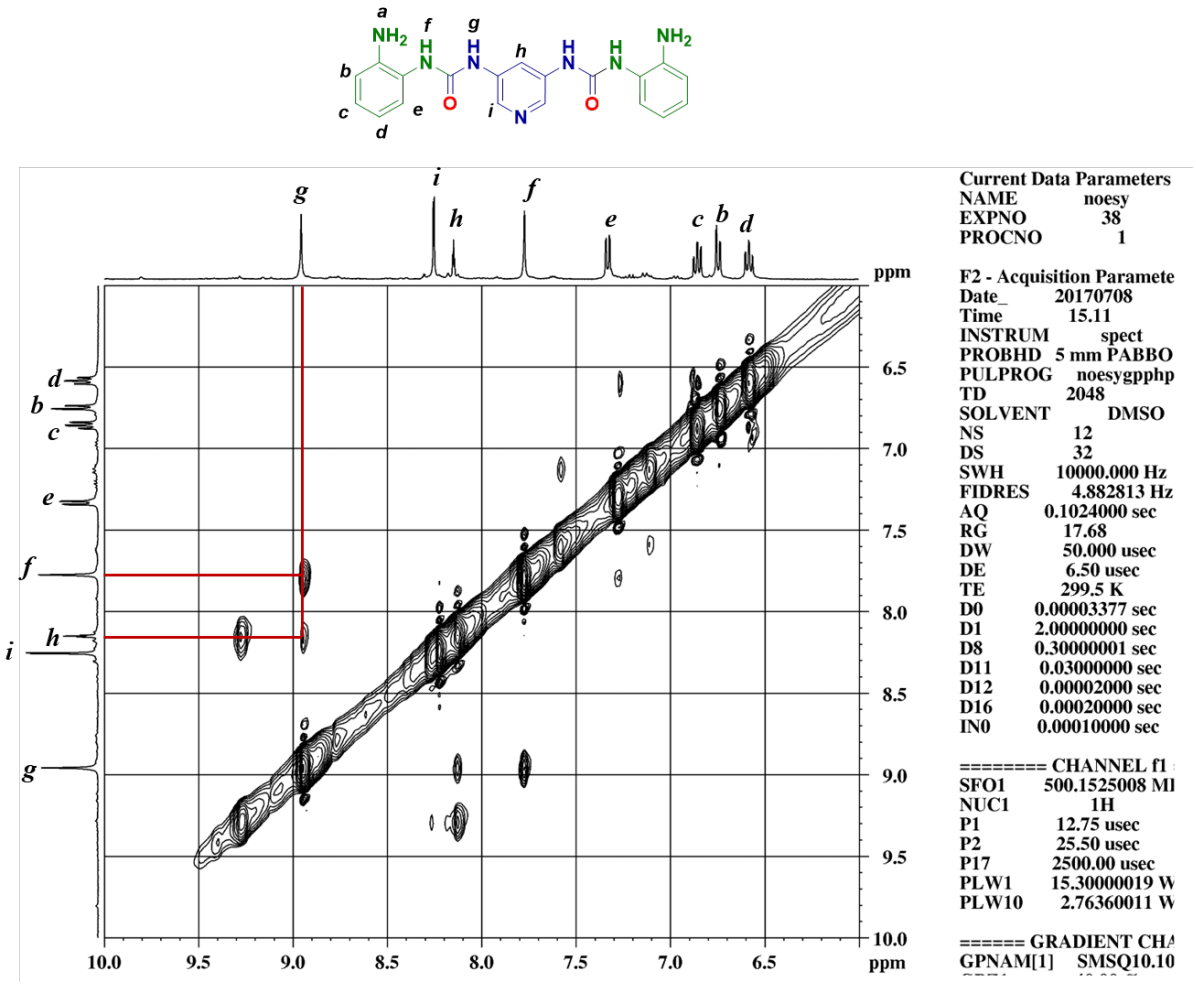

Fig. S7 500 MHz NOESY expansion spectrum of diamine **A** in DMSO-d_6.

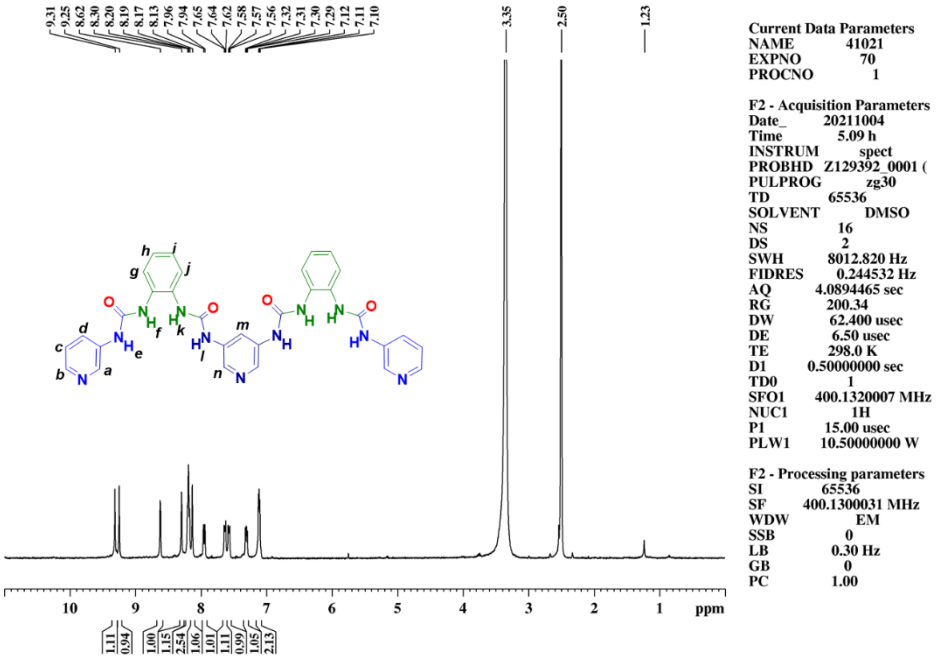

Fig. S8 400 MHz ^{1}H NMR spectrum of ligand **L4** in DMSO-d_6.

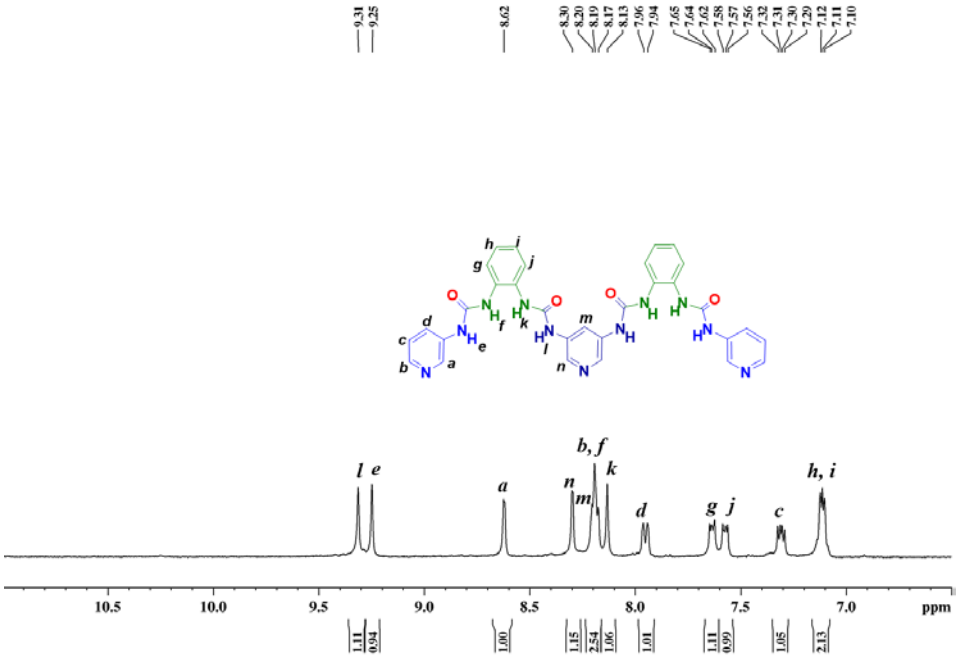

Fig. S9 400 MHz ^{1}H NMR expansion spectrum of ligand **L4** in DMSO-d_6.

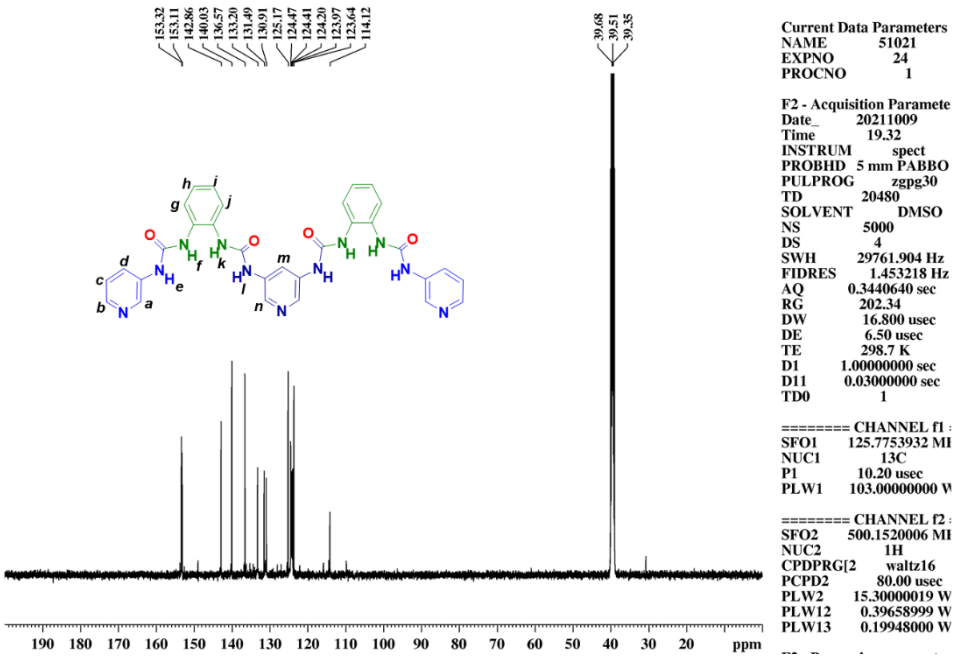

Fig. S10 125 MHz ^{13}C NMR spectrum of ligand **L4** in DMSO-d_6.

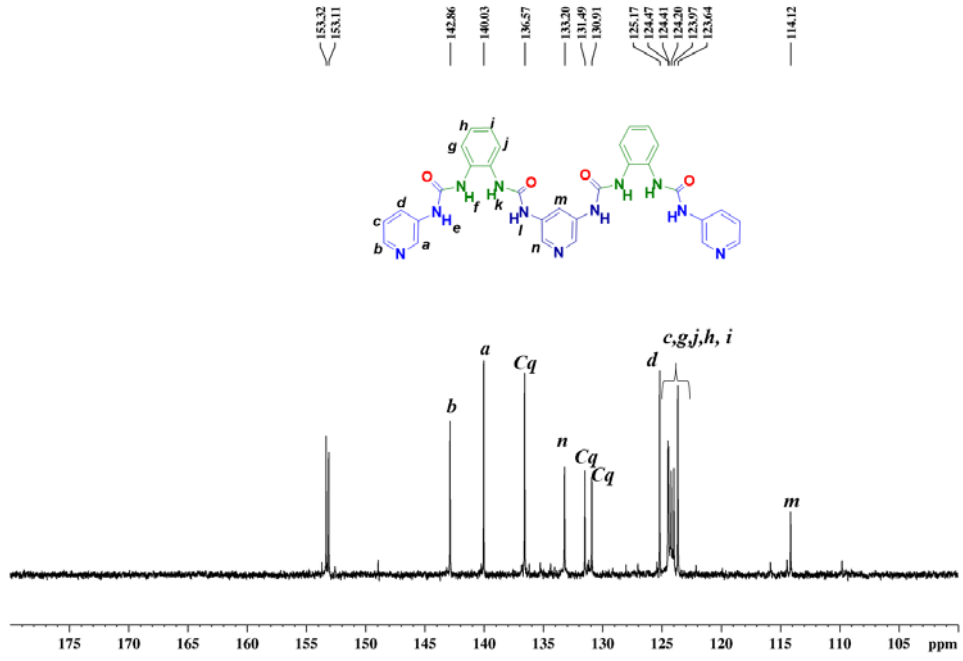

Fig. S11 125 MHz ^{13}C NMR expansion spectrum of ligand **L4** in DMSO-d_6.

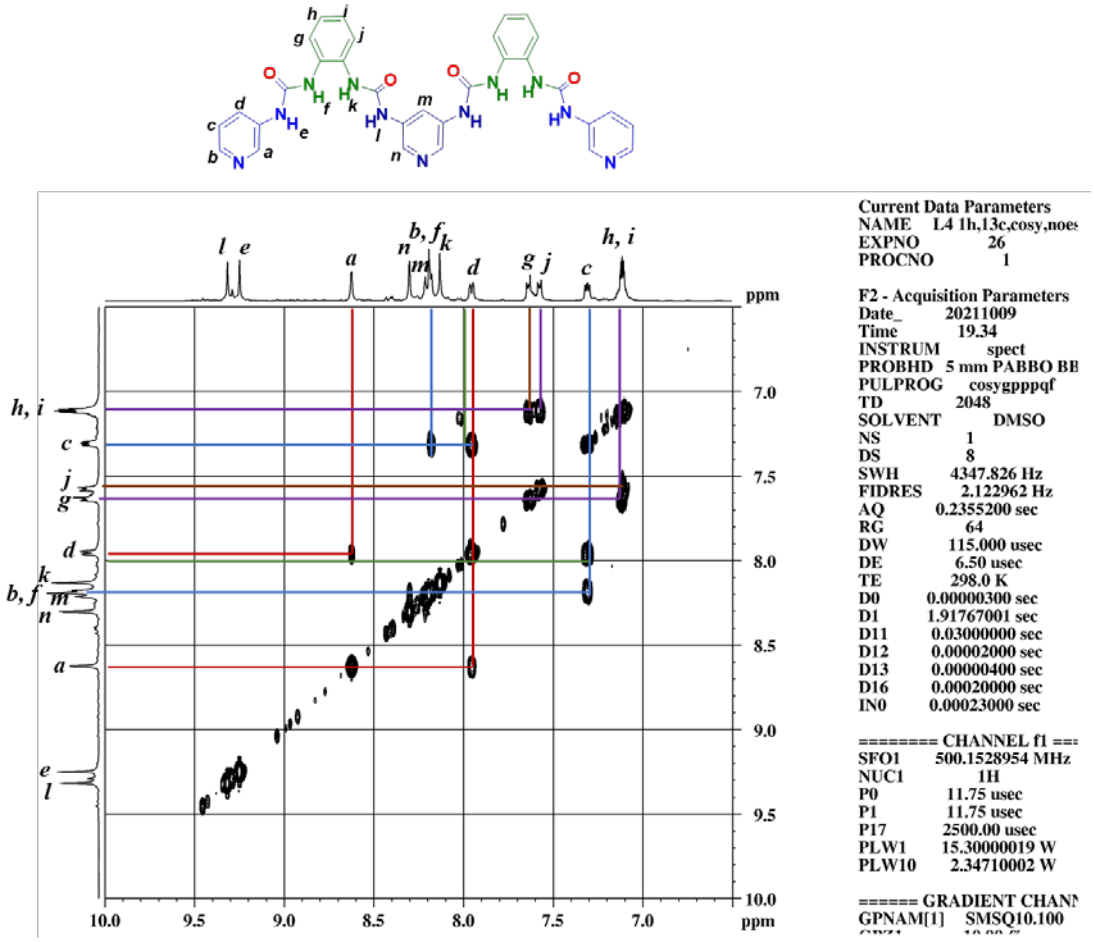

Fig. S12 500 MHz H-H COSY expansion spectrum of ligand **L4** in DMSO-d_6.

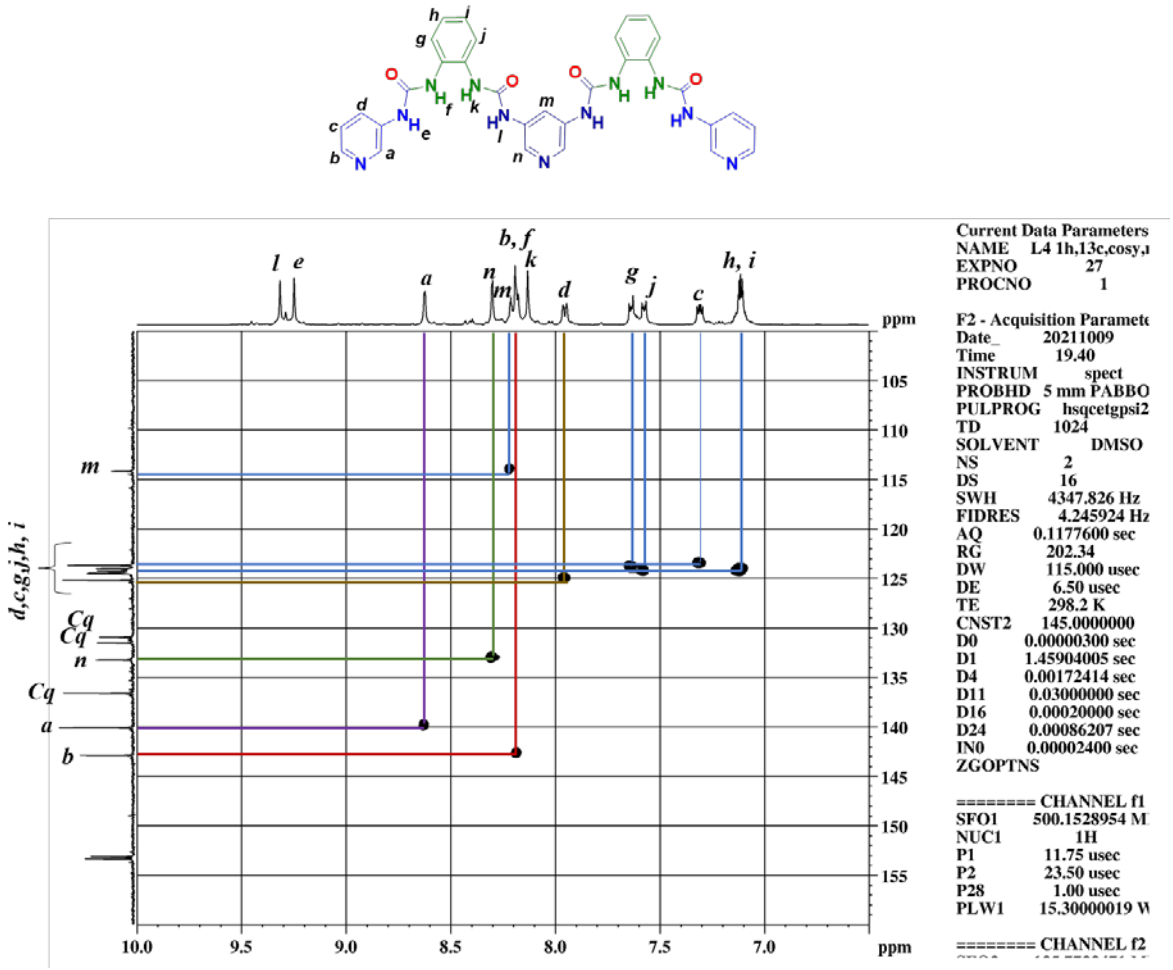

Fig. S13 500 MHz HSQC expansion spectrum of ligand **L4** in DMSO-d_6.

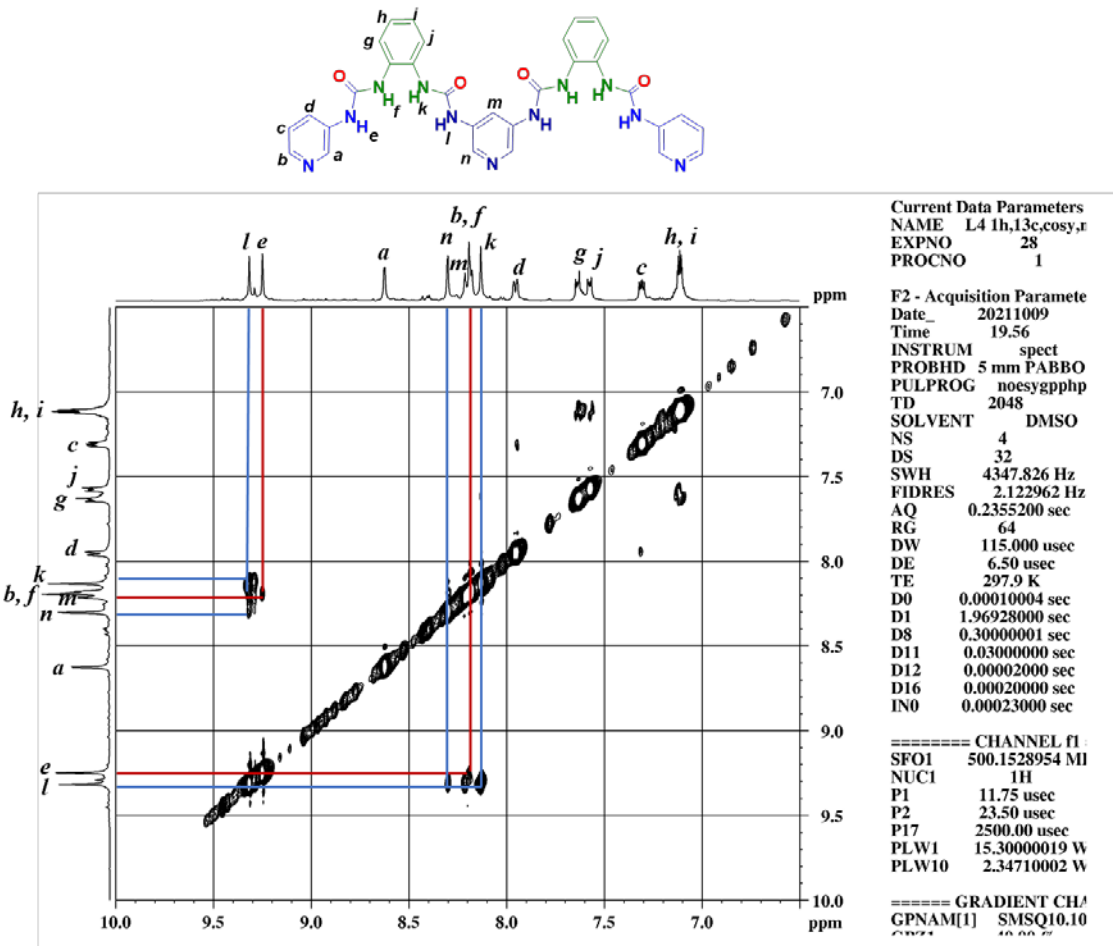

Fig. S14 500 MHz NOESY expansion spectrum of ligand **L4** in DMSO-d_6.

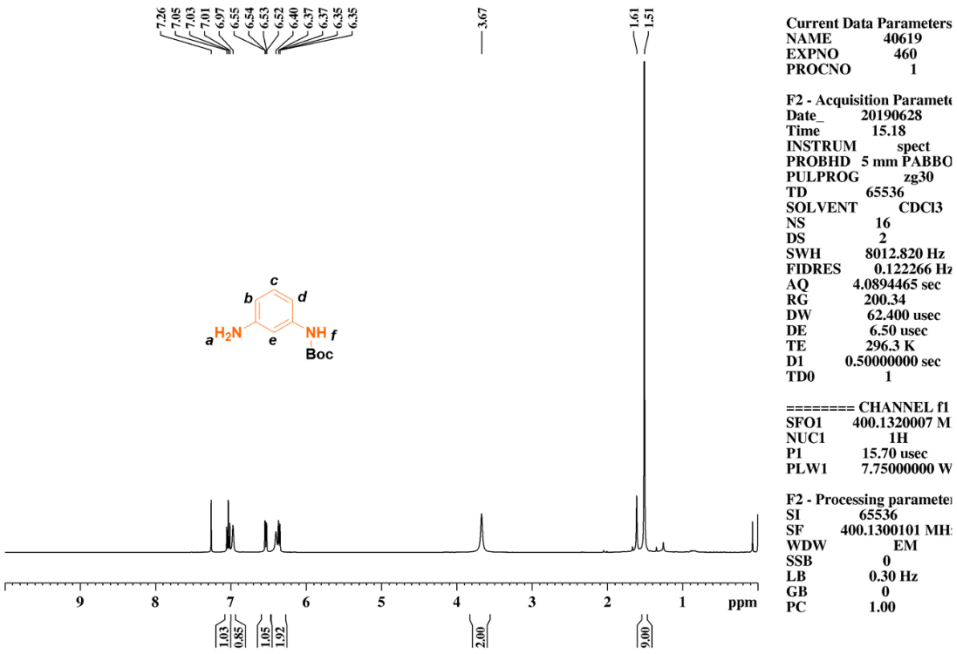

Fig. S15 400 MHz ^{1}H NMR spectrum of *N*-Boc-*m*-phenylenediamine in $CDCl_3$.

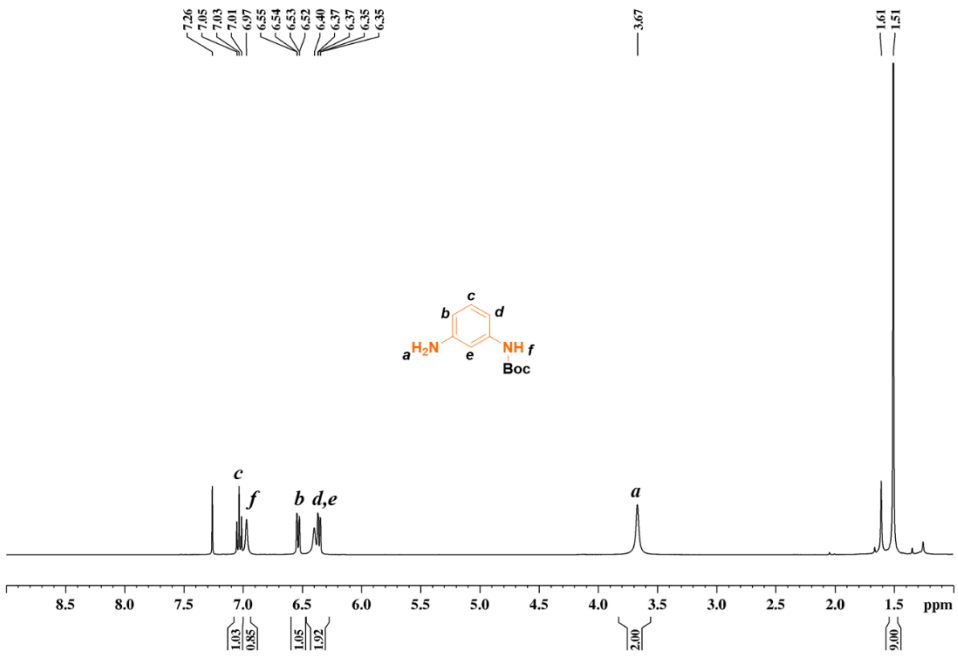

Fig. S16 400 MHz ^{1}H NMR expansion spectrum of *N*-Boc-*m*-phenylenediamine in $CDCl_3$.

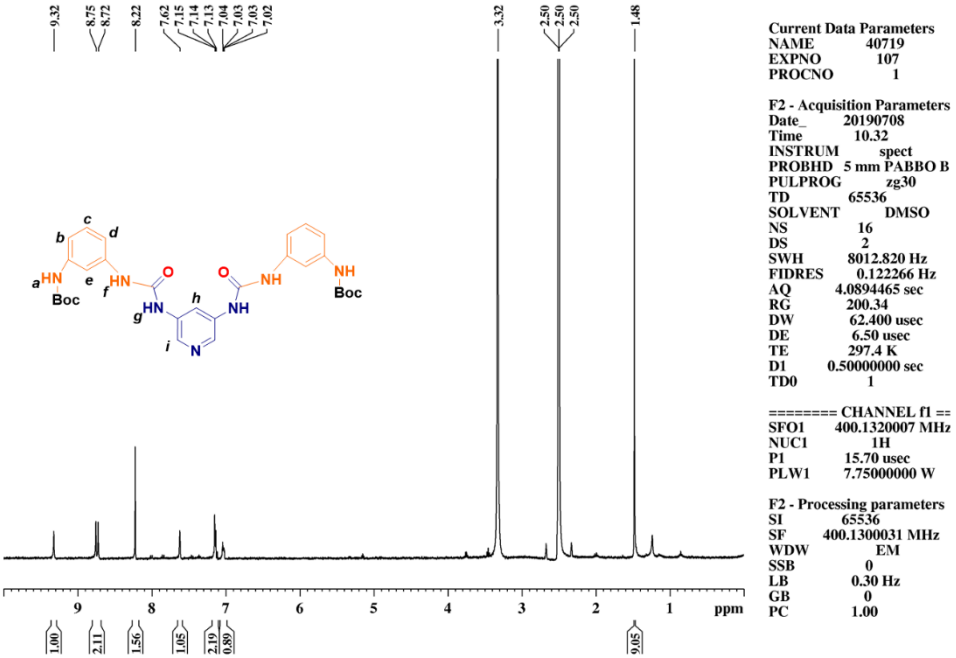

Fig. S17 400 MHz ^{1}H NMR spectrum of Boc protected diamine **B** in DMSO-d_6.

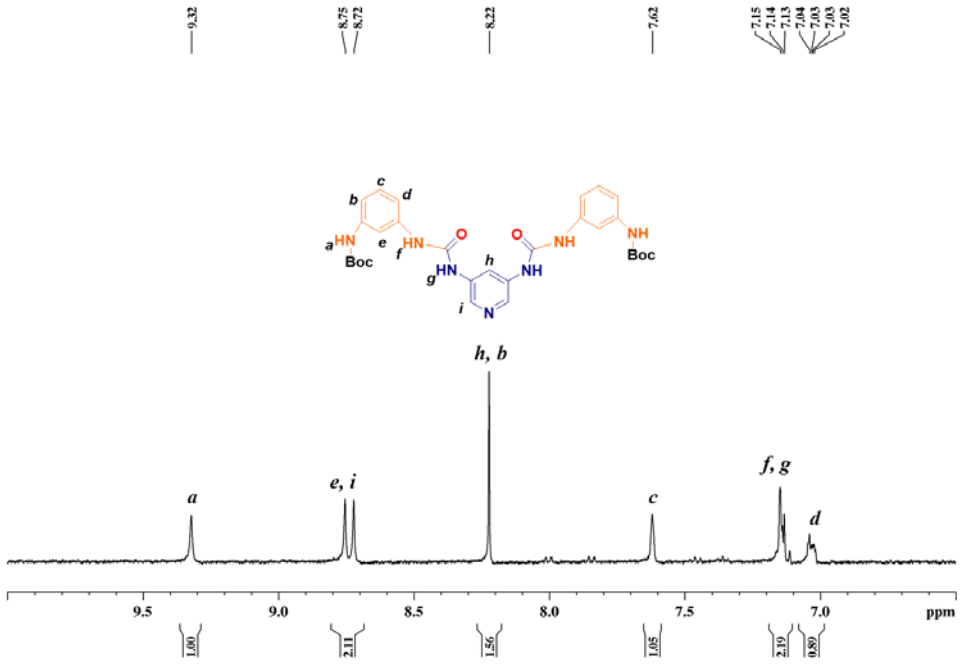

Fig. S18 400 MHz ^{1}H NMR expansion spectrum of Boc protected diamine **B** in DMSO-d_6.

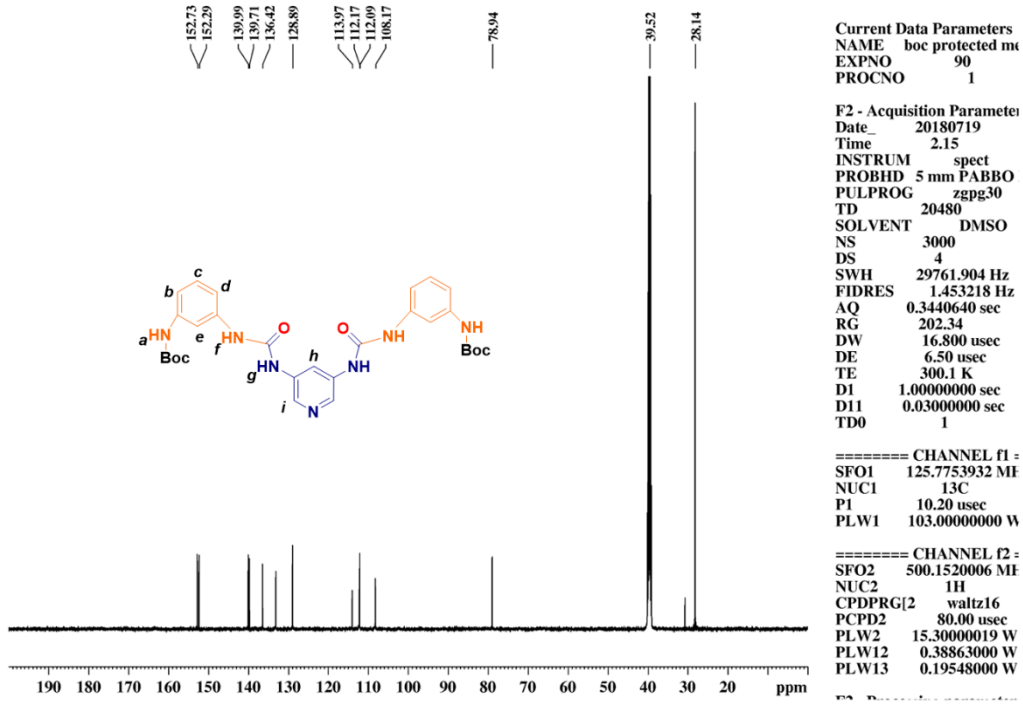

Fig. S19 125 MHz ^{13}C NMR spectrum of Intermediate **B** in DMSO-d_6.

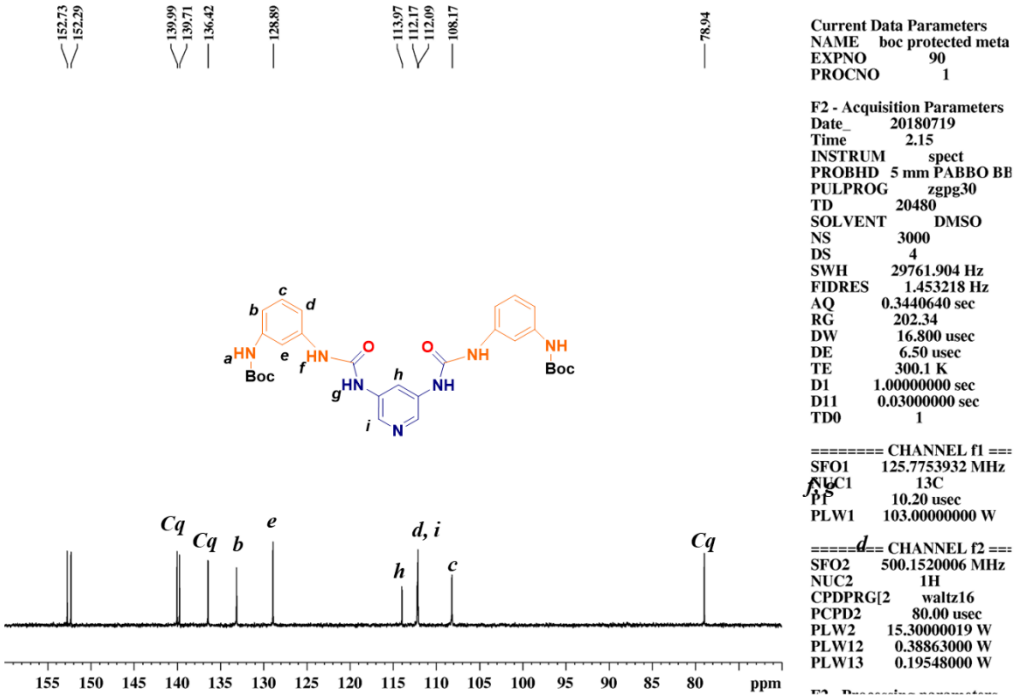

Fig. S20 125 MHz ^{13}C NMR expansion spectrum of Intermediate **B** in DMSO-d_6.

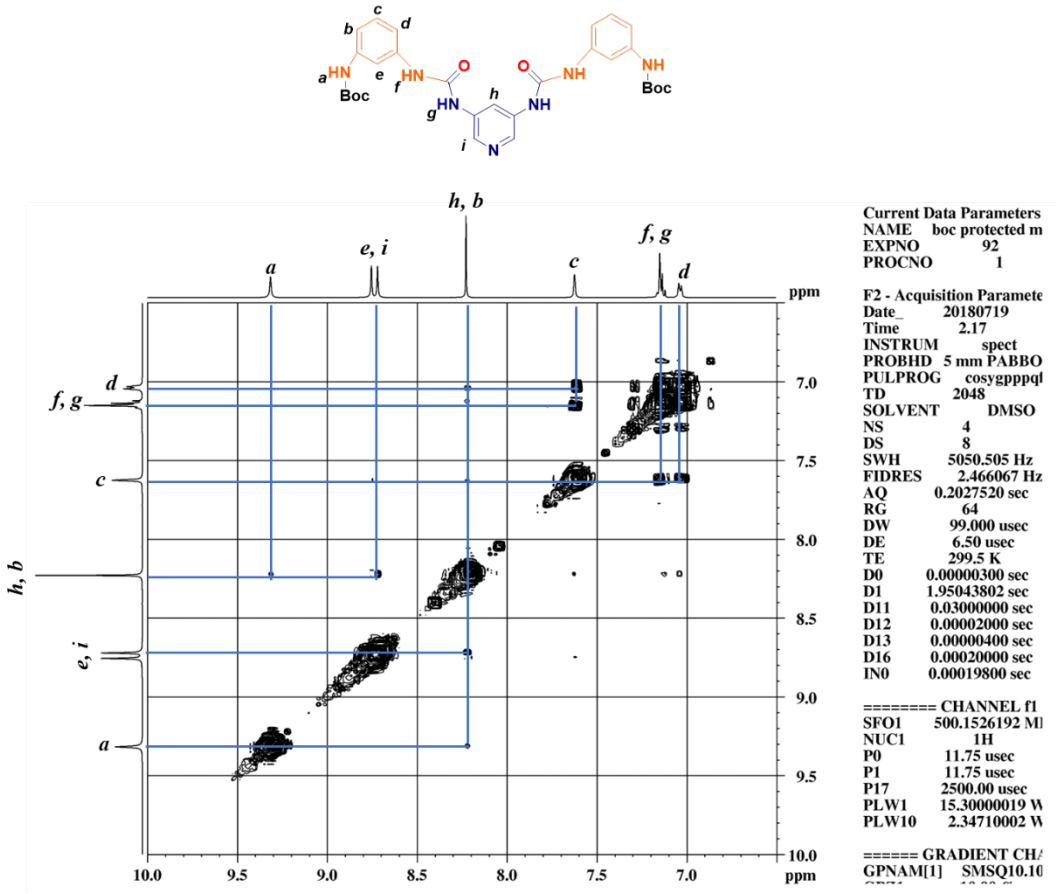

Fig. S21 500 MHz H-H COSY expansion spectrum of Intermediate **B** in DMSO-d_6.

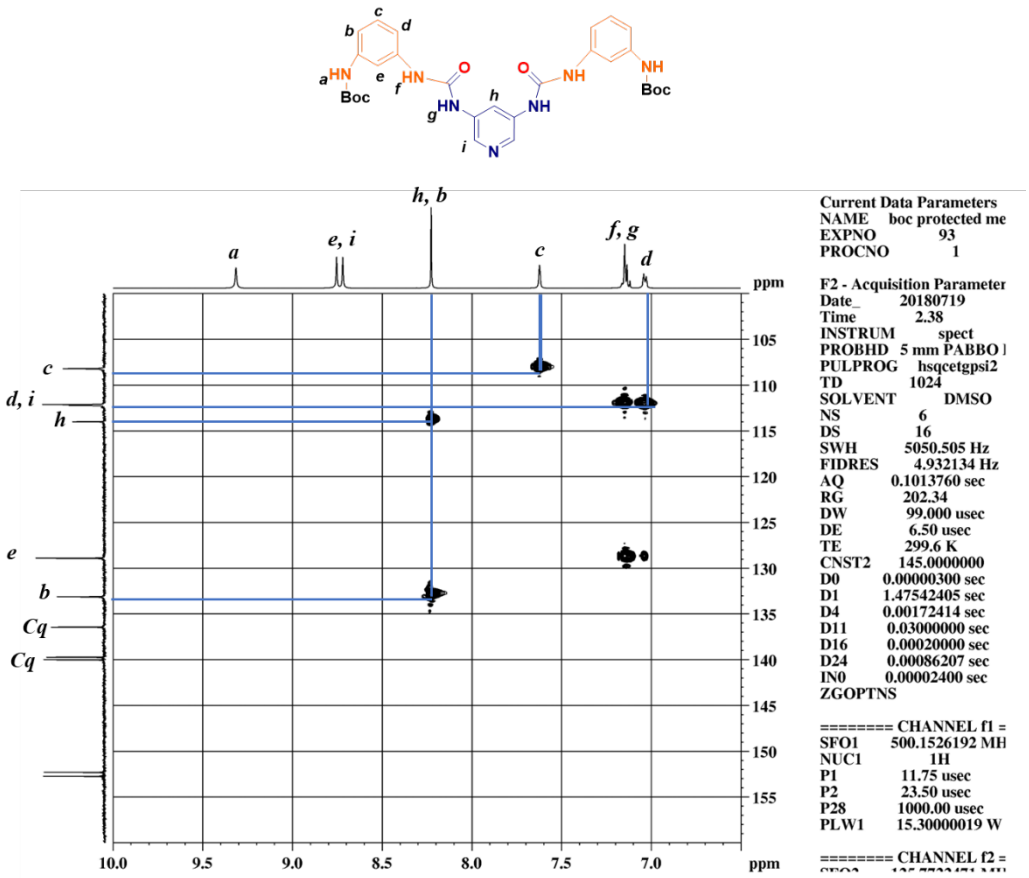

Fig. S22 500 MHz HSQC expansion spectrum of Intermediate **B** in DMSO-d_6.

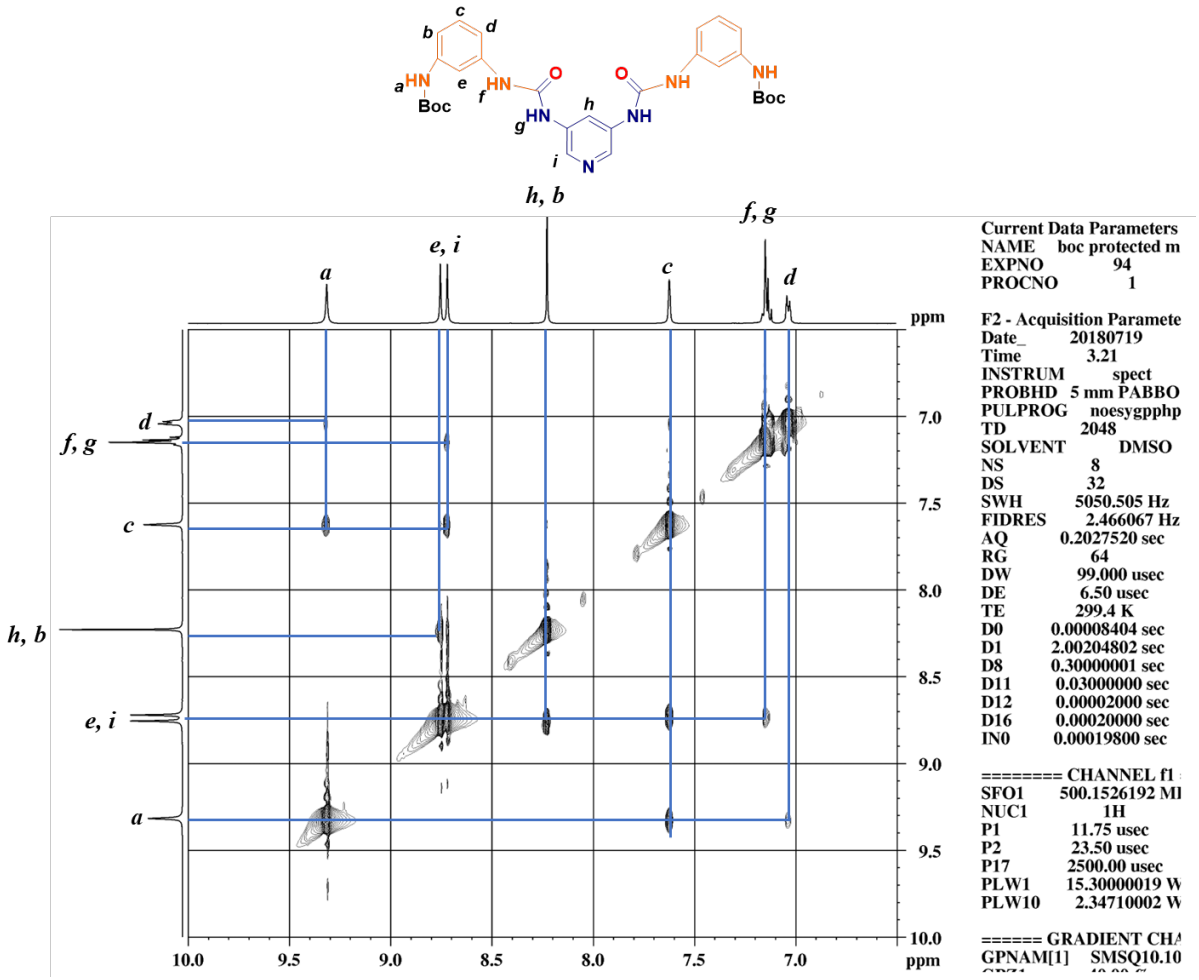

Fig. S23 500 MHz NOESY expansion spectrum of Intermediate **B** in DMSO-d_6.

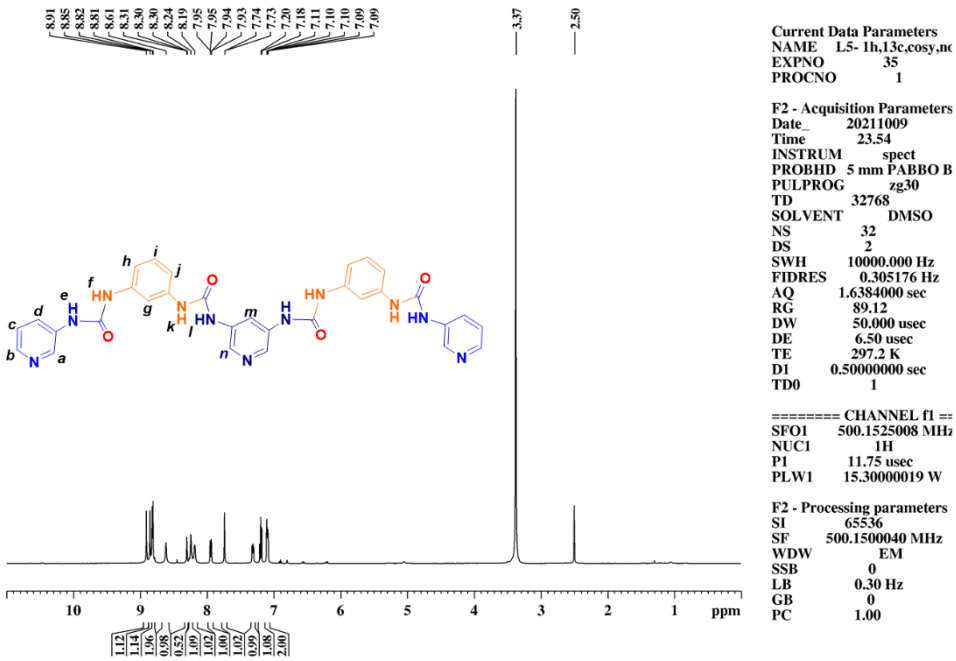

Fig. S24 400 MHz ^{1}H NMR spectrum of ligand **L5** in DMSO-d_6.

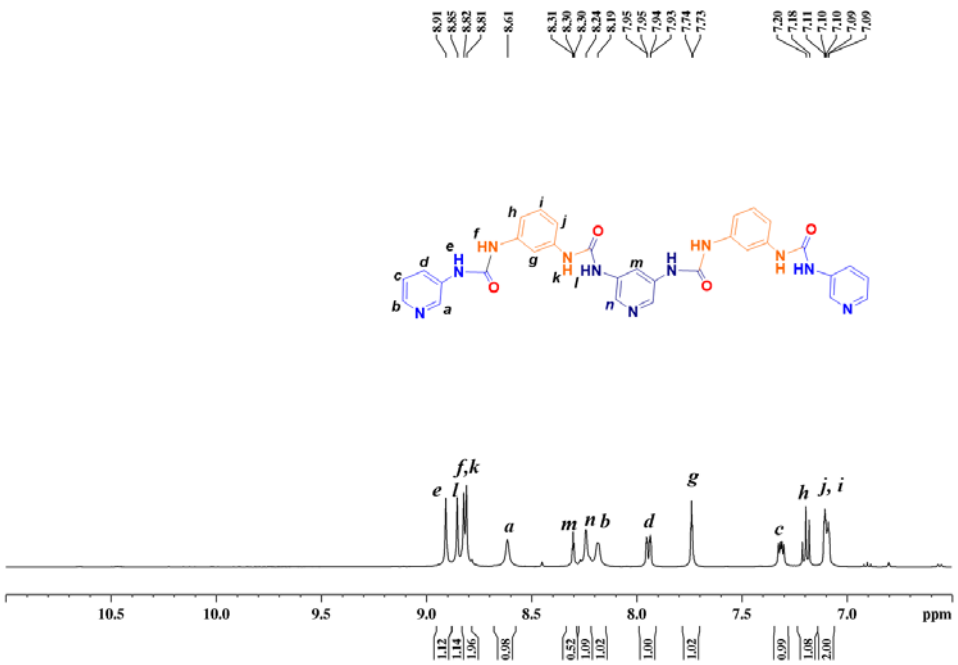

Fig. S25 400 MHz ^{1}H NMR expansion spectrum of ligand **L5** in DMSO-d_6.

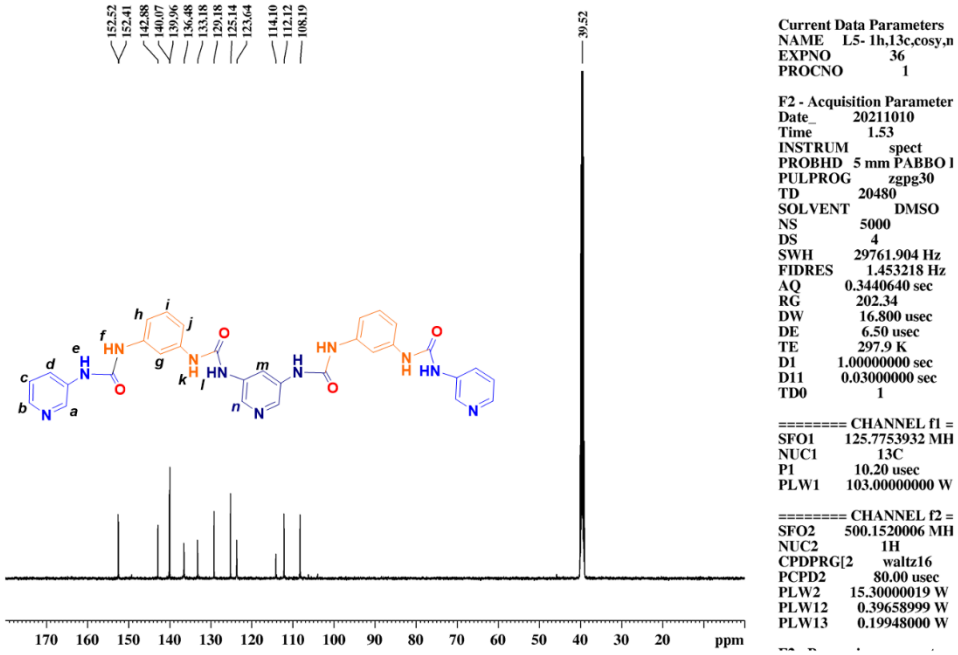

Fig. S26 125 MHz ^{13}C NMR spectrum of ligand **L5** in DMSO-d_6.

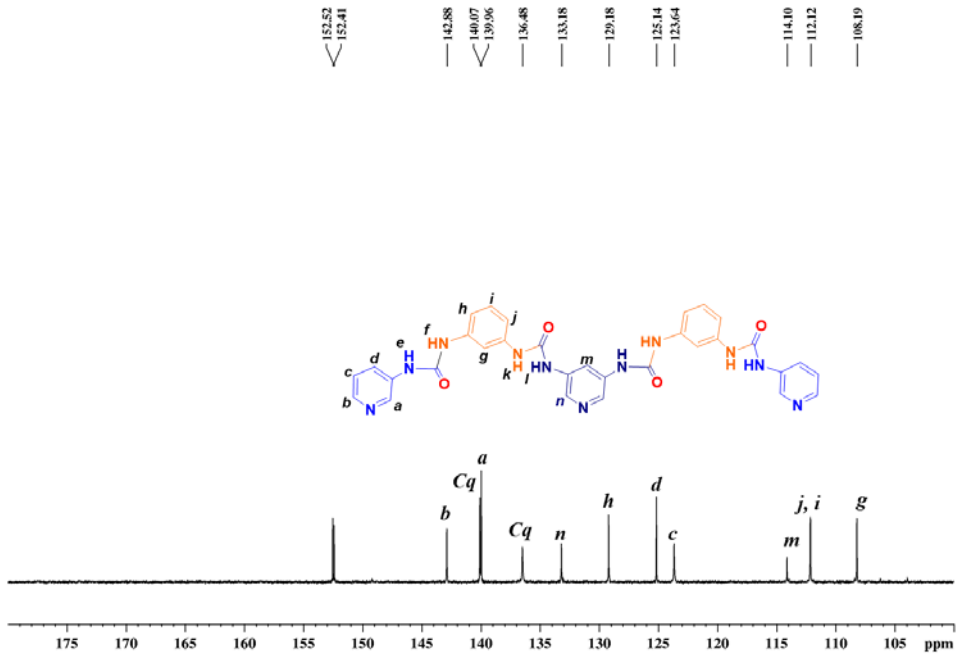

Fig. S27 125 MHz ^{13}C NMR expansion spectrum of ligand **L5** in DMSO-d_6.

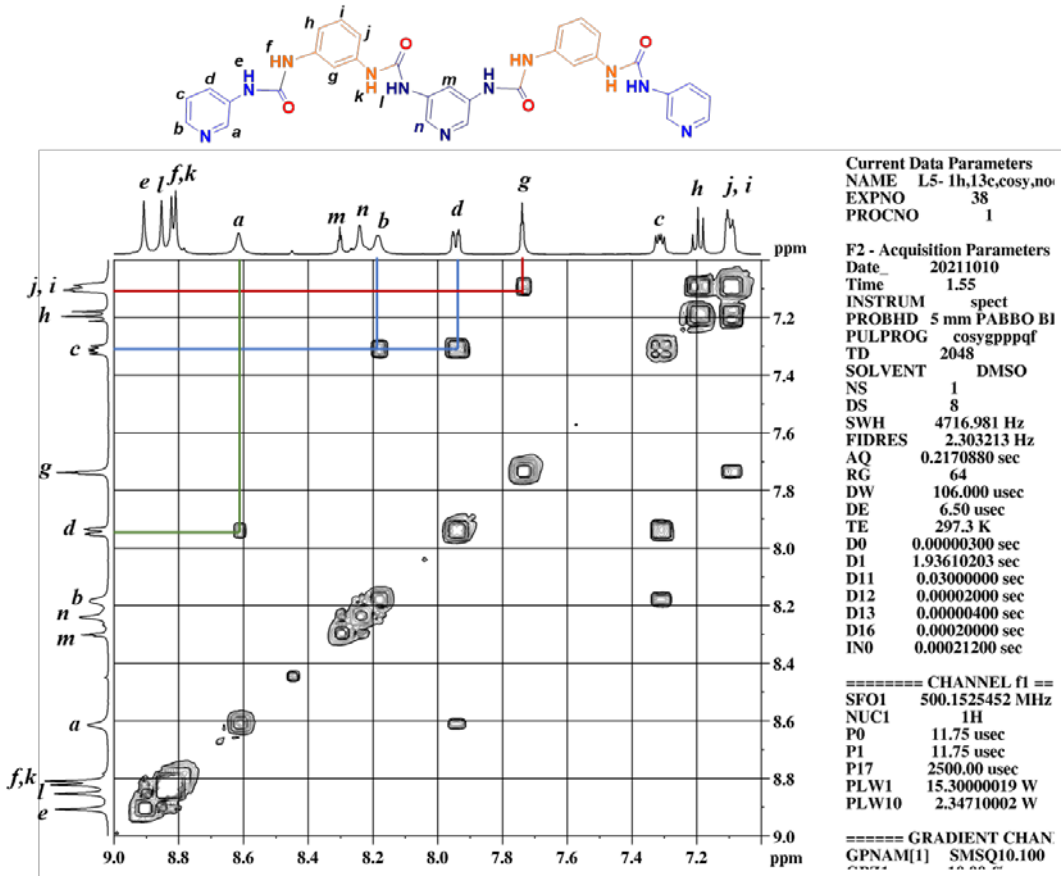

Fig. S28 500 MHz H-H COSY expansion spectrum of ligand **L5** in DMSO-d_6.

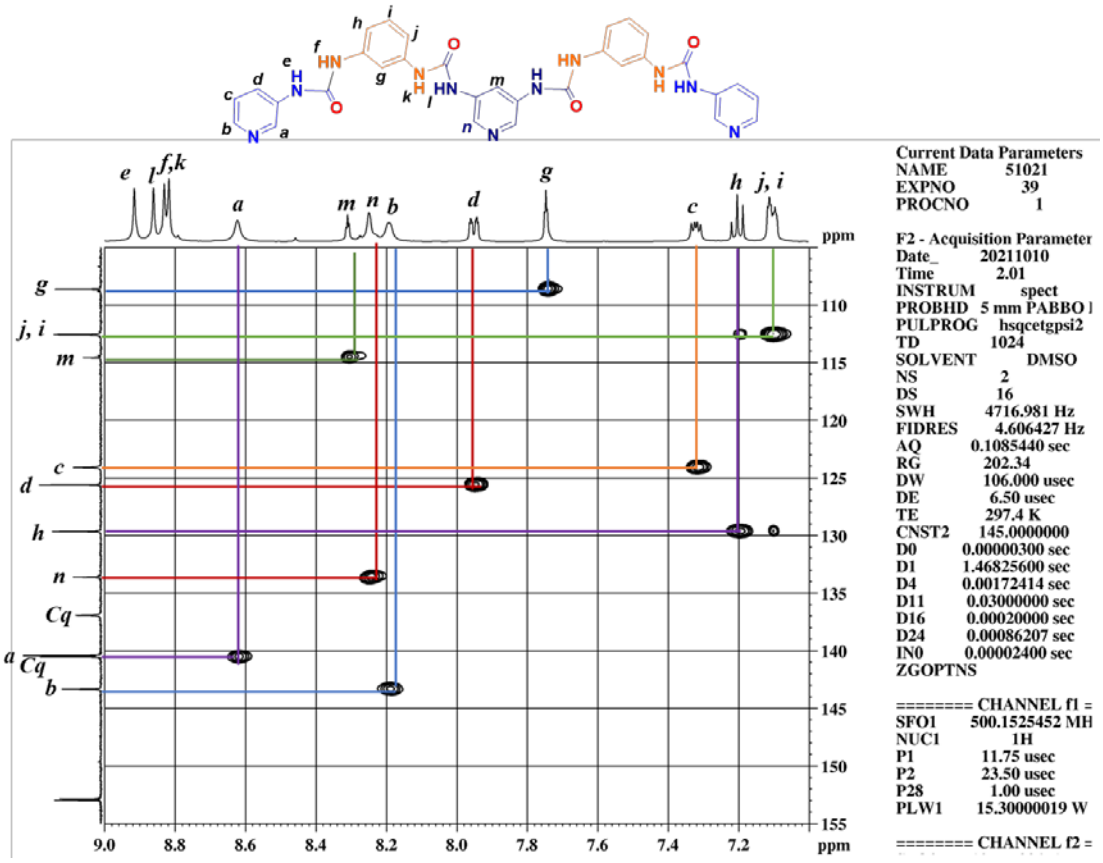

Fig. S29 500 MHz HSQC expansion spectrum of ligand **L5** in DMSO-d_6.

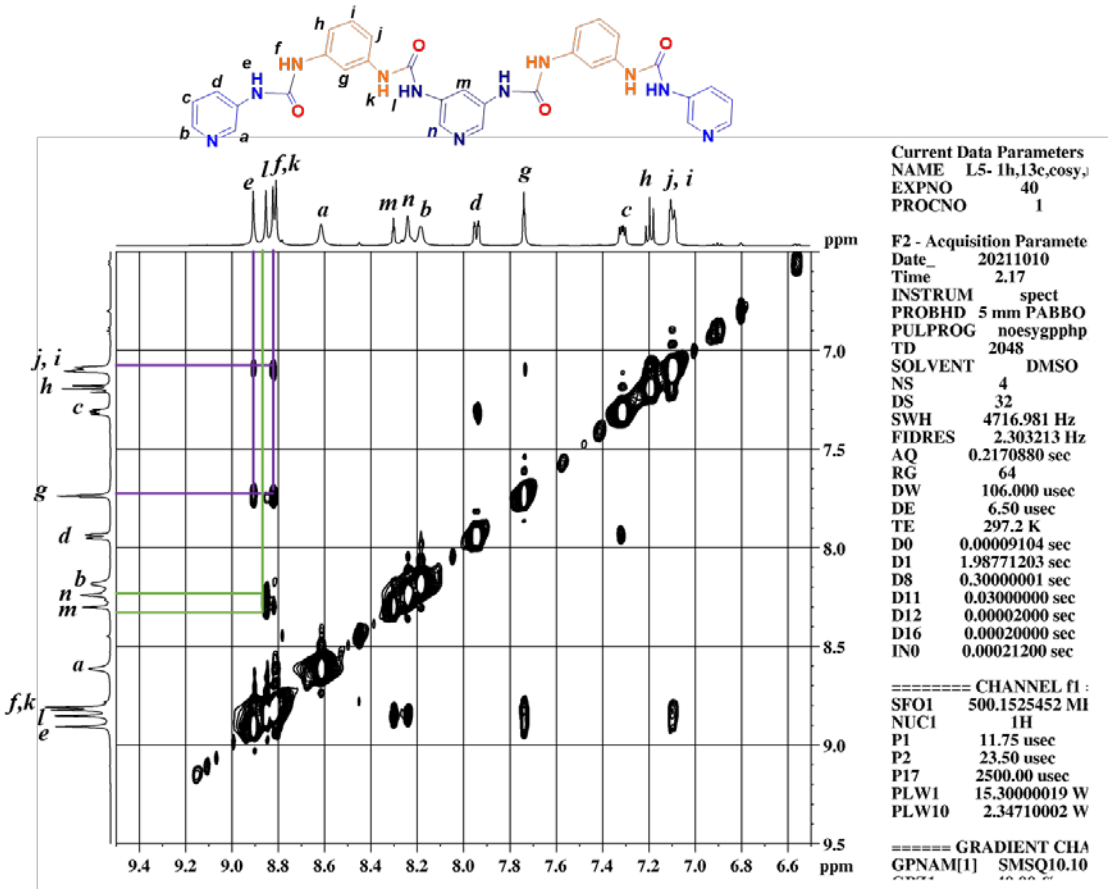

Fig. S30 500 MHz NOESY expansion spectrum of ligand **L5** in DMSO-d_6.

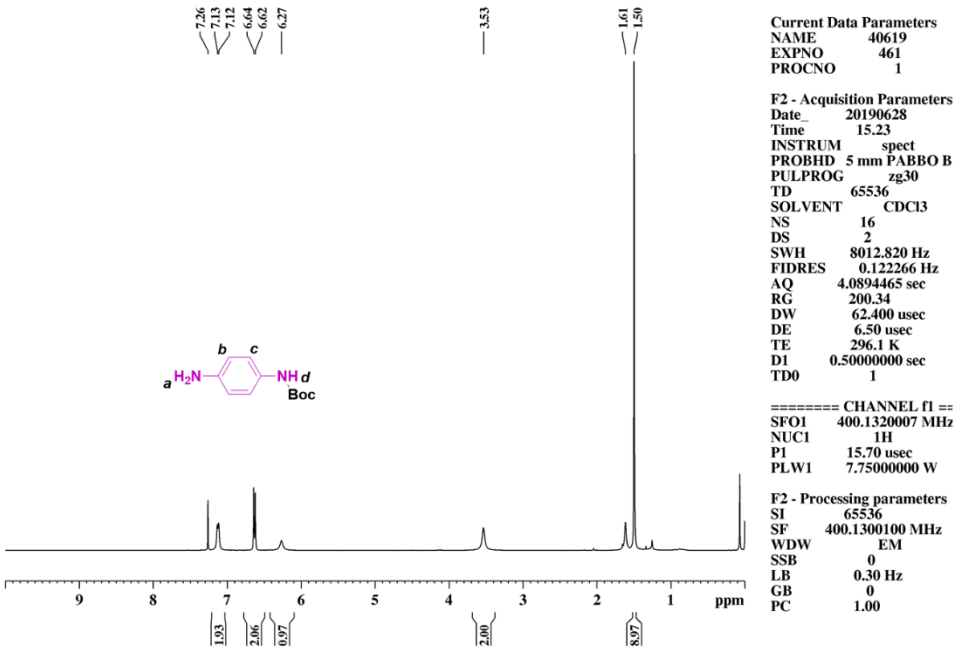

Fig. S31 400 MHz ^{1}H NMR spectrum of *N*-Boc-*p*-phenylenediamine in $CDCl_3$.

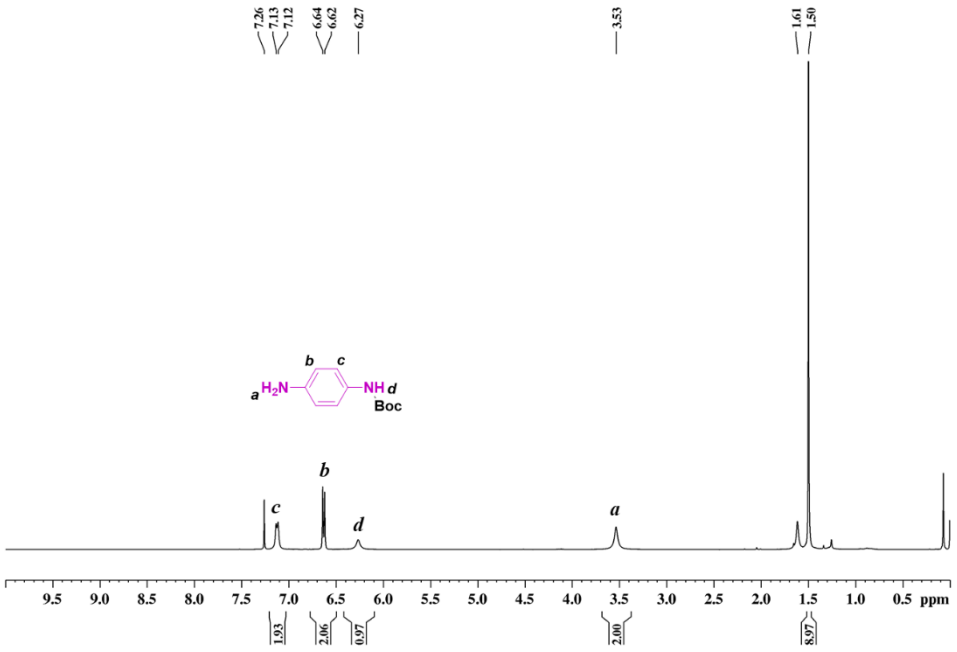

Fig. S32 400 MHz ^{1}H NMR expansion spectrum of *N*-Boc-*p*-phenylenediamine in $CDCl_3$.

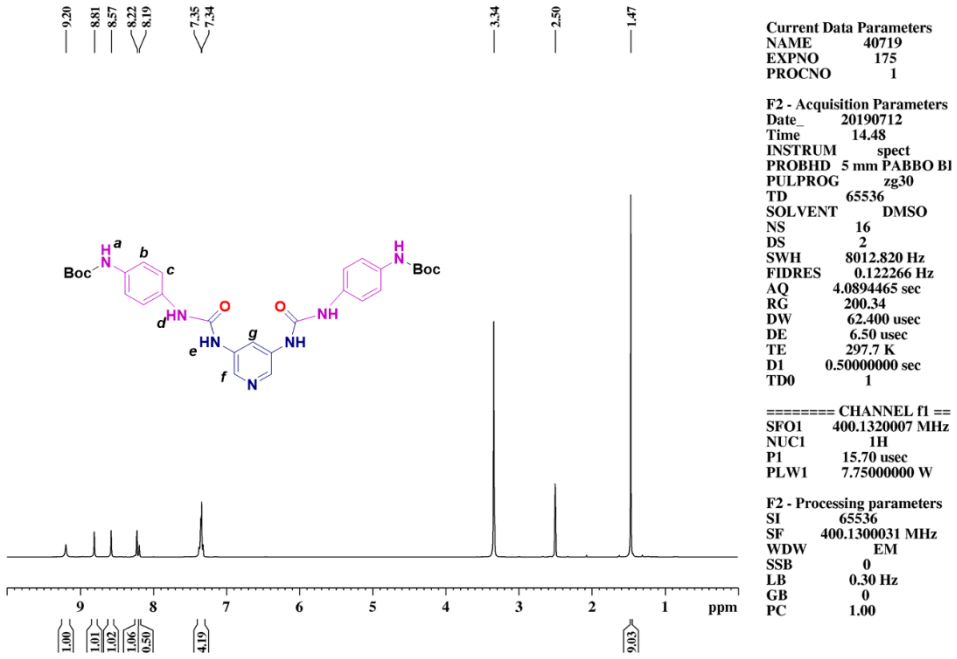

Fig. S33 400 MHz ^{1}H NMR spectrum of Boc protected diamine **D** in DMSO-d_6.

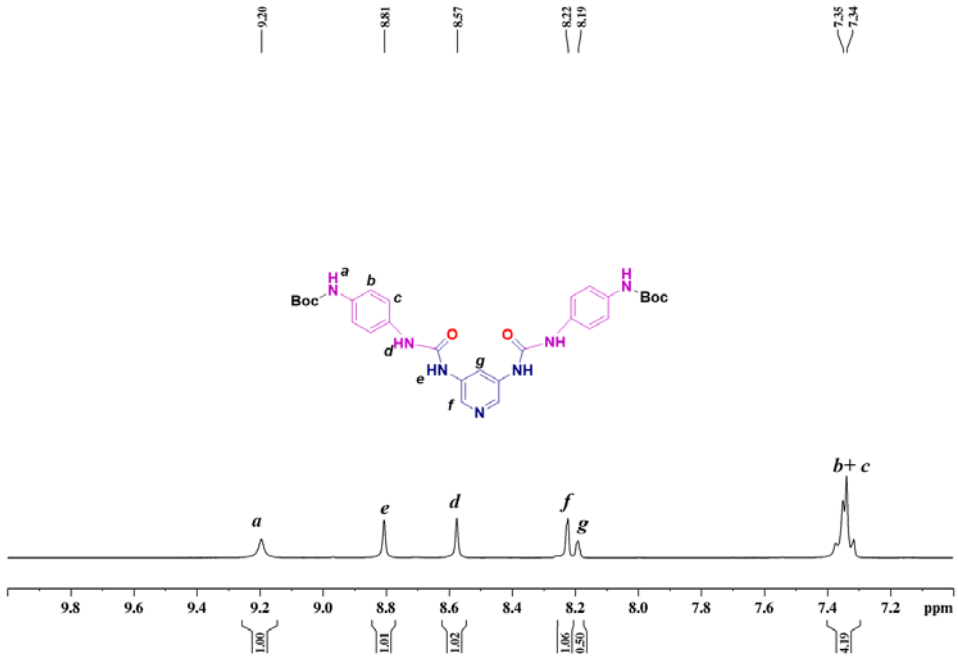

Fig. S34 400 MHz ^{1}H NMR expansion spectrum of Boc protected diamine **D** in DMSO-d_6.

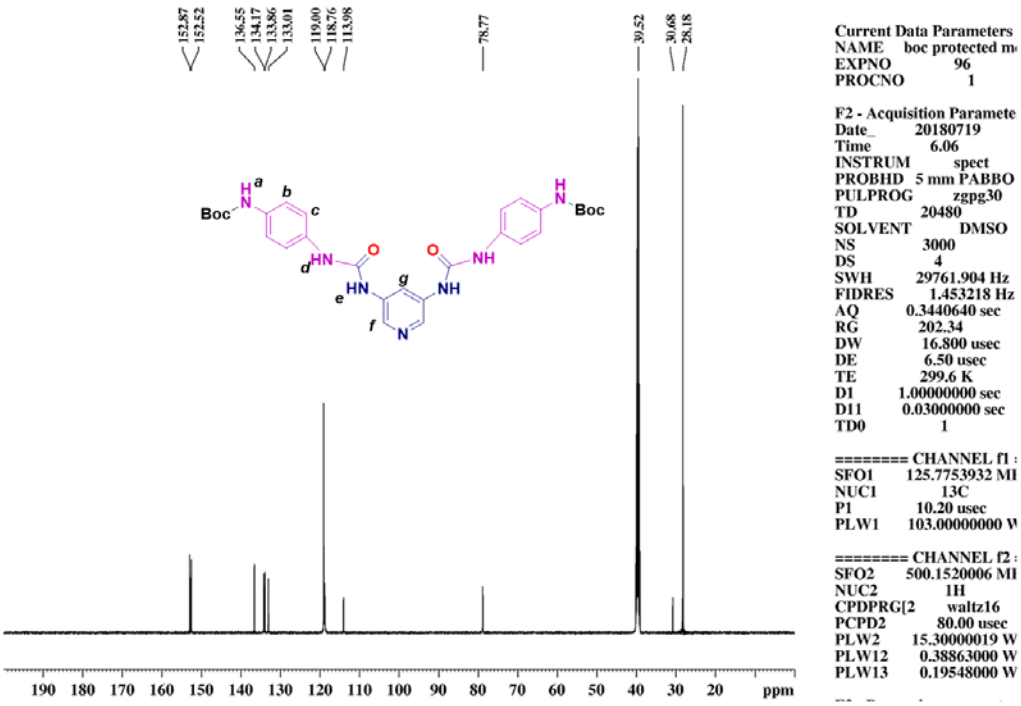

Fig. S35 125 MHz ^{13}C NMR spectrum of Intermediate **D** in DMSO-d_6.

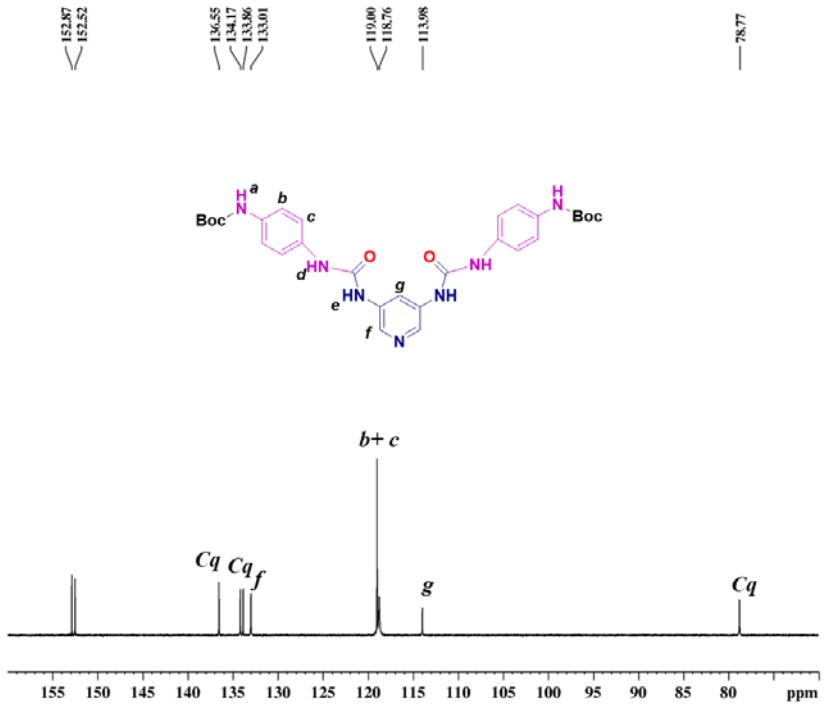

Fig. S36 125 MHz ^{13}C NMR expansion spectrum of Intermediate **D** in DMSO-d_6.

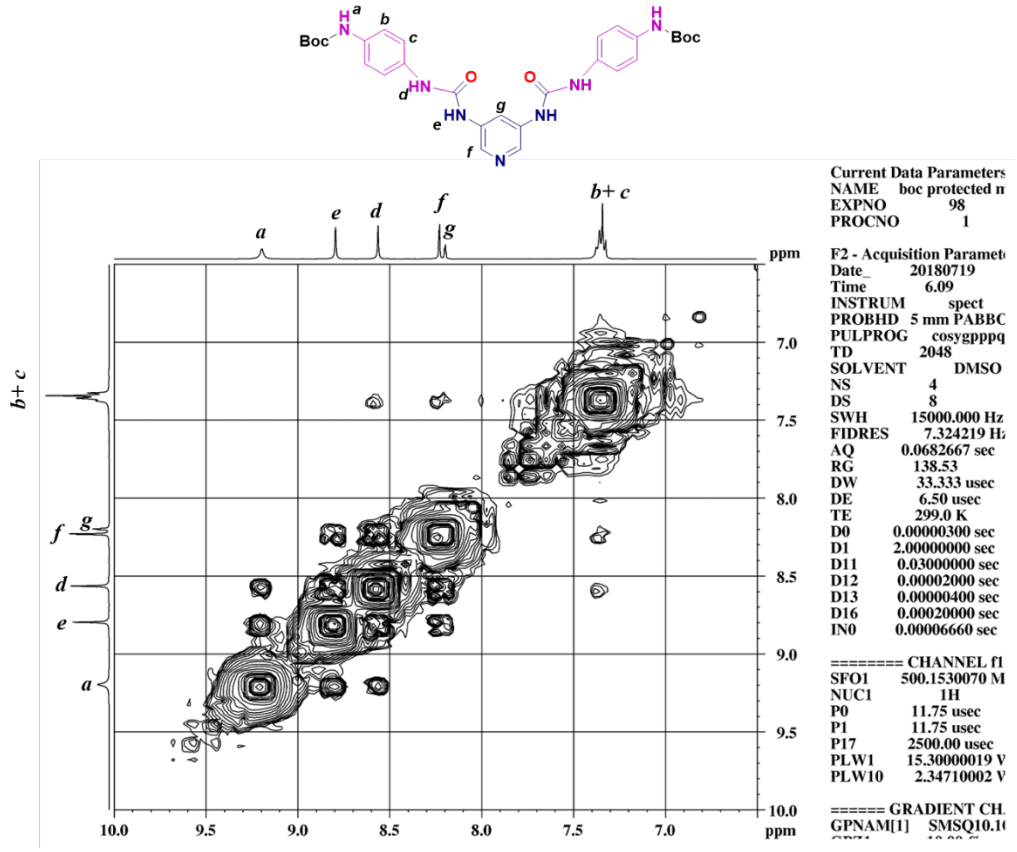

Fig. S37 500 MHz H-H COSY expansion spectrum of Intermediate **D** in DMSO-d_6.

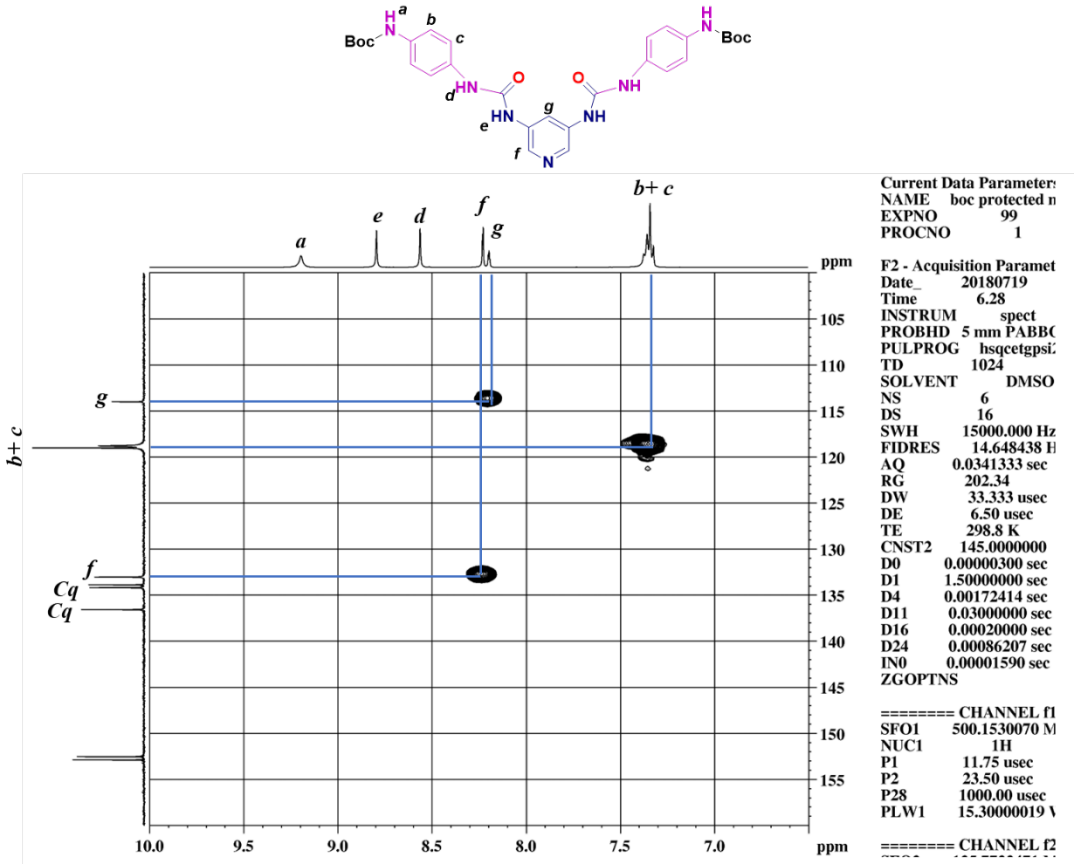

Fig. S38 500 MHz HSQC expansion spectrum of Intermediate **D** in DMSO-d_6.

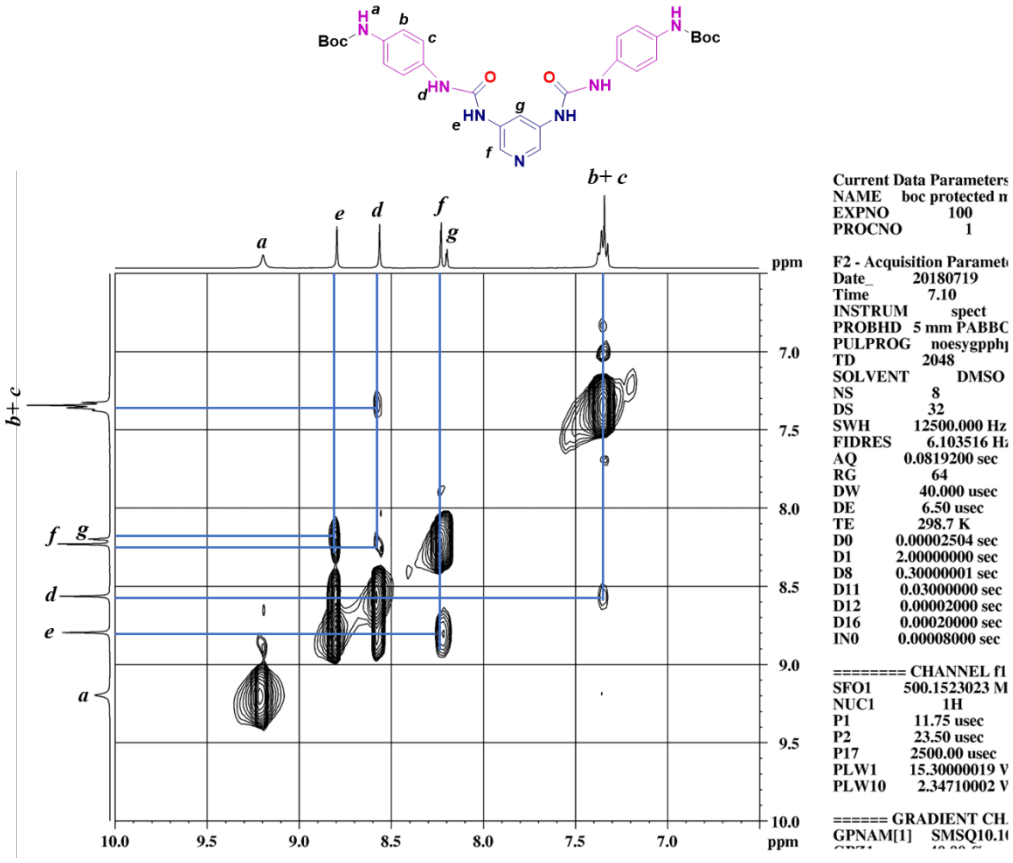

Fig. S39 500 MHz NOESY expansion spectrum of Intermediate **D** in DMSO-d_6.

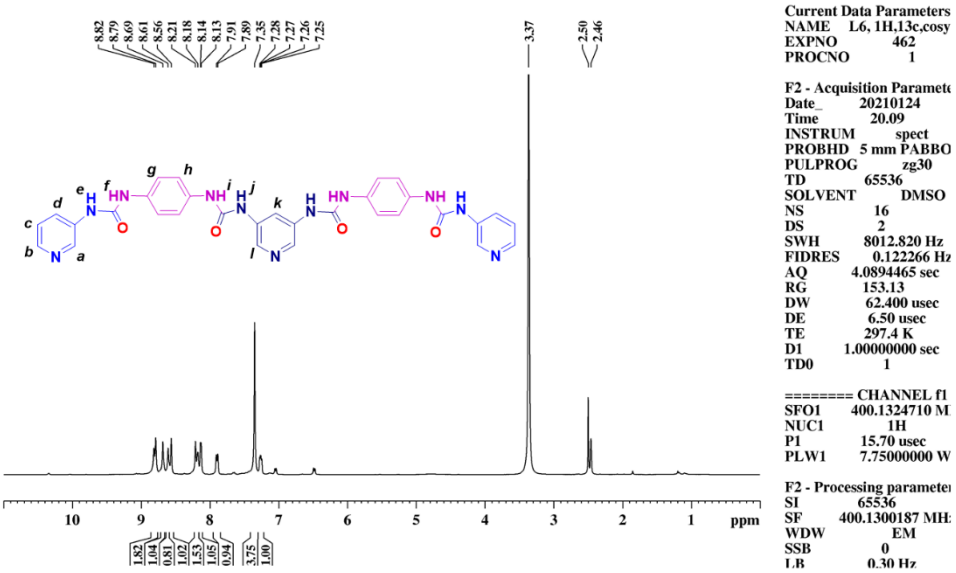

Fig. S40 400 MHz ^{1}H NMR spectrum of ligand **L6** in DMSO-d_6.

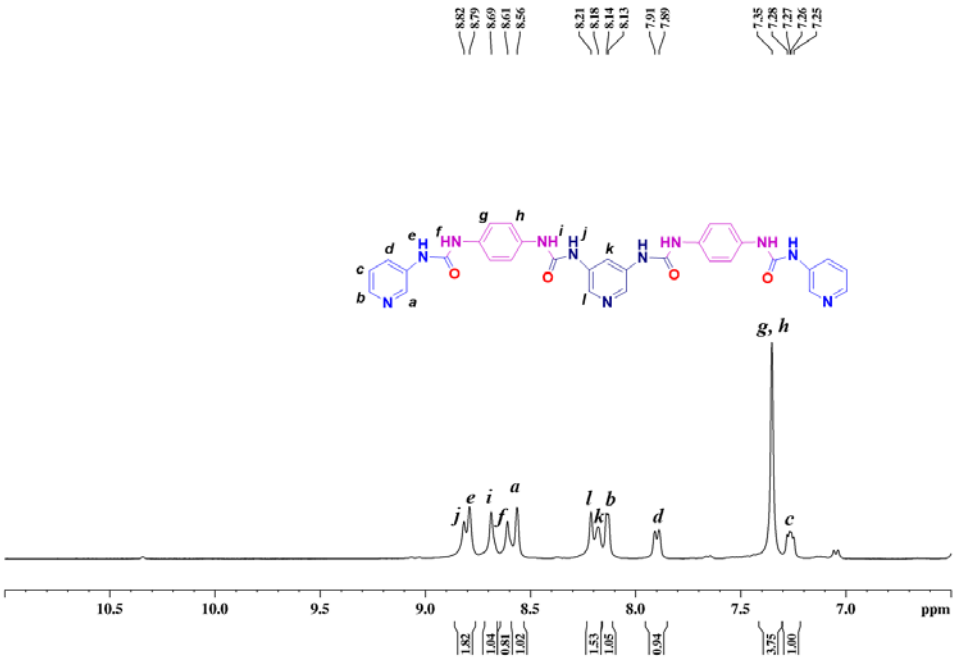

Fig. S41 400 MHz ^{1}H NMR expansion spectrum of ligand **L6** in DMSO-d_6.

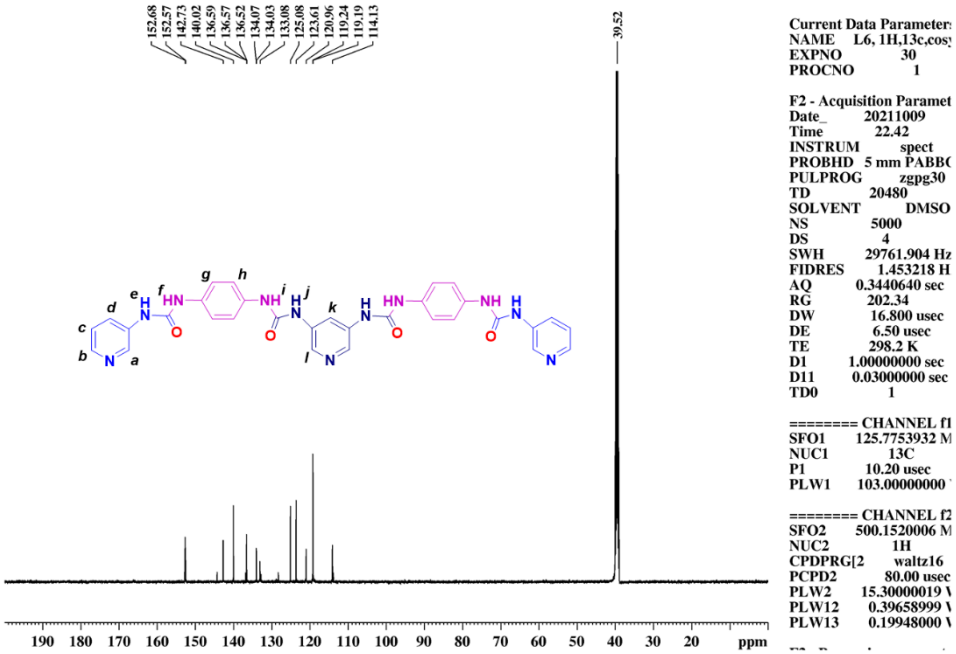

Fig. S42 125 MHz ^{13}C NMR spectrum of ligand **L6** in DMSO-d_6.

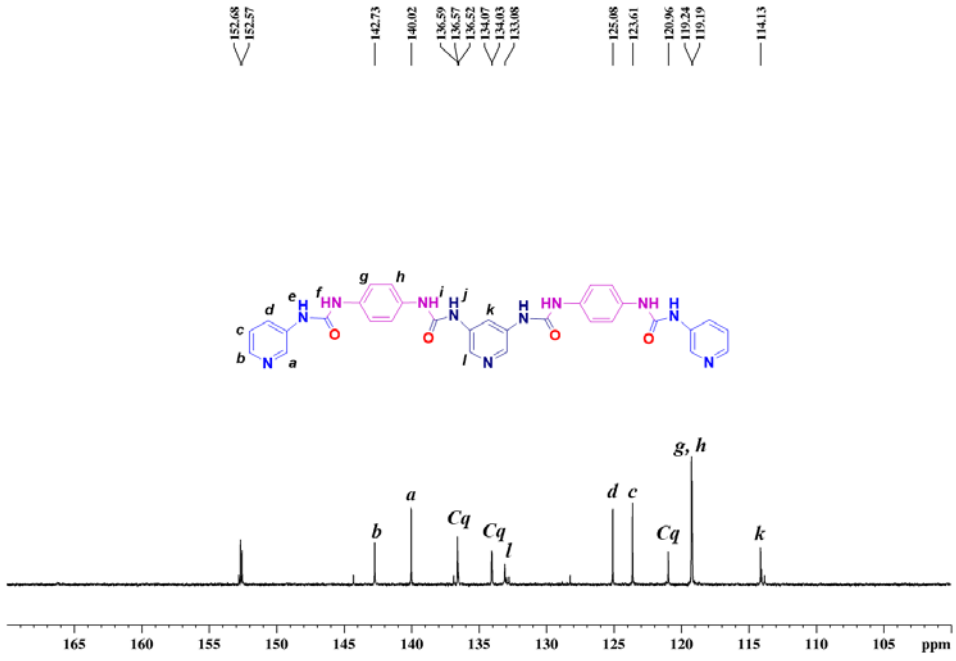

Fig. S43 125 MHz ^{13}C NMR expansion spectrum of ligand **L6** in DMSO-d_6.

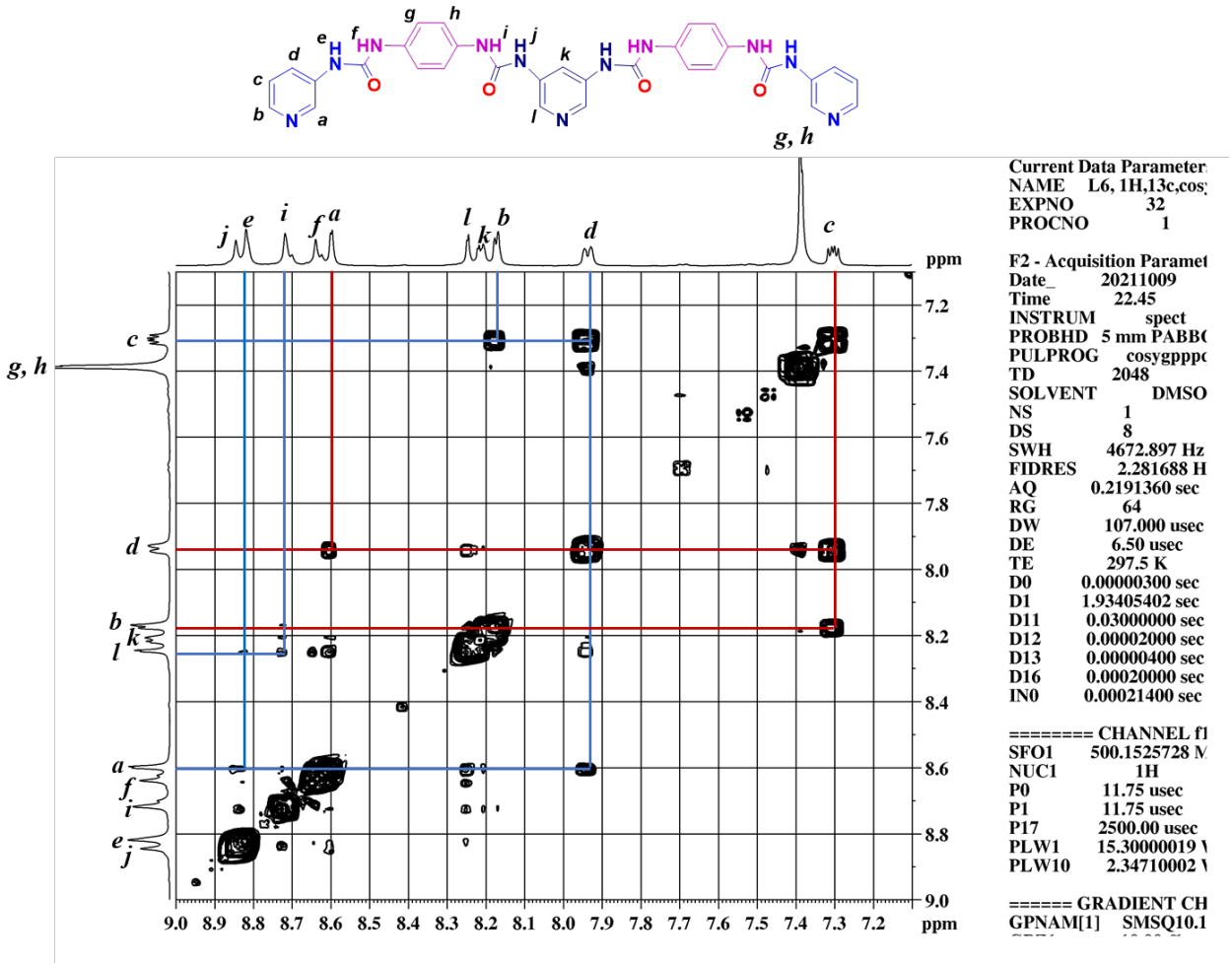

Fig. S44 500 MHz H-H COSY expansion spectrum of ligand **L6** in DMSO-d_6.

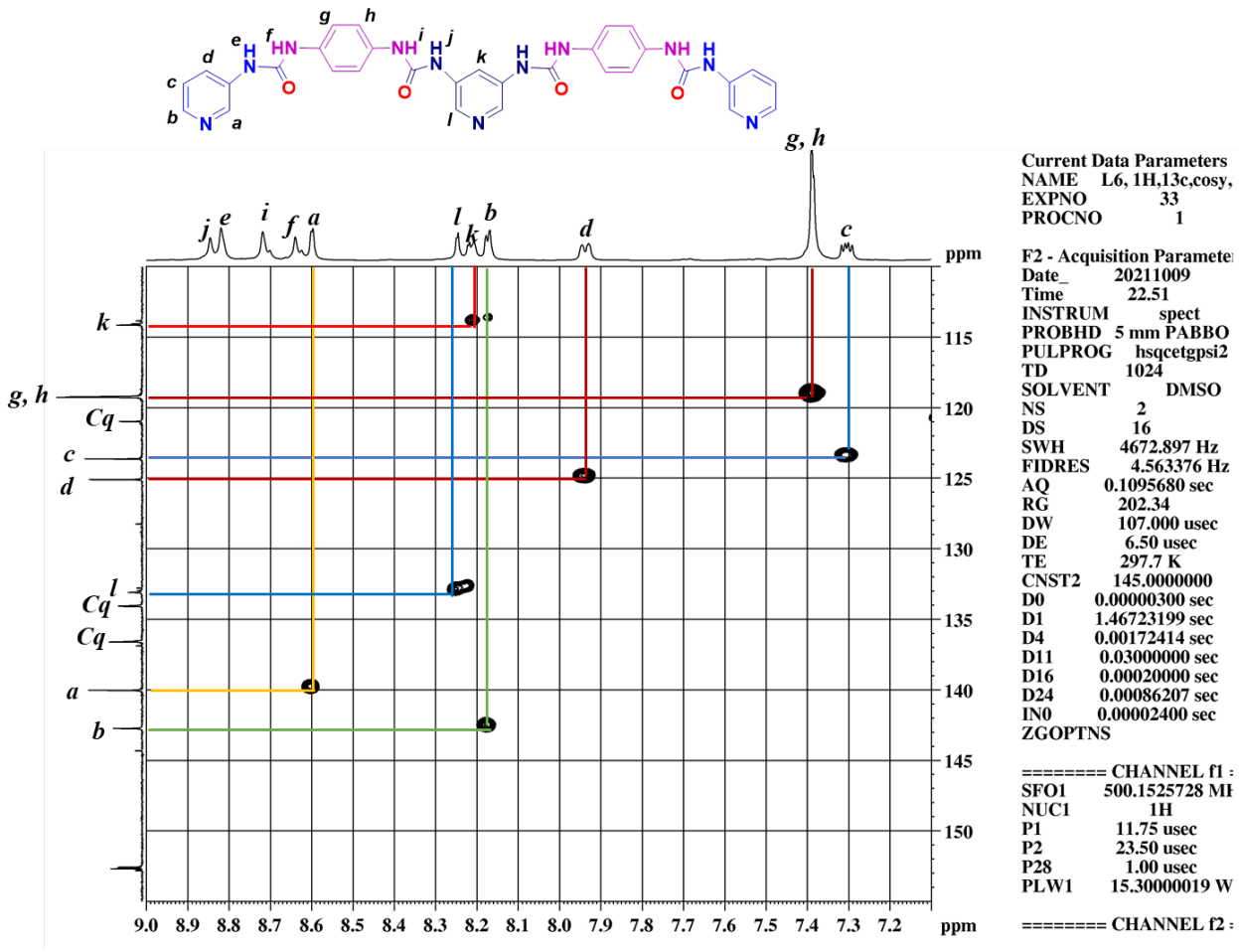

Fig. S45 500 MHz HSQC expansion spectrum of ligand **L6** in DMSO-d_6.

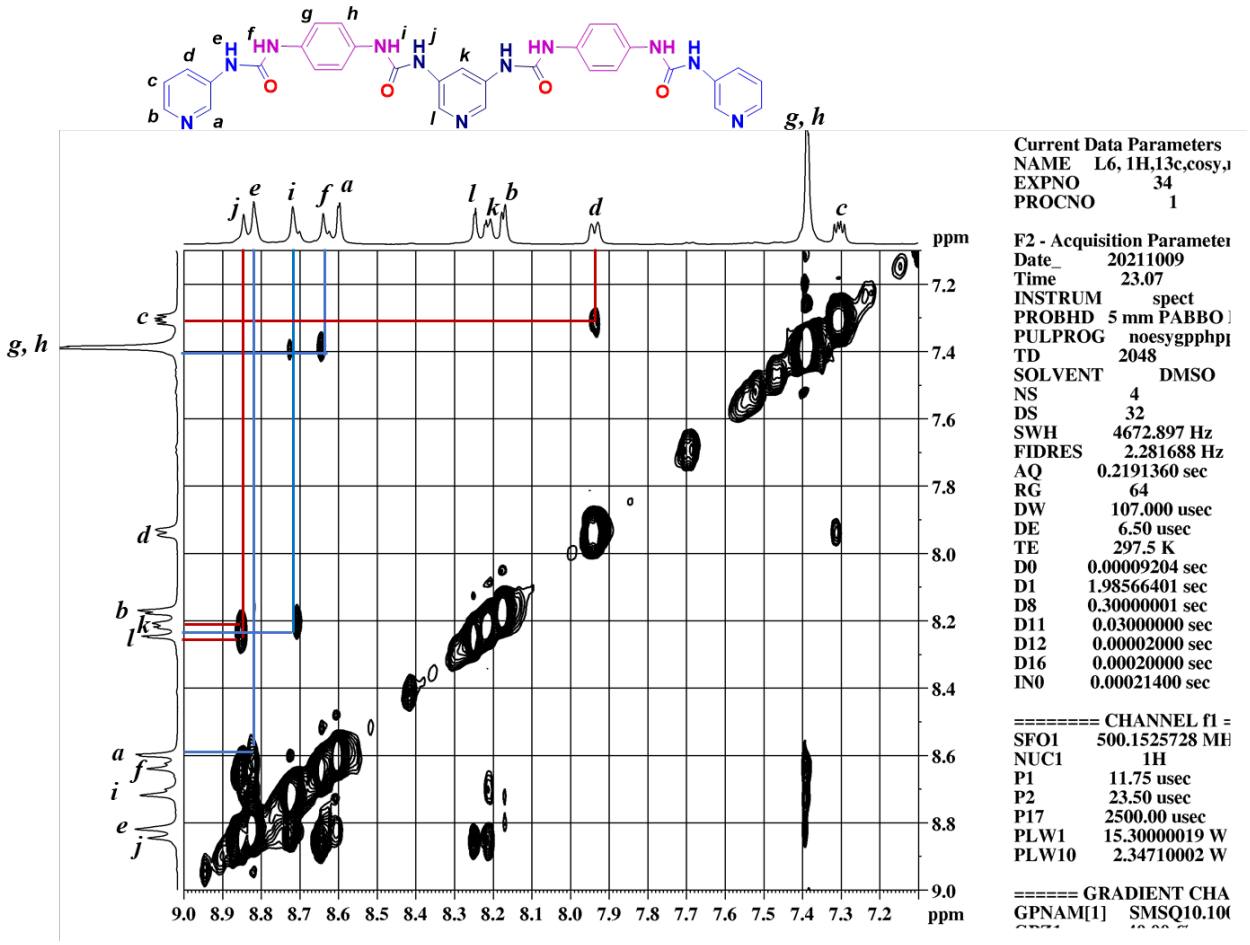

Fig. S46 500 MHz NOESY expansion spectrum of ligand **L6** in DMSO-d_6.

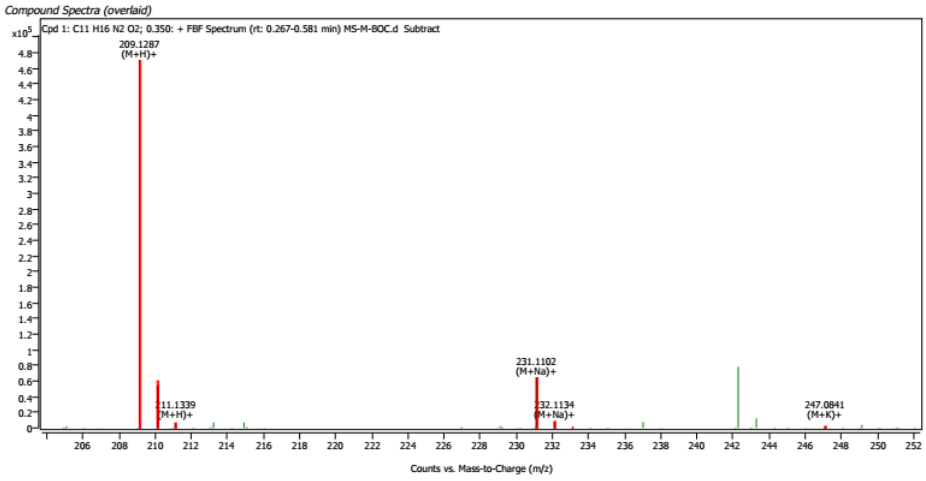

Compound ID Table

Cpd	Formula	Mass (Tgt)	Calc. Mass	Mass	Species	Diff(Tgt.ppm)	mDa
1	C11 H16 N2 O2	208.1212	208.1214	209.1287 231.1102 247.0841	(M+H)+ (M+Na)+ (M+K)+	0.92	0.19

Fig. S47 ESI-HRMS spectrum of *N*-Boc-*m*-phenylenediamine.

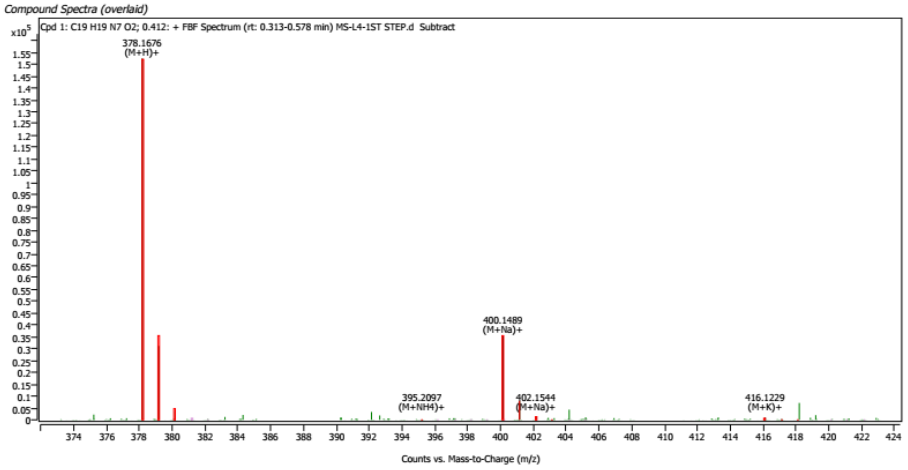

Compound ID Table

Cpd	Formula	Mass (Tgt)	Calc. Mass	Mass	Species	Diff(Tgt.ppm)	mDa
1	C19 H19 N7 O2	377.1600	377.1601	378.1676 395.2097 400.1489 416.1229	(M+H)+ (M+NH4)+ (M+Na)+ (M+K)+	0.31	0.12

Fig. S48 ESI-HRMS spectrum of diamine **A**.

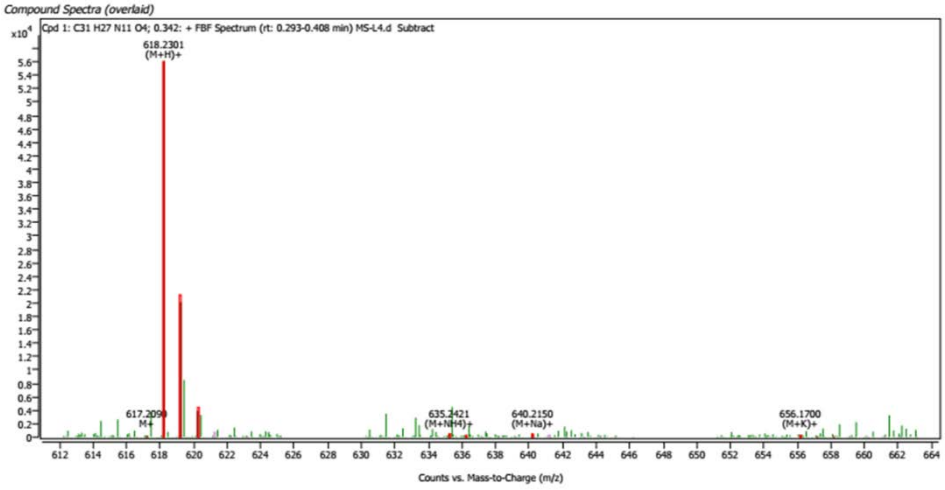

Compound ID Table

Cpd	Formula	Mass (Tgt)	Calc. Mass	Mass	Species	Diff(Tgt.ppm)	mDa
1	C31 H27 N11 O4	617.2247	617.2226	617.2090 618.2301 635.2421 640.2150 656.1700	M+ (M+H)+ (M+NH4)+ (M+Na)+ (M+K)+	-3.56	-2.20

Fig. S49 ESI-HRMS spectrum of ligand **L4**.

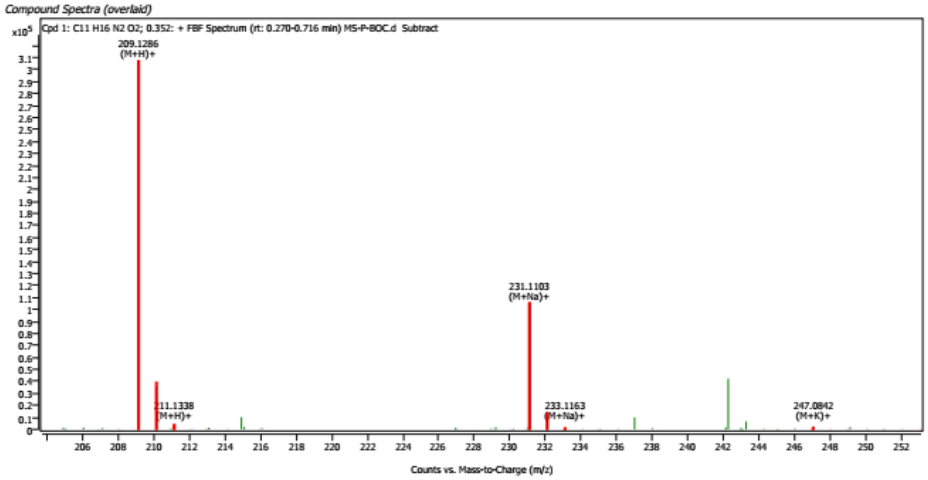

Compound ID Table

Cpd	Formula	Mass (Tgt)	Calc. Mass	Mass	Species	Diff(Tgt.ppm)	mDa
1	C11 H16 N2 O2	208.1212	208.1213	209.1286 231.1103 247.0842	(M+H)+ (M+Na)+ (M+K)+	0.38	0.08

Fig. S50 ESI-HRMS spectrum of *N*-Boc-*p*-phenylenediamine.

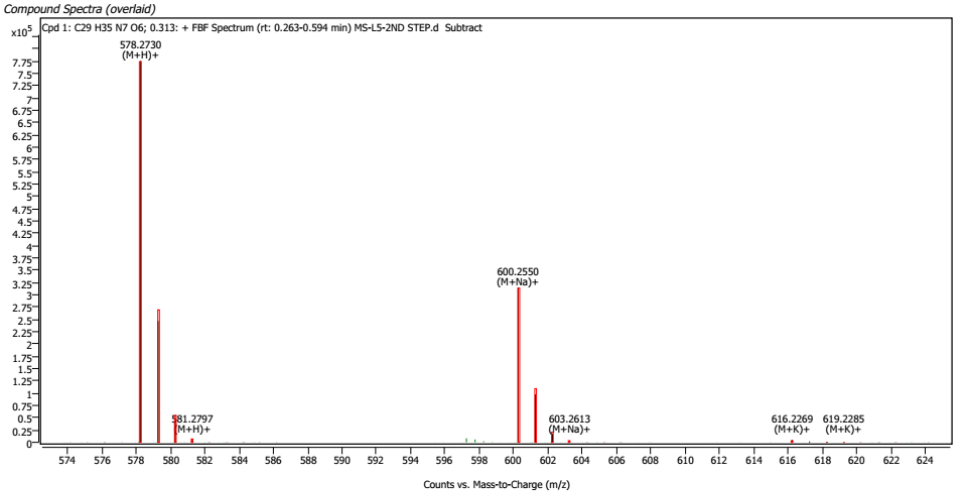

Compound ID Table

Cpd	Formula	Mass (Tgt)	Calc. Mass	Mass	Species	Diff(Tgt.ppm)	mDa
1	C29 H35 N7 O6	577.2649	577.2656	578.2730 600.2550 616.2269	(M+H)+ (M+Na)+ (M+K)+	1.29	0.74

Fig. S51 ESI-HRMS spectrum of intermediate **B**.

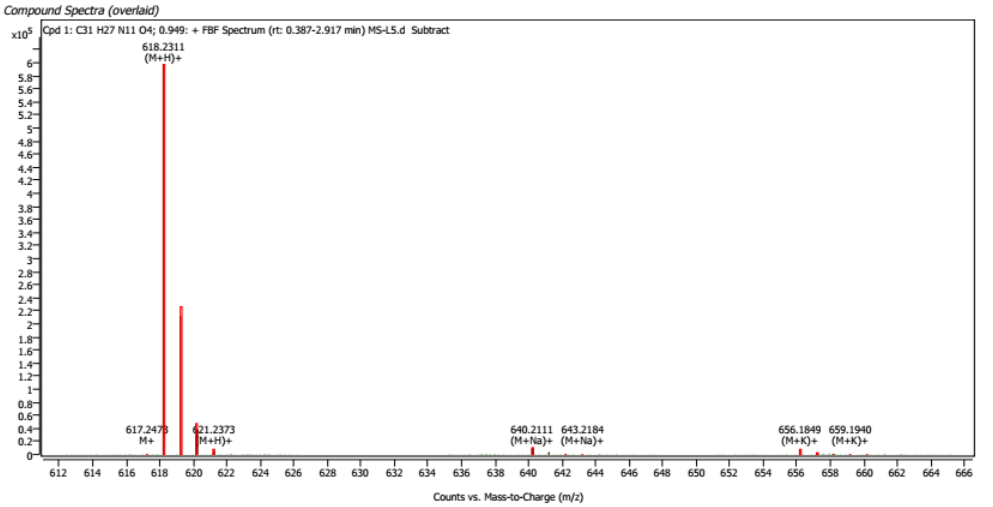

Compound ID Table

Cpd	Formula	Mass (Tgt)	Calc. Mass	Mass	Species	Diff(Tgt.ppm)	mDa
1	C31 H27 N11 O4	617.2247	617.2236	617.2473 618.2311 640.2111 656.1849	M+ (M+H)+ (M+Na)+ (M+K)+	-1.84	-1.14

Fig. S52 ESI-HRMS spectrum of ligand **L5**.

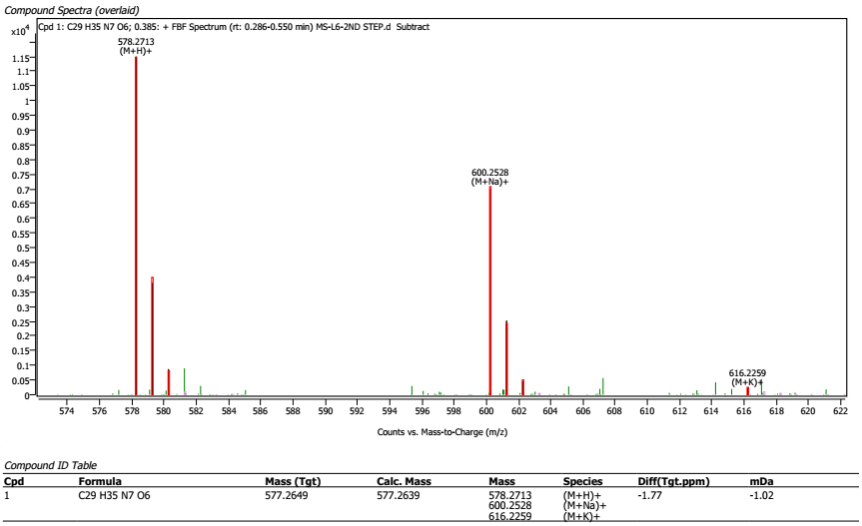

Compound ID Table

Cpd	Formula	Mass (Tgt)	Calc. Mass	Mass	Species	Diff(Tgt.ppm)	mDa
1	C29 H35 N7 O6	577.2649	577.2639	578.2713 600.2528 616.2259	(M+H)+ (M+Na)+ (M+K)+	-1.77	-1.02

Fig. S53 ESI-HRMS spectrum of intermediate **D**.

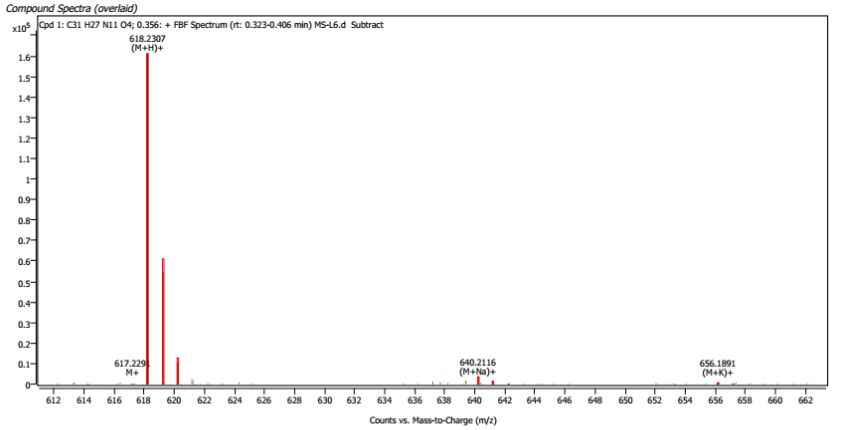

Compound ID Table

Cpd	Formula	Mass (Tgt)	Calc. Mass	Mass	Species	Diff(Tgt.ppm)	mDa
1	C31 H27 N11 O4	617.2247	617.2232	617.2291 618.2307 640.2116 656.1891	M+ (M+H)+ (M+Na)+ (M+K)+	-2.45	-1.51

Fig. S54 ESI-HRMS spectrum of ligand **L6**.

3. Synthesis and characterization of Pd_3L_4 type complexes

Complexation of $Pd(NO_3)_2$ with ligands L4, L5, and L6 in 3:4 metal to ligand ratio

To a solution of commercially available $Pd(NO_3)_2$ (8.07 mg, 0.04 mmol) in DMSO (7 mL), ligand **L4** (28.82 mg, 0.05 mmol) was added and the reaction mixture was stirred at 70 ºC for 16 h to allow the complexation reaction. The desired complexes **4a** and **4a′** were precipitated from the clear solution so obtained using excess ethyl acetate, which were separated by centrifugation method. The isolated solid was washed with ethyl acetate and vacuum dried to afford the cage **4a** and **4a′** as white solid. The cages **5b**, **5b′**, and **6a** were prepared in a similar

manner by the complexation of $Pd(CH_3CN)_4(BF_4)_2$ and $Pd(NO_3)_2$ solution in DMSO with ligands **L5** and **L6**, respectively in separate experiments.

$[Pd_3(L4)_4](NO_3)_6$ (4a and 4a′). Yield: (33.73 mg, 80%). Melting point = 260 °C. ^{1}H NMR (500 MHz, DMSO-d_6) δ = 9.63 (s, 16H, H_l^D and H_l^H), 9.57 (s, 16H, H_e^D and H_e^H), 9.32 (s, 8H, H_a^H), 8.86-8.82 (m, 32H, Ha^D, H_b^H, H_n^H, and H_n^D), 8.70 (s, 8H, H_m^D, and H_m^H), 8.56 (brs, 16H, H_f^H and H_k^H), 8.22-8.17 (m, 40H, H_b^D, H_d^D, H_d^H, H_f^D, and H_k^D), 7.76 (brs, 16H, H_g^H and H_j^H), 7.62-7.52 (m, 32H, H_c^D, H_c^H, H_g^D, and H_j^D), 7.20-7.11 (m, 32H, H_h^D, H_h^H, H_j^D, and H_i^H) *ppm* (D and H denote double decker and hour-glass shaped Pd_3L_4 cages, respectively). ESI-MS: *m/z* calculated for [**4a**-$3NO_3$]$^{3+}$ and [**4a**-$4NO_3$]$^{4+}$ are 991.8602 and 728.3983; observed, 991.8531 and 728.3911.

$[Pd_3(L5)_4](BF_4)_6$ (5b and 5b′). Yield: (33.70 mg, 82%). Melting point = 235 °C. ^{1}H NMR (500 MHz, DMSO-d_6) δ = 9.73 (s, 8H, H_a^H), 9.62 (s, 8H, H_a^D), 9.32 (s, 8H, H_n^D), 9.13 (d, *J* = 4.87 Hz, 8H, H_b^H), 9.01 (brs, 16H, H_e^D and H_e^H), 8.94-8.91 (m, 24H, H_f^D, and H_b^D), 8.87 (s, 8H, H_n^H), 8.85 (s, 8H, H_l^H), 8.80 (s, 8H, H_l^D), 8.74 (brs, 8H, H_m^D and H_m^H), 8.61 (s, 8H, H_k^H), 8.58 (s, 8H, H_k^D), 8.09-7.07 (m, 16H, H_d^H and H_d^D), 7.68 (s, 8H, H_g^D), 7.61-7.58 (m, 16H, H_c^H and H_c^H), 7.52-7.50 (m, 16H, H_g^H and H_j^D), 7.23-7.12 (m, 40H, H_h^D, H_h^H, H_j^D, H_i^H and H_j^H) *ppm* (D and H denote double decker and hour-glass shaped Pd_3L_4 cages, respectively). ESI-MS: *m/z* calculated for [**5b**-$6BF_4$]$^{6+}$, [**5b**-$5BF_4$]$^{5+}$, and [**5b**-$4BF_4$]$^{4+}$are 464.9350, 575.3244, and 740.6561; observed, 464.9367, 575.3249, and 740.6561.

$[Pd_3(L6)_4](NO_3)_6$ (6a). Yield: (34.94 mg, 85%). Melting point = 275 °C. ^{1}H NMR (500 MHz, DMSO-d_6) δ = 10.18 (s, 8H, H_a^D), 9.87 (s, 8H, H_l^D), 9.21-9.12 (m, 16H, H_j^D and H_e^D), 9.06 (d, J= 5.22 Hz, 8H, H_b^D), 8.97-8.92 (m, 20H, H_f^D, H_k^D and H_i^D), 7.59-7.44 (m, 48H, H_c^D, H_d^D, H_g^D and H_h^D) *ppm* (D denotes double decker Pd_3L_4 cage). ESI-MS: *m/z* calculated for [**6a**-$6NO_3$]$^{6+}$ and [**6a**-$5NO_3$]$^{5+}$ are 464.9367 and 570.3212; observed, 464.9326 and 570.3165.

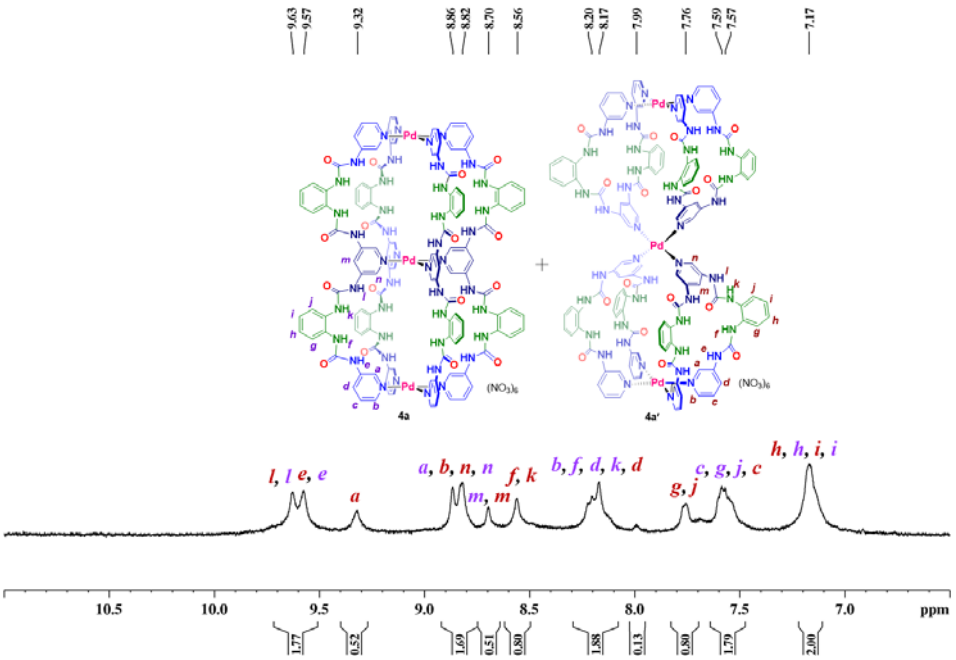

Fig. S55 400 MHz ^{1}H NMR spectrum of cages **4a** and **4a′** in DMSO-d_6

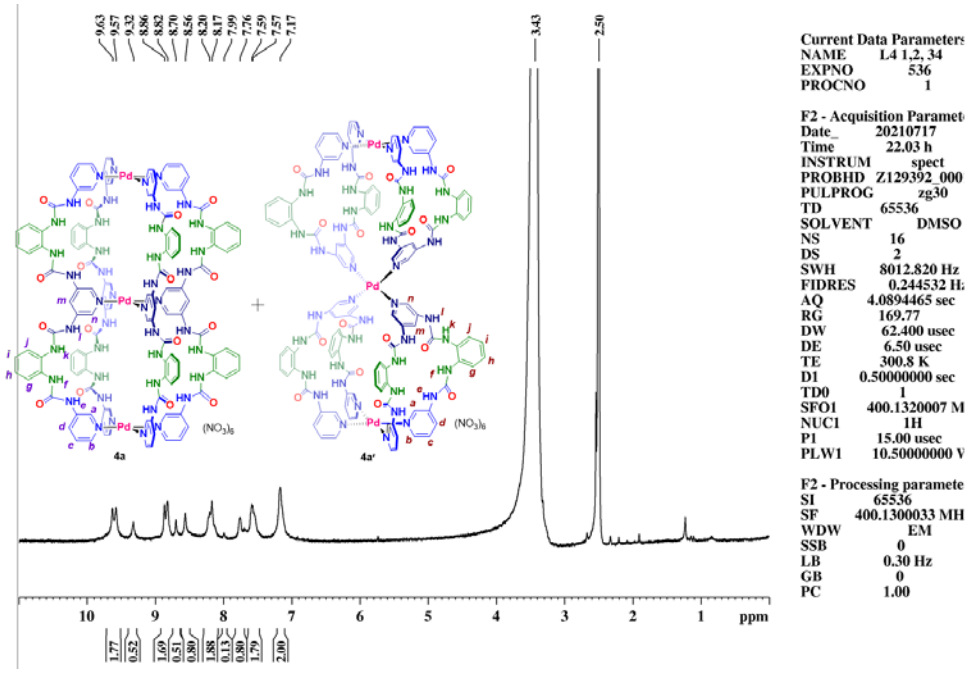

Fig. S56 400 MHz ^{1}H NMR expansion spectrum of cages **4a** and **4a′** in DMSO-d_6. (Colours: dark red = hour-glass shaped and purple = double-decker type Pd_3L_4 cages)

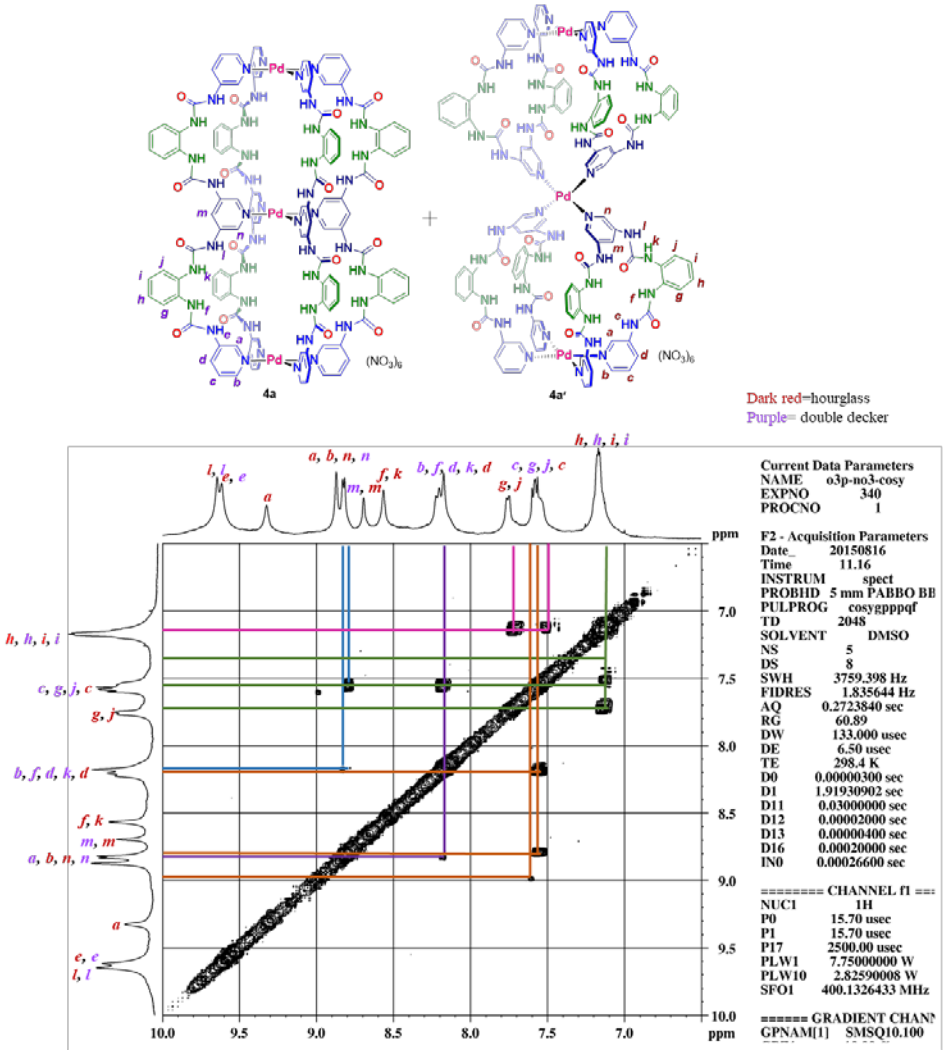

Fig. S57 500 MHz H-H COSY expansion spectrum of cages **4a** and **4a′** in DMSO-d_6.

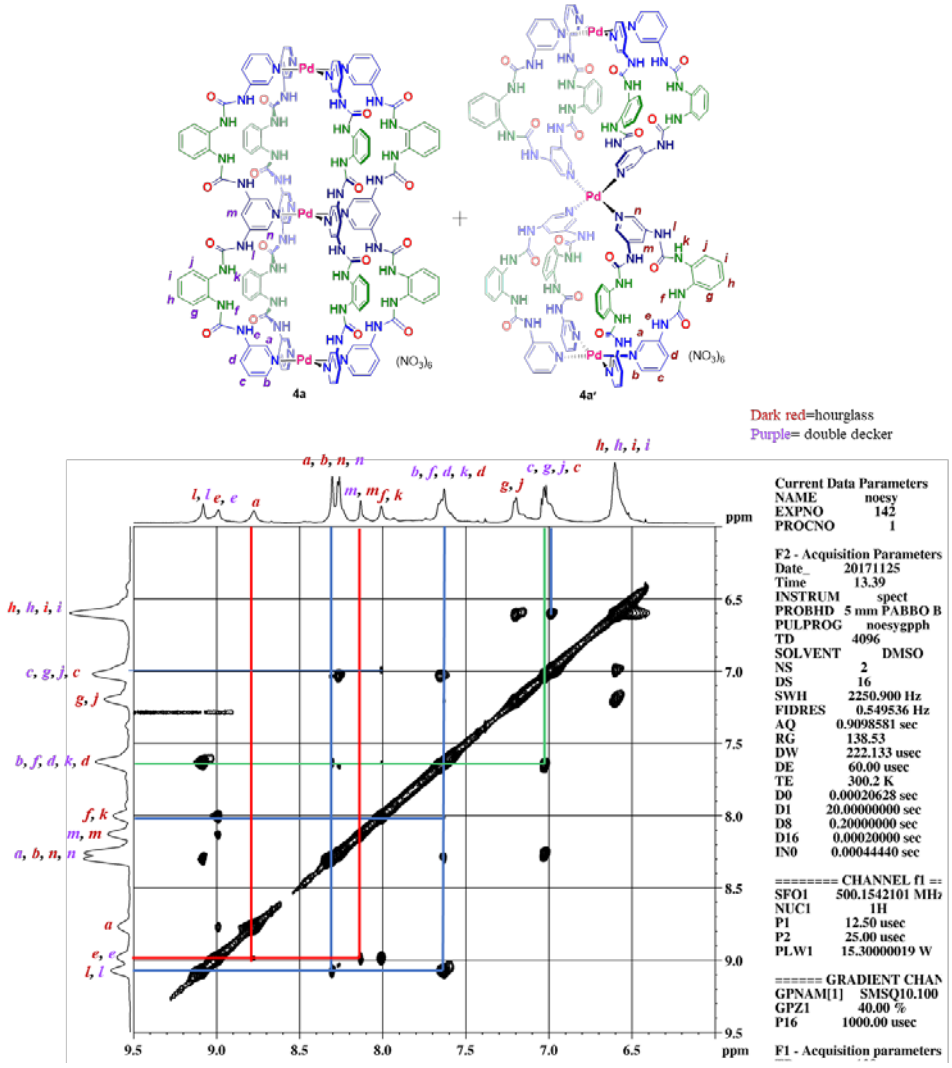

Fig. S58 500 MHz NOESY expansion spectrum of cages **4a** and **4a′** in DMSO-d_6.

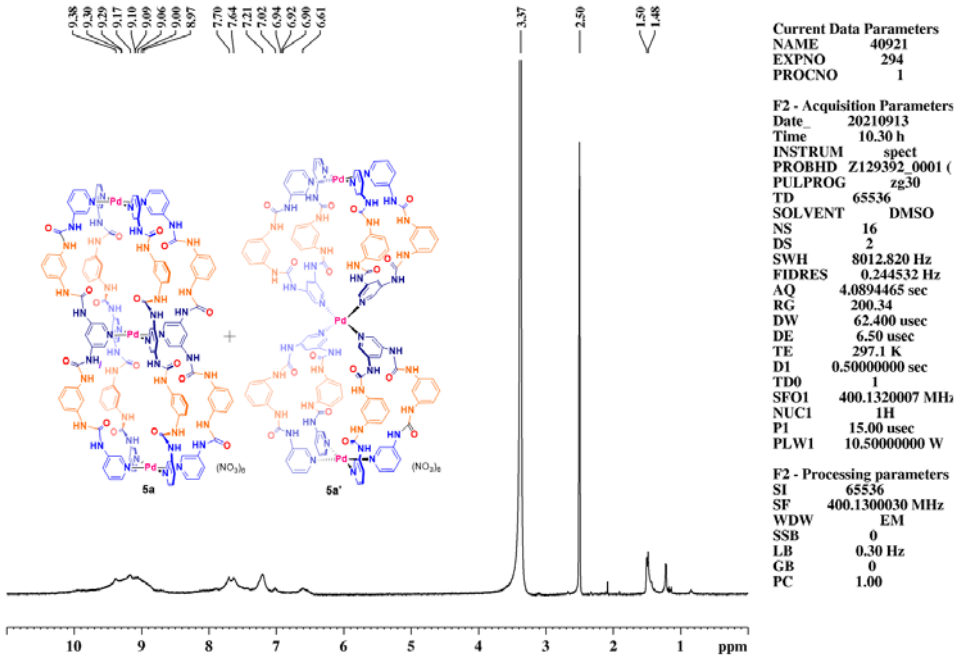

Fig. S59 400 MHz ^{1}H NMR spectrum of cages **5a** and **5a′** in DMSO-d_6, recorded at rt.

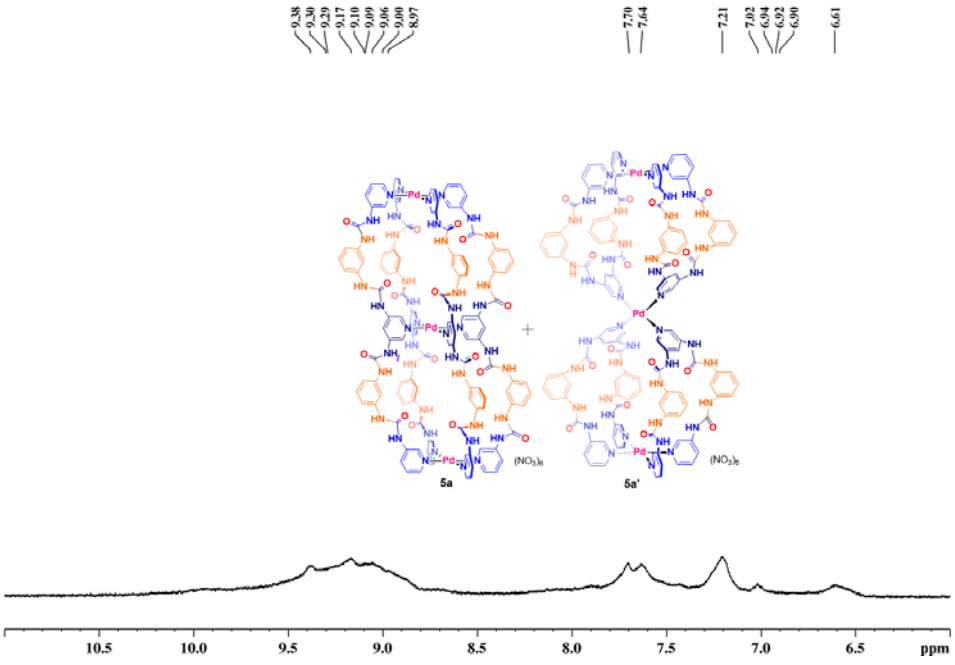

Fig. S60 400 MHz ^{1}H NMR expansion spectrum of cages **5a** and **5a′** in DMSO-d_6, recorded at rt.

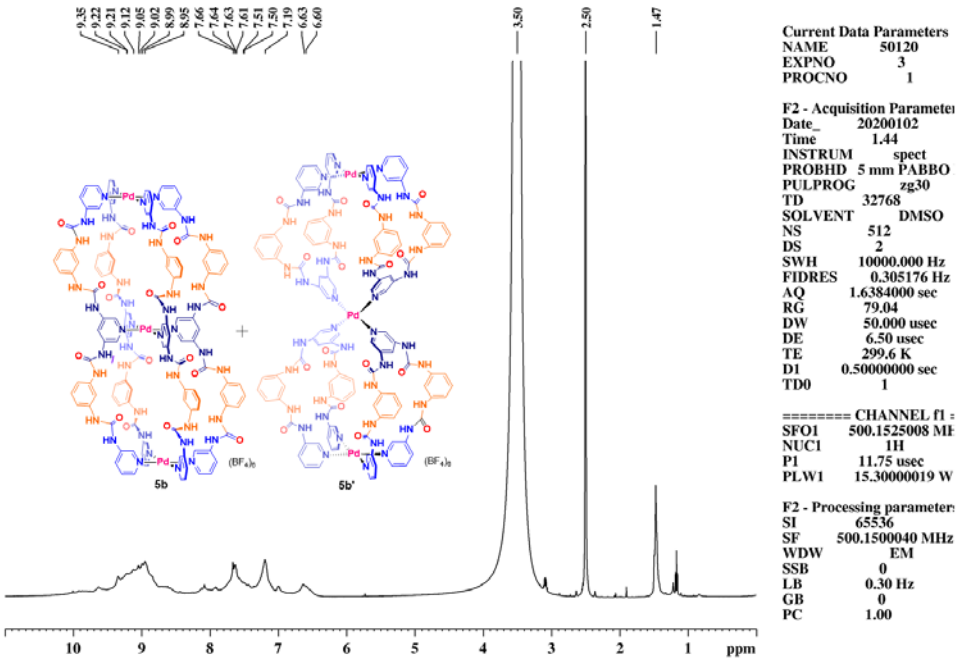

Fig. S61 500 MHz ^{1}H NMR spectrum of cages **5b** and **5b′** in DMSO-d_6, recorded at rt.

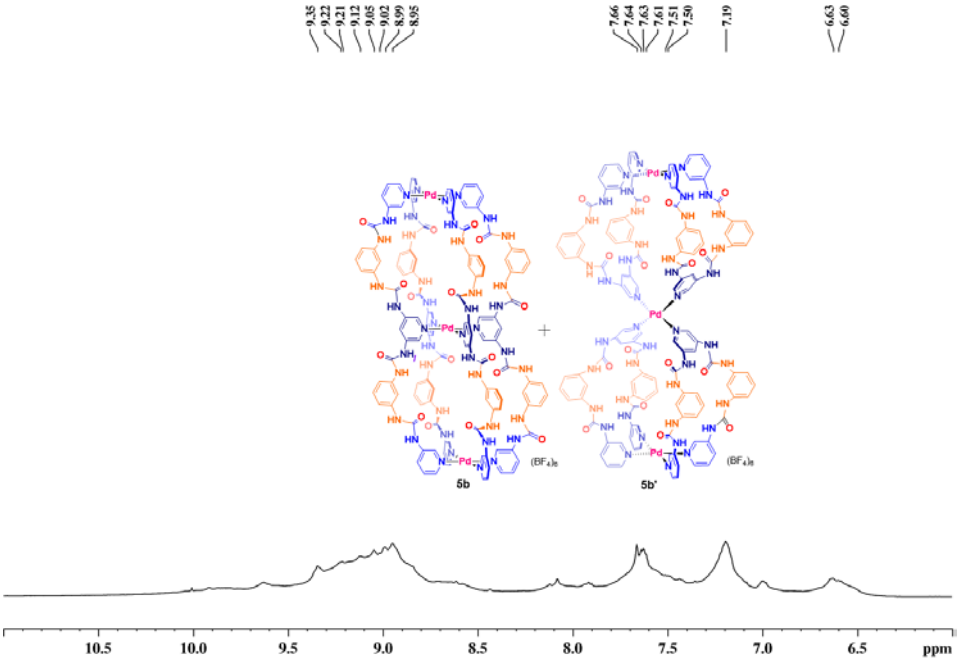

Fig. S62 500 MHz ^{1}H NMR expansion spectrum of cages **5b** and **5b′** in DMSO-d_6, recorded at rt.

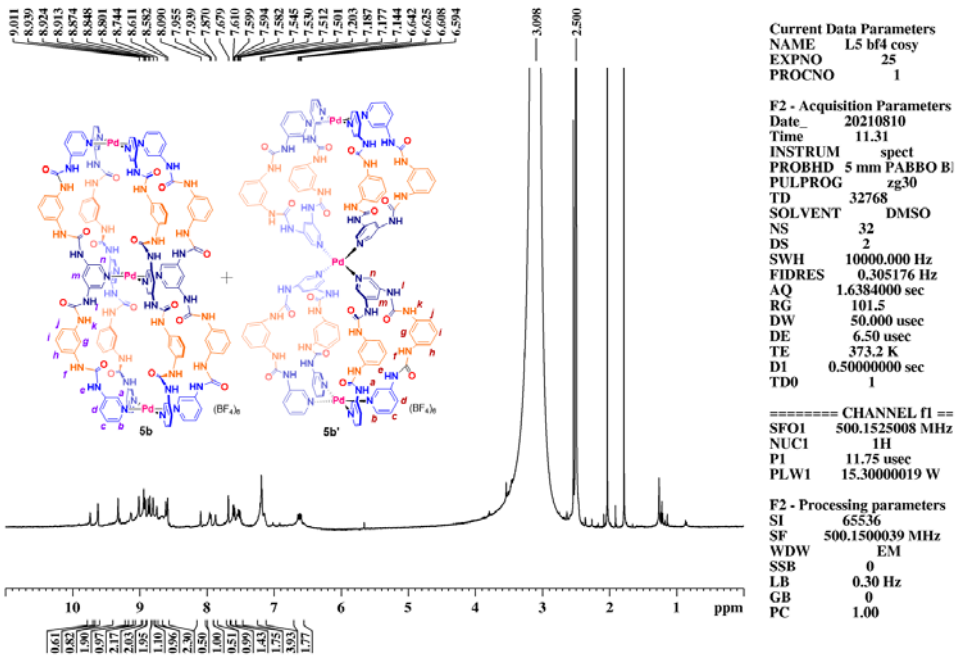

Fig. S63 500 MHz ^{1}H NMR spectrum of cages **5b** and **5b′** in DMSO-d_6, recorded at 100°C.

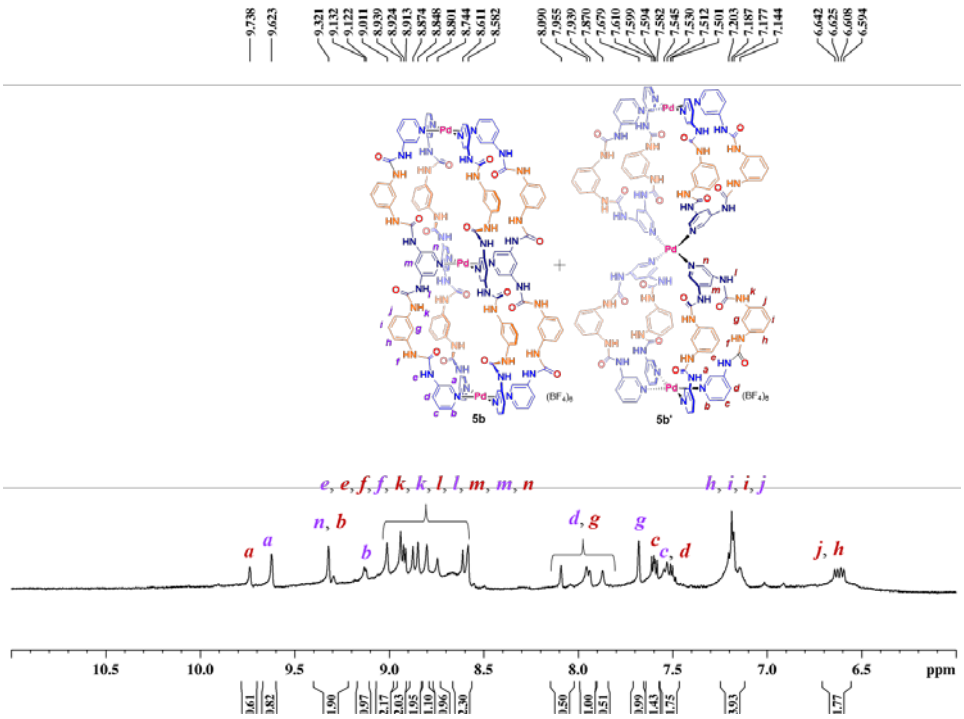

Fig. S64 500 MHz ^{1}H NMR expansion spectrum of cages **5b** and **5b′** in DMSO-d_6, recorded at 100 °C. (Colours: dark red = hour-glass shaped and purple = double-decker type Pd_3L_4 cages)

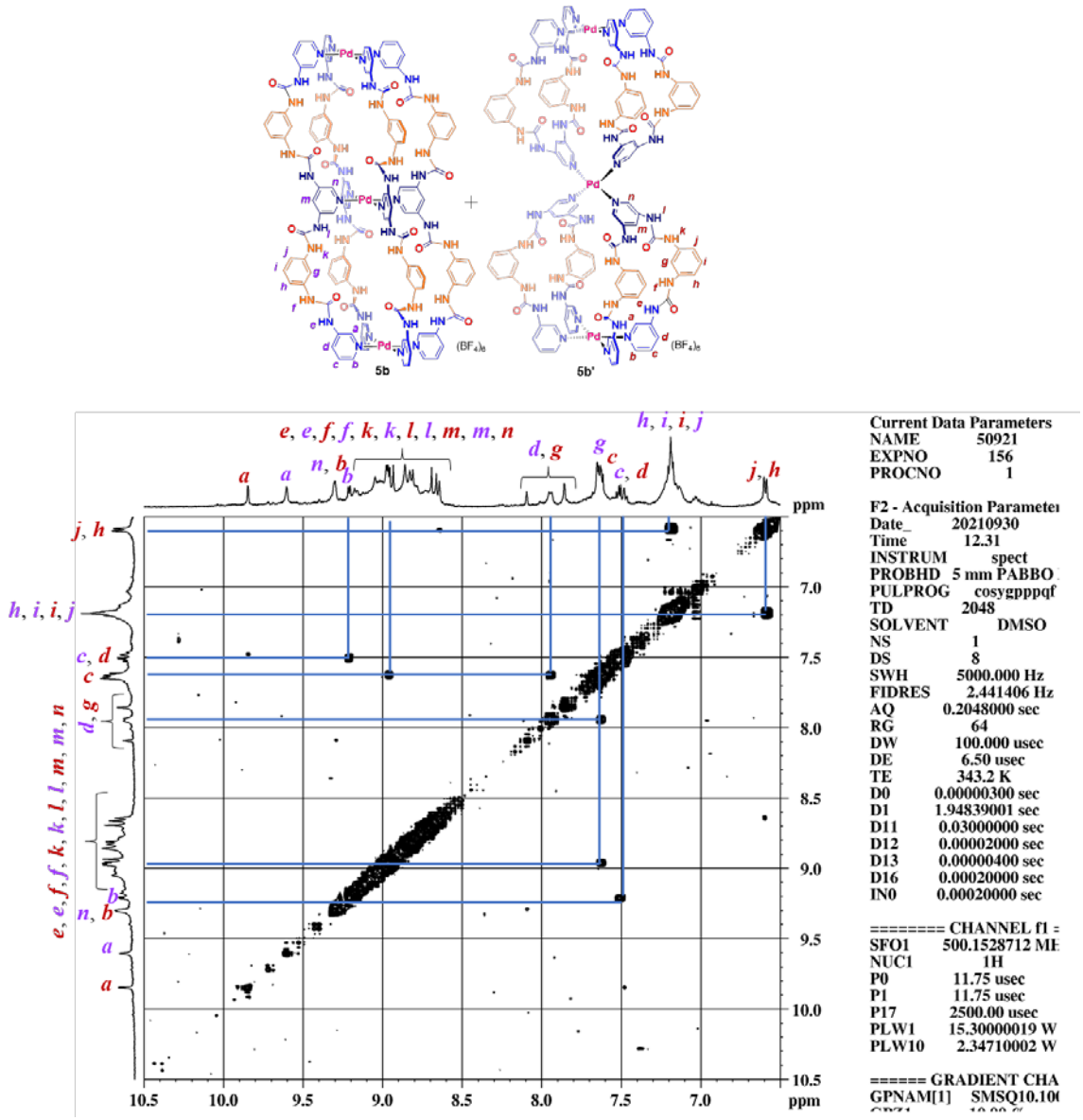

Fig. S65 500 MHz H-H COSY expansion spectrum of cages **5b** and **5b′** in DMSO-d_6, recorded at 70 °C.

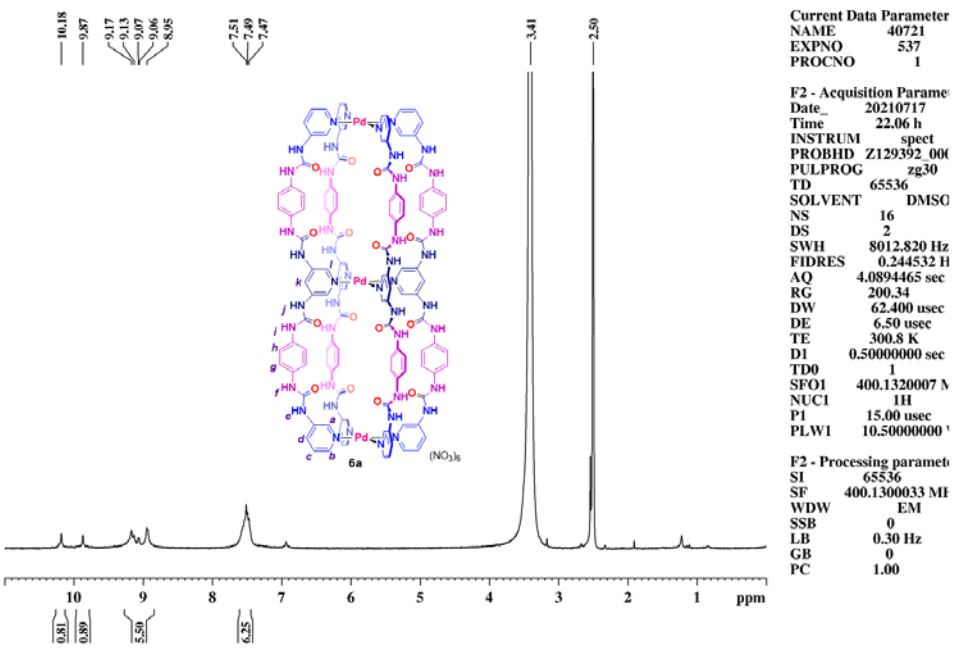

Fig. S66 400 MHz ^{1}H NMR spectrum of cage **6a** in DMSO-d_6.

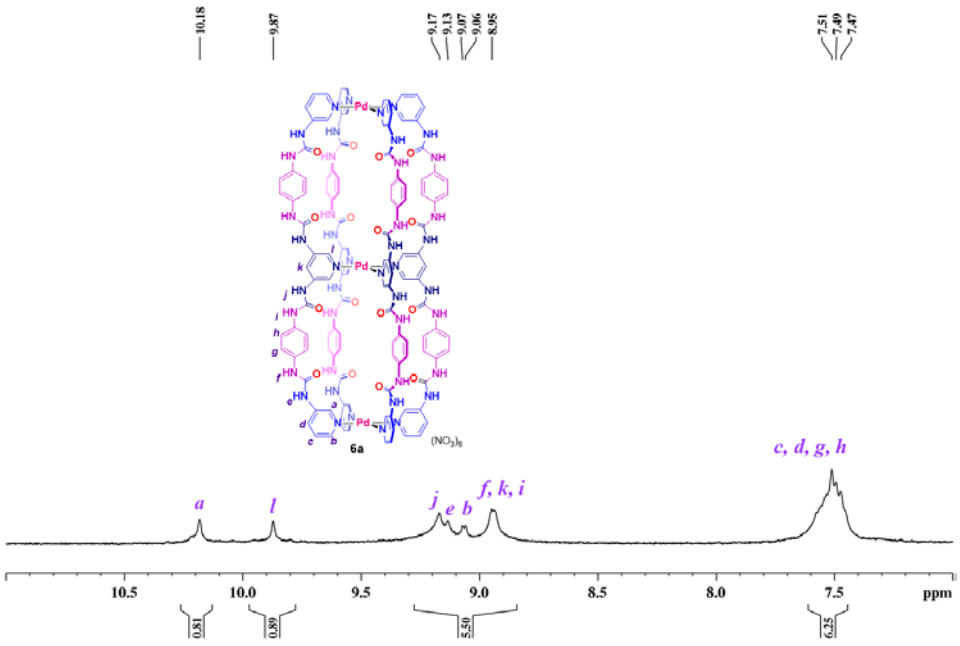

Fig. S67 400 MHz ^{1}H NMR expansion spectrum of cage **6a** in DMSO-d_6.

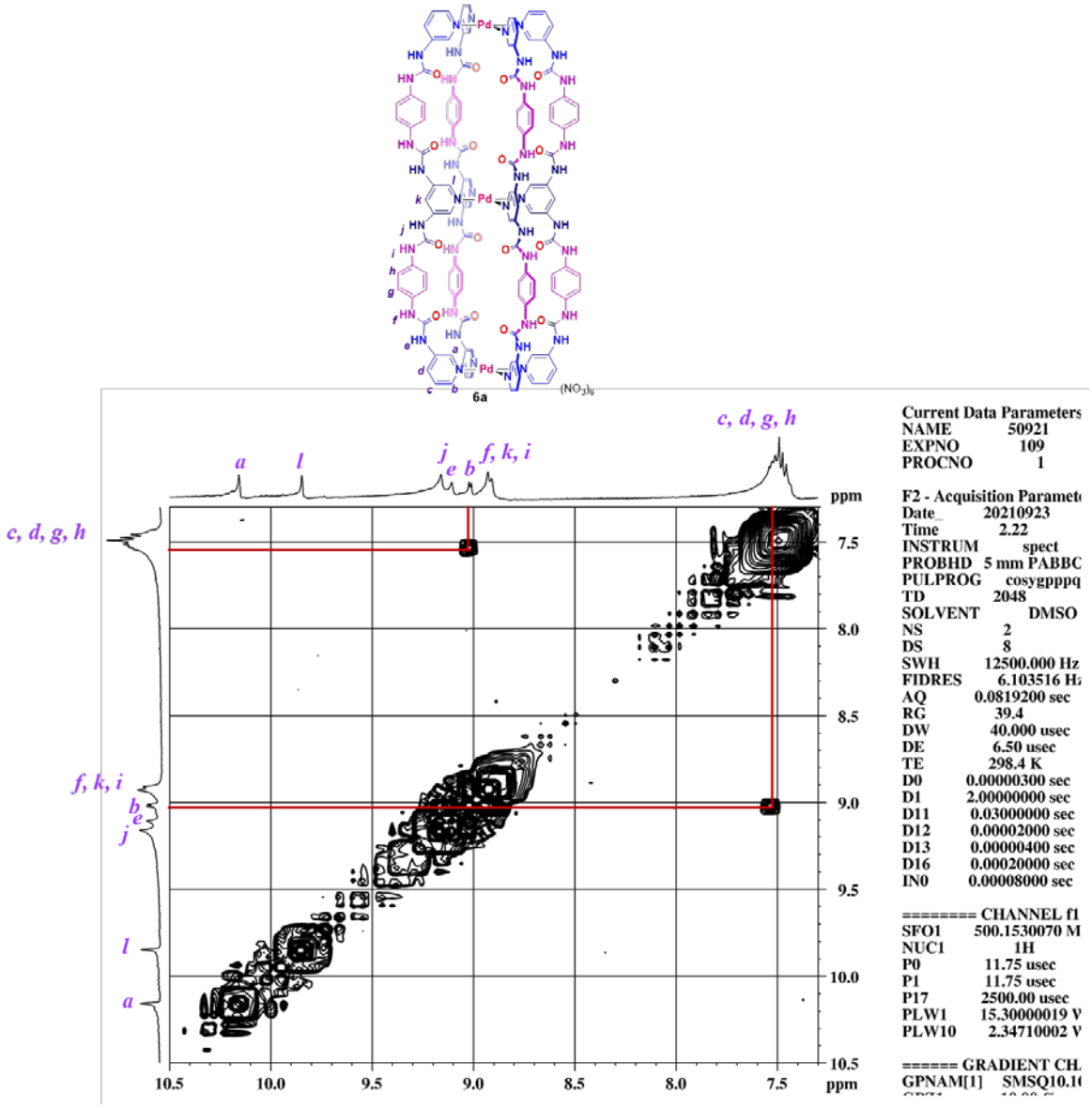

Fig. S68 500 MHz H-H COSY expansion spectrum of cage **6a** in DMSO-d_6.

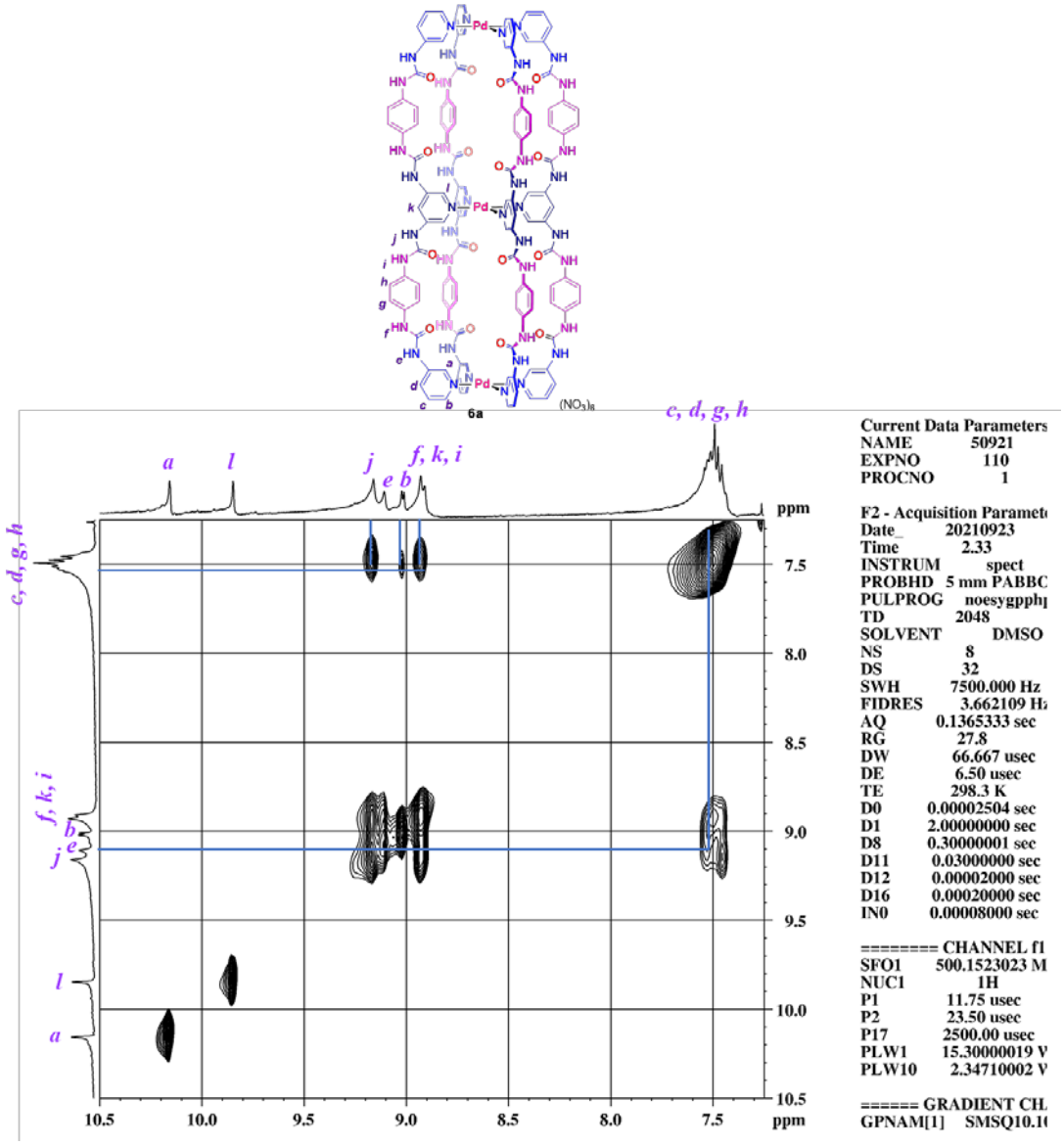

Fig. S69 500 MHz NOESY expansion spectrum of cage **6a** in DMSO-d_6.

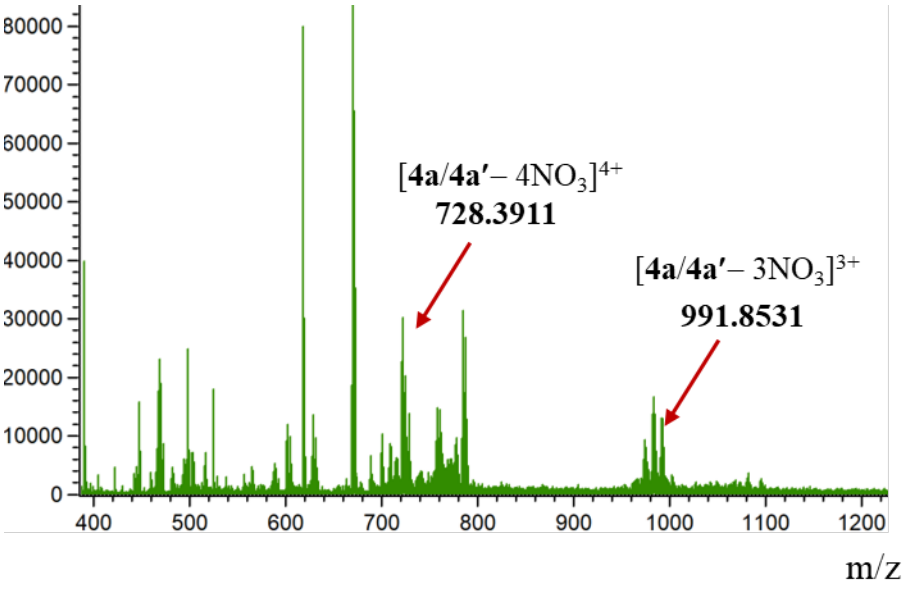

Fig. S70 ESI-MS spectrum of trinuclear cages $[Pd_3(\mathbf{L4})_4](NO_3)_6$, **4a** and **4a′**.

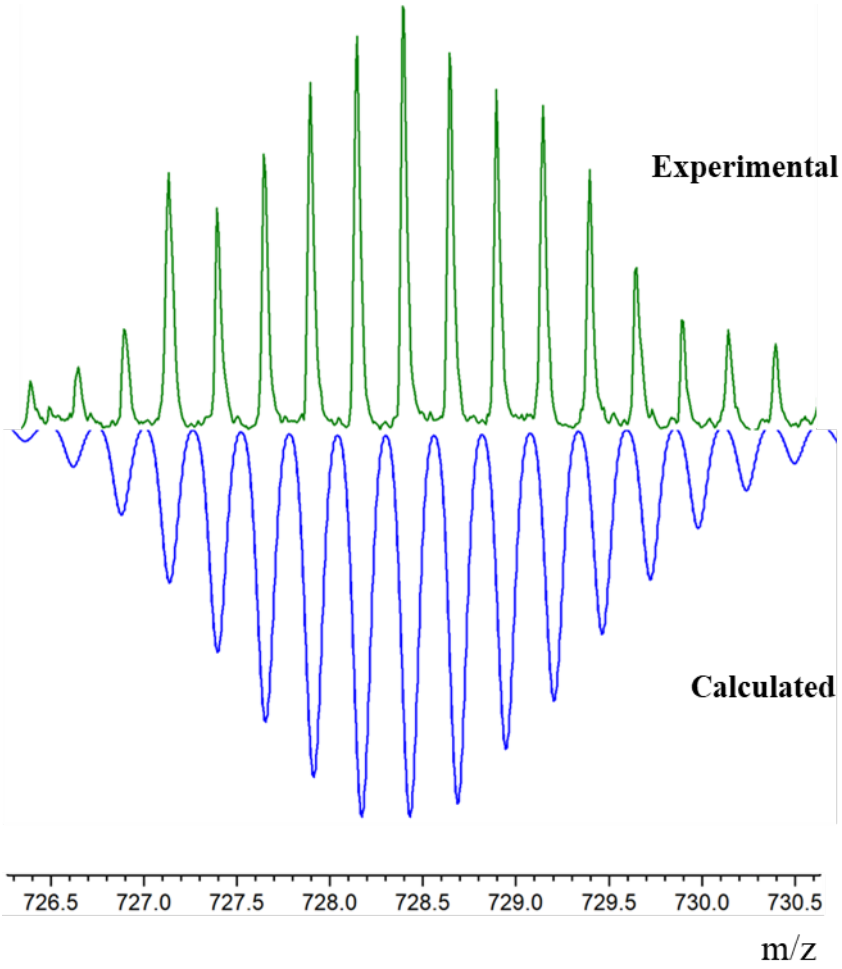

Fig. S71 Isotopic pattern of the trinuclear cage [**4a**/**4a′**-4NO_3]$^{4+}$ (top) and calculated pattern (bottom).

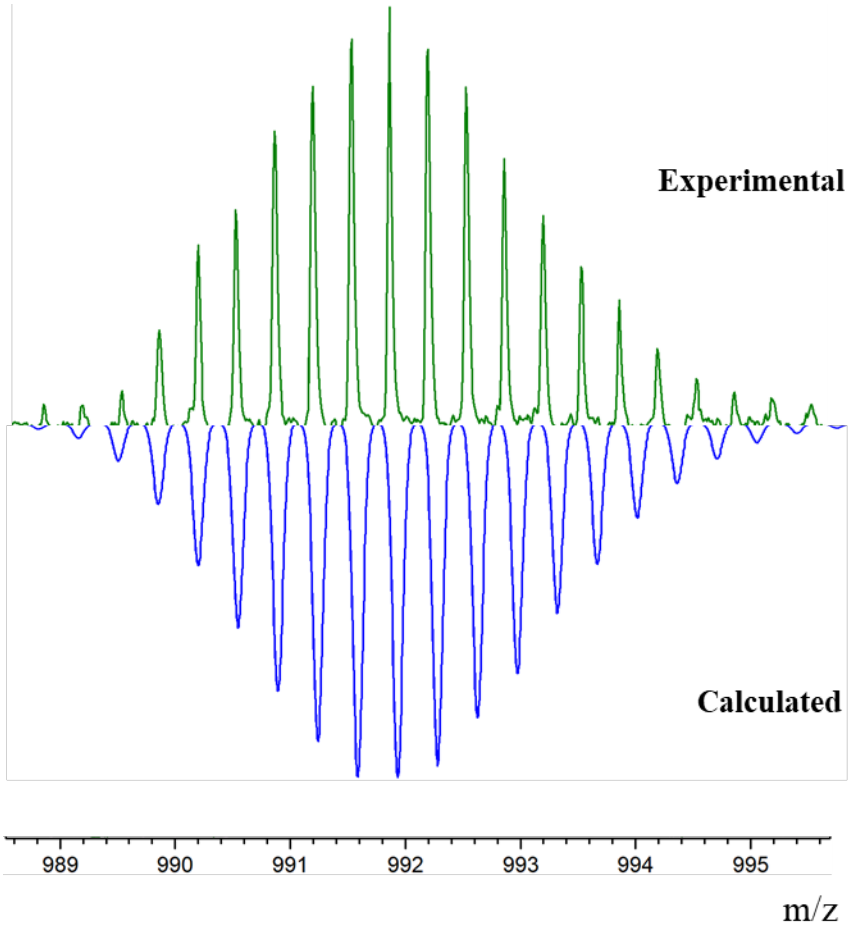

Fig. S72 Isotopic pattern of the trinuclear cage [**4a**/**4a′**-3NO_3]$^{3+}$ (top) and calculated pattern (bottom).

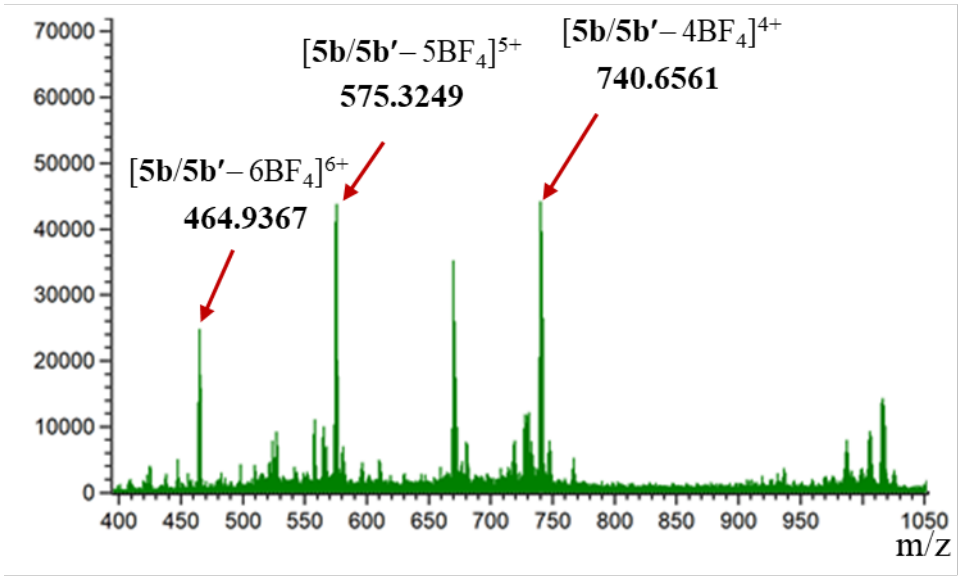

Fig. S73 ESI-MS spectrum of trinuclear cages [Pd_3(**L5**)$_4$](BF_4)$_6$, **5b** and **5b′**.

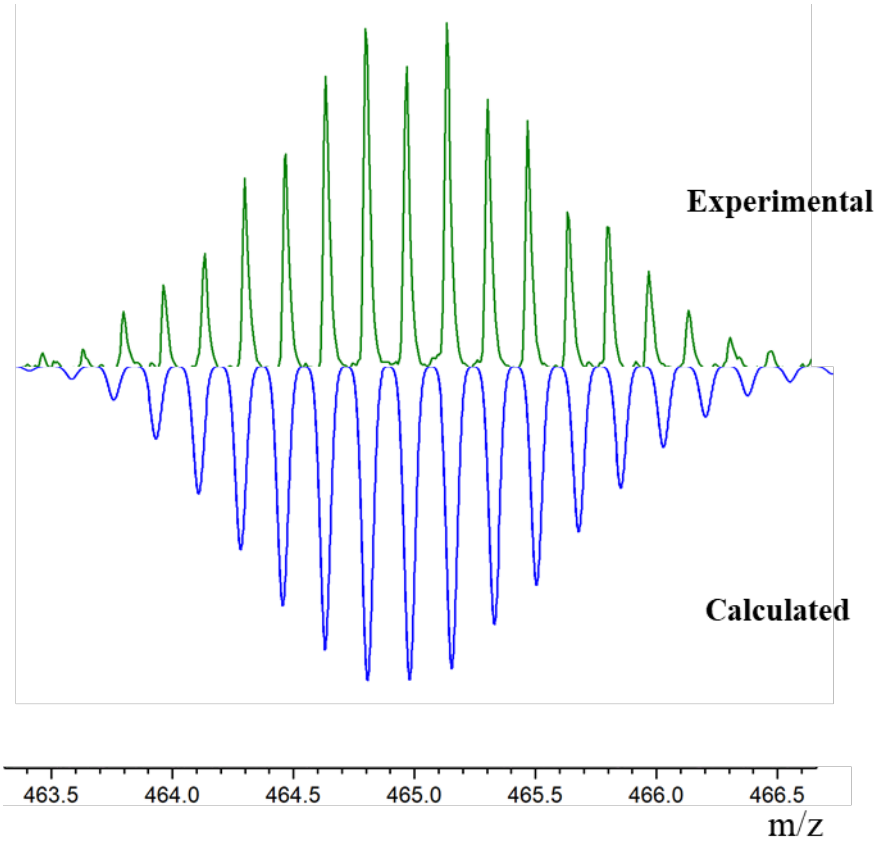

Fig. S74 Isotopic pattern of the trinuclear cage [**5b**/**5b′**-6BF_4]$^{6+}$ (top) and calculated pattern (bottom).

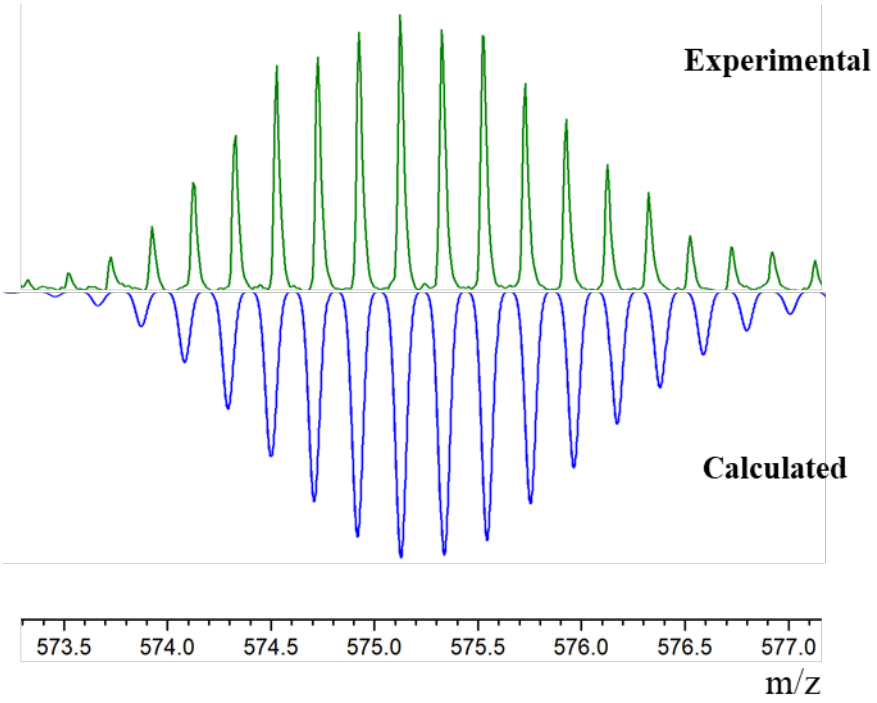

Fig. S75 Isotopic pattern of the trinuclear cage [**5b**/**5b′**-5BF_4]$^{5+}$ (top) and calculated pattern (bottom).

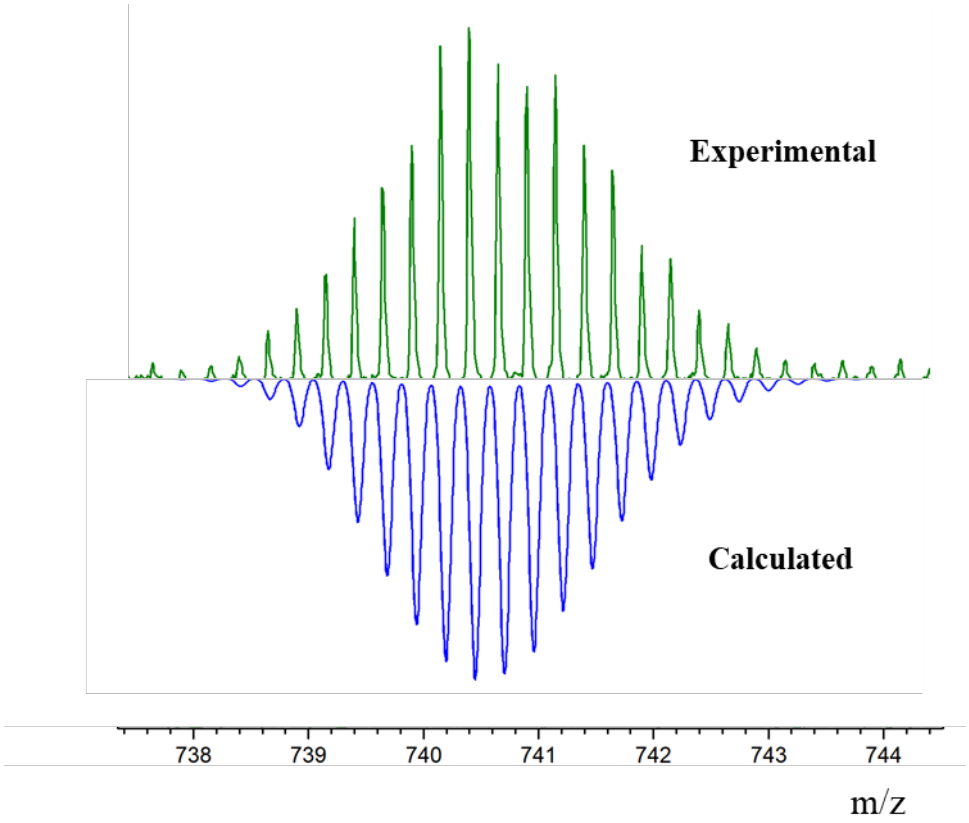

Fig. S76 Isotopic pattern of the trinuclear cage [**5b**/**5b′**-4BF_4]$^{4+}$ (top) and calculated pattern (bottom).

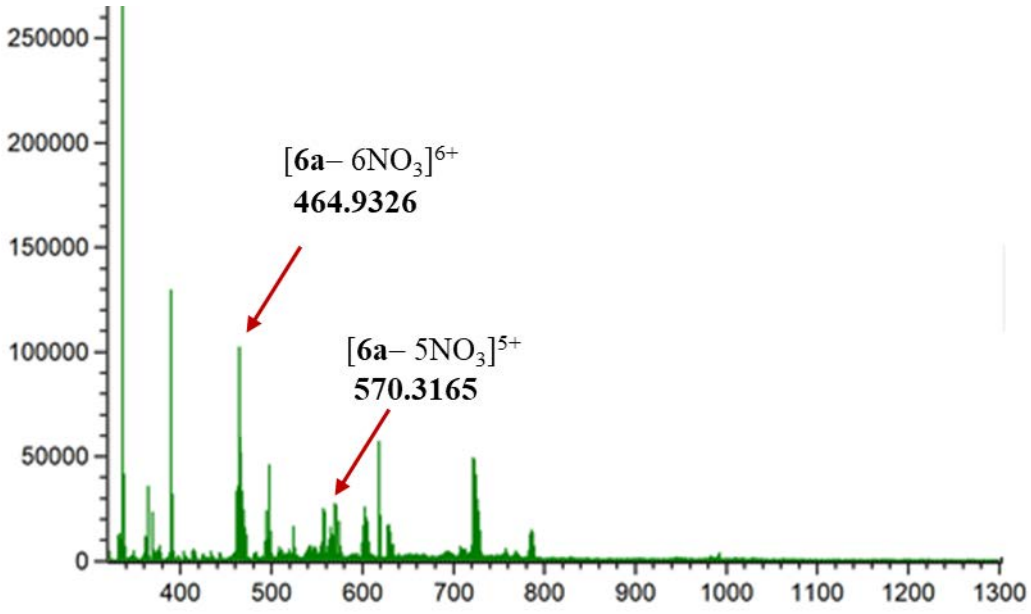

Fig. S77 ESI-MS spectrum of trinuclear cage [Pd_3(**L6**)$_4$](NO_3)$_6$, **6a**.

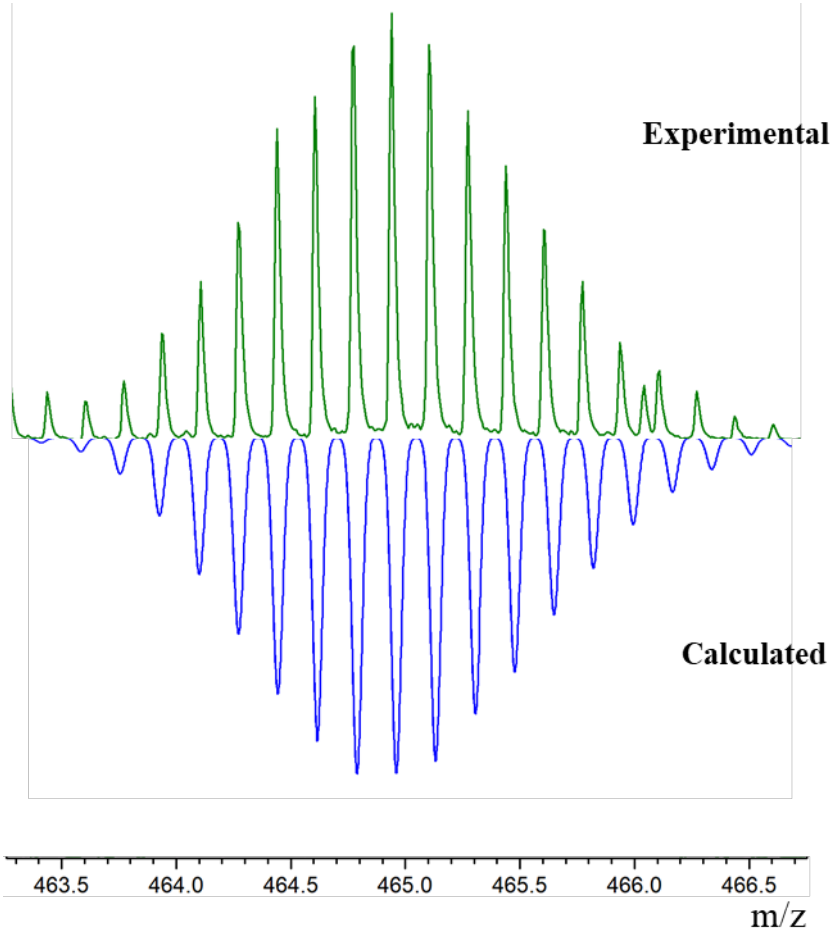

Fig. S78 Isotopic pattern of the trinuclear cage [**6a**-6NO_3]$^{6+}$ (top) and calculated pattern (bottom).

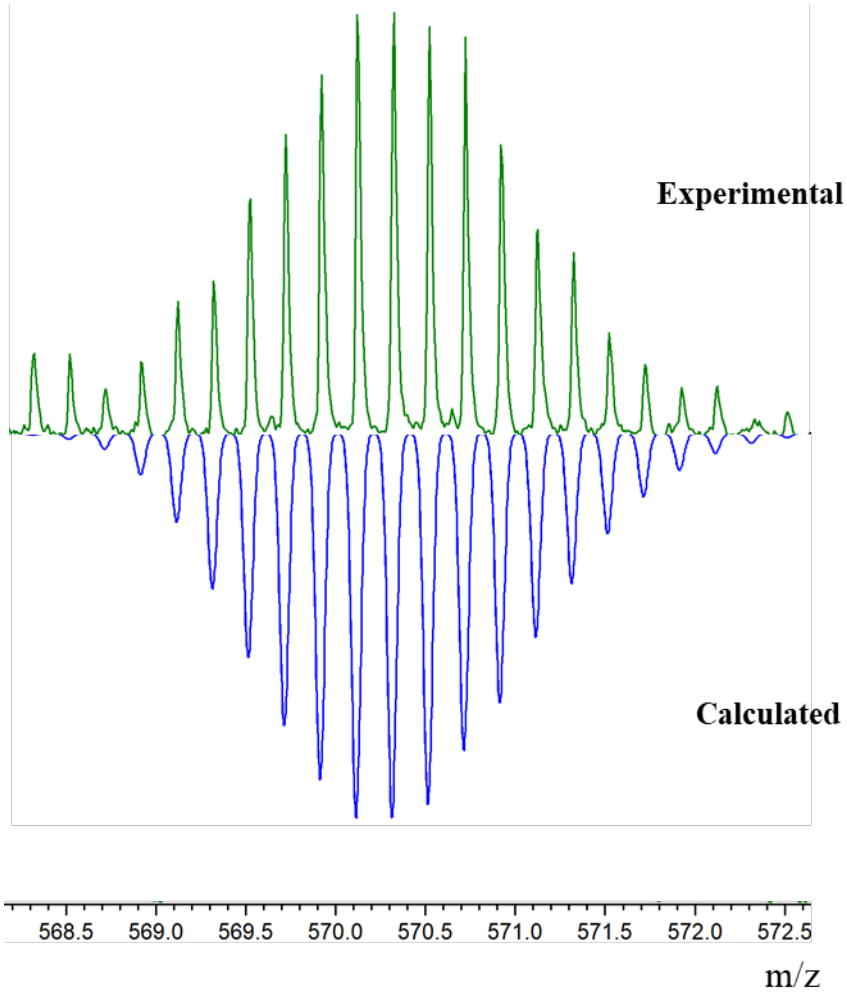

Fig. S79 Isotopic pattern of the trinuclear cage [**6a**-5NO_3]$^{5+}$ (top) and calculated pattern (bottom).

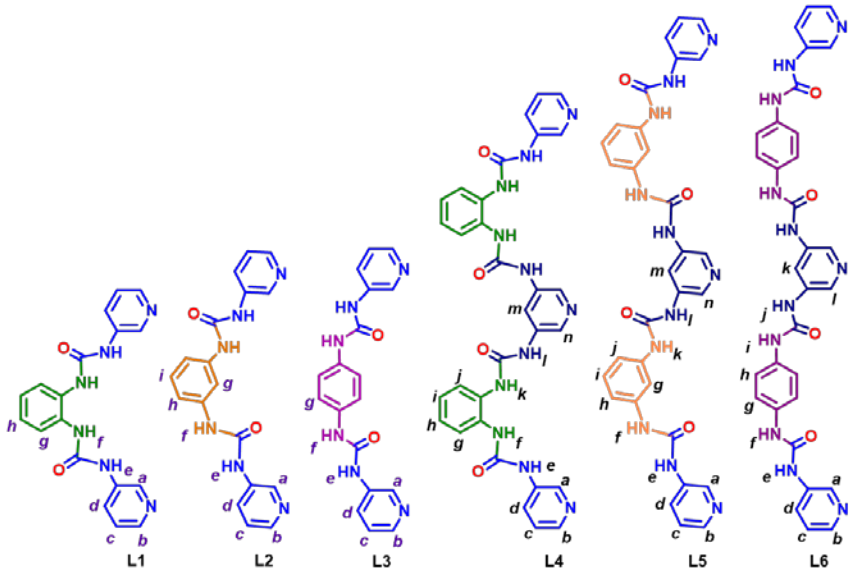

Fig. S80 Nonchelating regioisomeric bi-[5] and tridentate ligands **L1**, **L2**, **L3**, **L4**, **L5**, and **L6**.

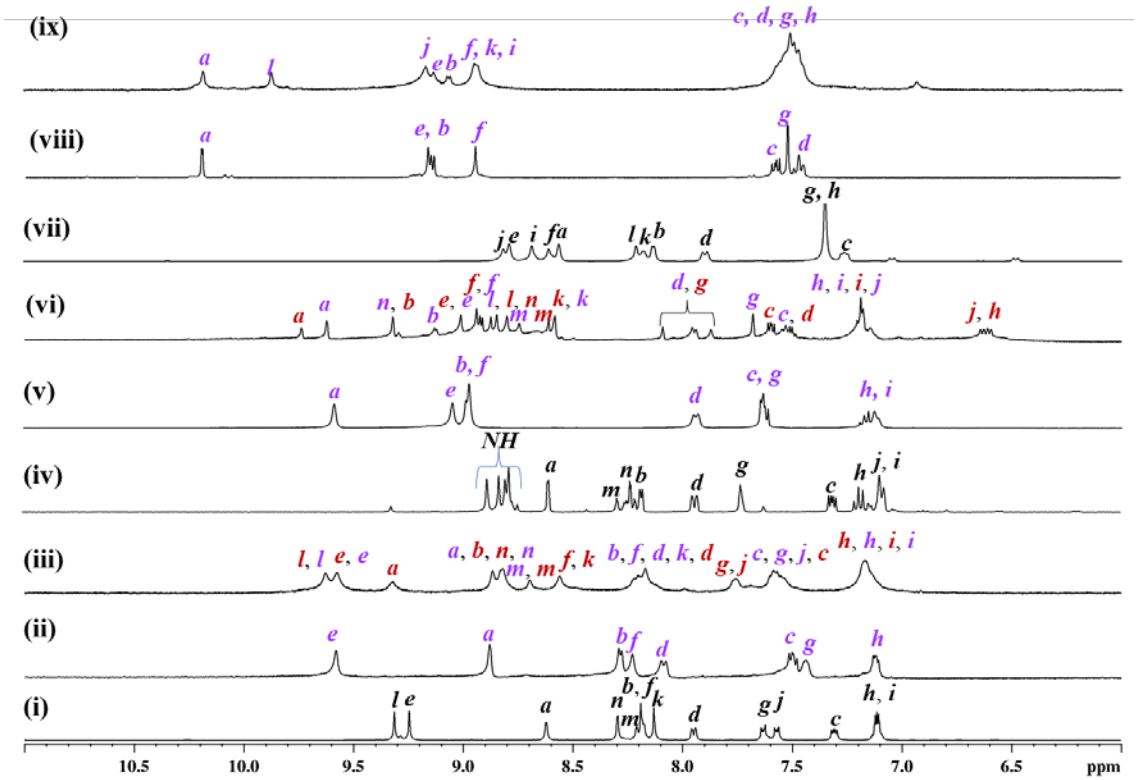

Fig. S81 500 MHz ^{1}H NMR expansion spectra of (i) ligand **L4**; (ii) cage $[Pd_2(\mathbf{L1})_4](NO_3)_4$, **1**; (iii) cages ($[Pd_3(\mathbf{L4})_4](NO_3)_6$) **4a** and **4a′**; (iv) ligand **L5**; (v) cage $[Pd_2(\mathbf{L2})_4](NO_3)_4$, **2**; (vi) cages ($[Pd_3(\mathbf{L5})_4](BF_4)_6$) **5b** and **5b′**; (vii) ligand **L6**; (viii) cage $[Pd_2(\mathbf{L3})_4](NO_3)_4$, **3**; (ix) cage ($[Pd_3(\mathbf{L4})_4](NO_3)_6$) **6a** in DMSO-$d_6$. (Colours: dark red = hour-glass shaped and purple = double-decker type Pd_3L_4 cages)

4. Theoretical calculations

The preferential formation of an hourglass shaped trinuclear $Pd_3\mathbf{L}_4$ cage in gaseous state was further supported by the DFT calculations using Gaussian 16 software package.[6] The B3LYP (Becke's three parameter hybrid functional using the LYP correlation)[7] functional was used for geometry optimizations and frequencies with LANL2DZ for palladium, and the 6-31G* basis set for carbon, nitrogen, oxygen, and hydrogen. Frequency calculations were performed for the optimized structures to confirm the absence of any imaginary frequencies

DFT calculations of trinuclear Pd_3L_4 type cages. To further understand the role of ligand design on the formation of an "hour-glass" shaped unique trinuclear Pd_3L_4 type assembly, density functional theory (DFT) calculations in gaseous state were employed to calculate the energy of possible diastereomers of Pd_3L_4 cages (Fig. S83). For cages **4a a**nd **4a′**, the energy difference between the energy-minimized structures of the cationic fragments of the "double-decker" type and "hour-glass" shaped unusual Pd_3L_4 cages is 96.98 kcal/mol and the unusual trinuclear cage was found to be energetically more favourable. Particularly, this moderate energy difference favours the formation of an "hour-glass" shaped self-assembly in solid state with high purity whereas in solution state both the Pd_3L_4 type cages remain in equal ratio. The DFT calculations for cages **5a**/**5b** and **5a′**/**5b′** showed that the "double-decker" type assembly was found to be energetically more favourable than the "hour-glass" shaped architecture with energy difference of ΔE = 15.39 kcal/mol, which was confirmed by the complicated ^{1}H NMR spectrum. Because of very low energy difference between two diastereomers of cages **5a**/**5b** and **5a′**/**5b′**, we are not successful to obtain any exclusive Pd_3L_4 architecture in solid state after several attempts. However, in case of cages **6a** and **6a′**, exclusively double-decker type Pd_3L_4 cage was observed in both solution and solid state. The DFT calculations for cage **6a** supported

double decker architecture instead of “hour-glass” shaped assembly with energy difference of ΔE = 75.28 kcal/mol.

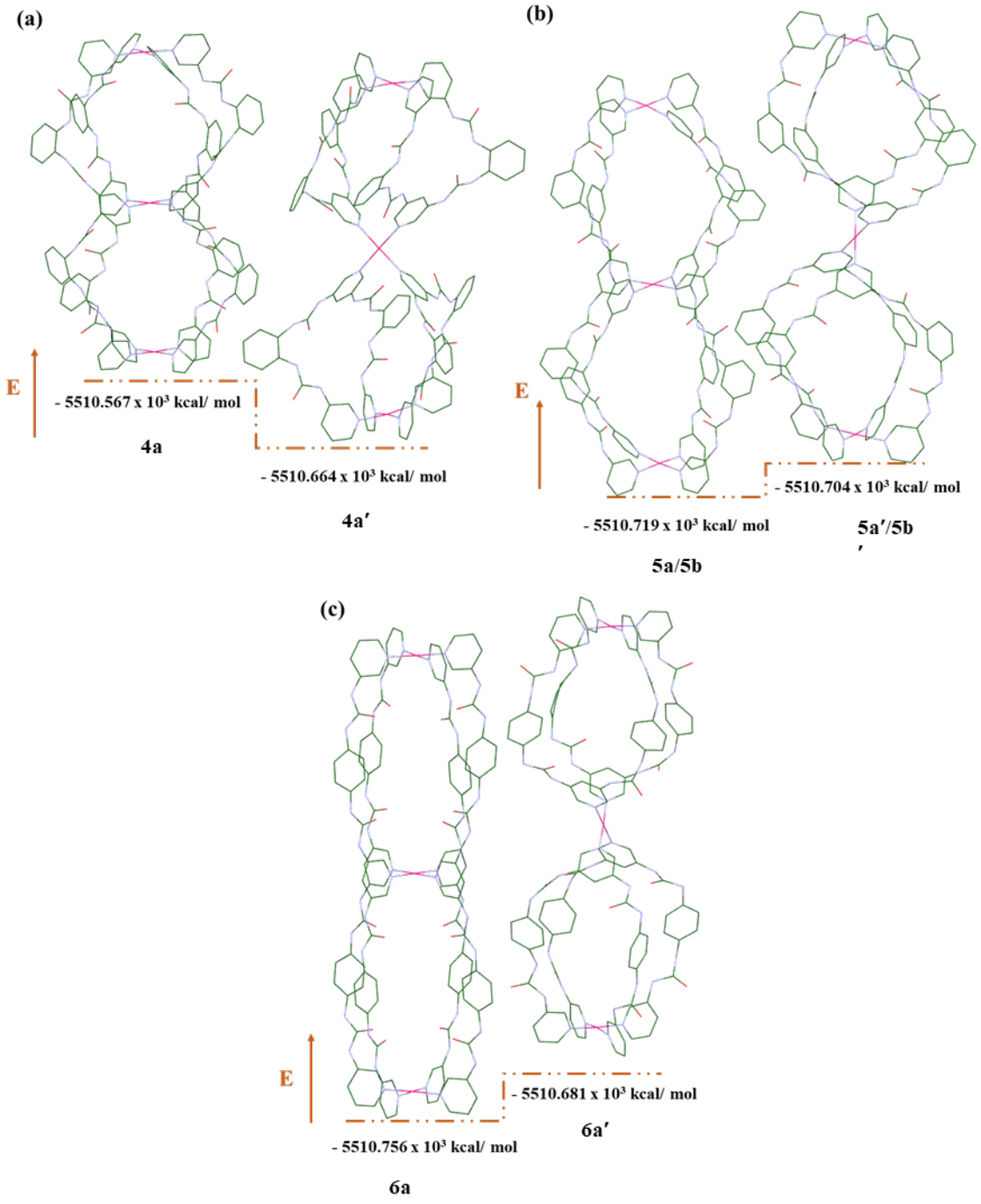

Fig. S82 Calculated structures (B3LYP/6-31G*) of the double decker type and unusual “hour-glass” shaped Pd_3L_4 assemblies of cages (a) **4a** and **4a′**; (b) **5b** and **5b′**; and (c) **6a** and **6a′** with energies (Hydrogen atoms are omitted for clarity) (anions are not employed during calculations)

The coordination of “E”-shaped tridentate ligands with palladium (II) units in 2:1 and 4:3 molar ratios results a structural motif of PdL_2 and Pd_3L_4 type cages.[8, 9] In mononuclear “spiro-type” type PdL_2 macrocycles,[8] the coordination environment around the PdN_4 square plane is satisfied by two ligand moieties. Each of the terminal pyridine of the individual ligand strand occupy cis-positions at Pd(II) centre to create a macrocyclic ring keeping the middle pyridine uncoordinated. Both the macrocyclic ligand loops are oriented in an alternate manner one pointing upward and another pointing downward with respect to the coordination square plane. If both the ligand loops converge toward same direction i.e “up-up” or “down-down” then there is a possibility to achieve the unusual “hour-glass” shaped configuration of trinuclear Pd_3L_4-type cage. The basic requirements to form coordination complexes with square planar geometry of Pd(II) unit are - (i) the Pd-N distances in complex are in the range of 2.01-2.03 Å and (ii) the cis-N-Pd-N bond angle should be close to 90°. However, the “spiro-type” PdL_2 type assemblies so far known in literature are not suitable to satisfy the basic requirement for the formation of unusual “hour-glass” shaped trinuclear Pd_3L_4-type cage. The construction of the familiar “double-decker” type Pd_3L_4 cage is feasible when all the coordination vectors of a “E”-shaped tridentate ligand are pointed unidirectionally, parallel to each other and remain on the same plane upon combination of ligand with Pd(II) units. On the contrary, an “hour-glass” shaped Pd_3L_4 cage displays middle PdN_4 plane perpendicular to terminal PdN_4 planes where both the terminal pyridine moieties of an individual ligand strand converge to a same Pd(II) centre and the central pyridine group coordinates to another Pd(II) ion.

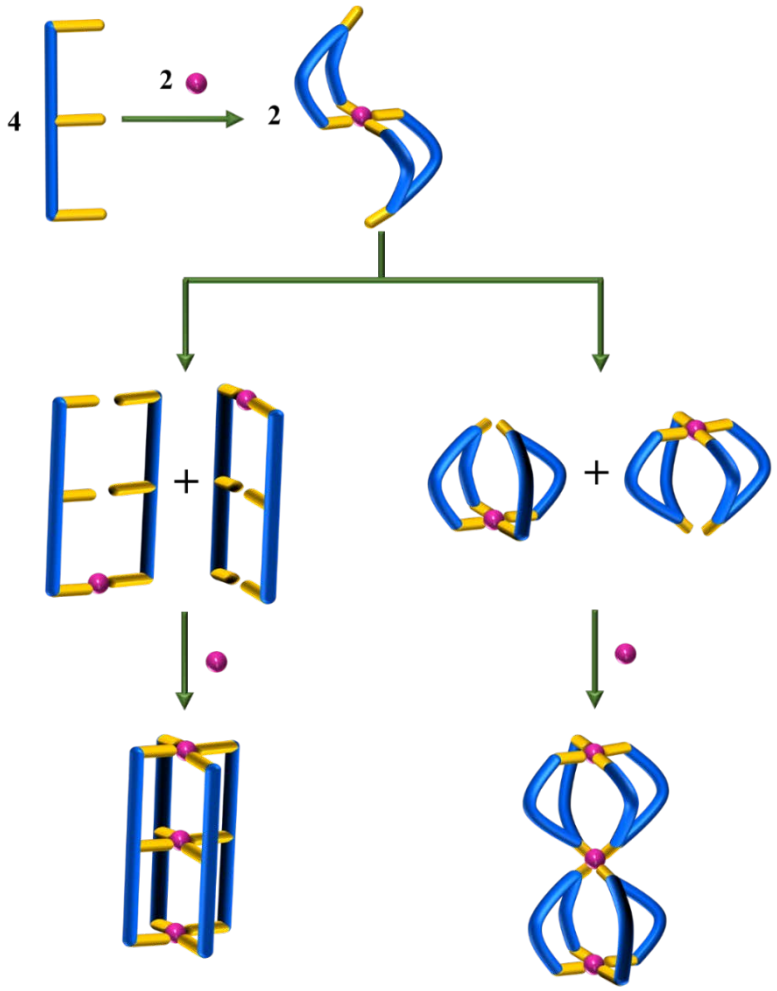

Fig. S83 Schematic cartoon representation for the formation of mononuclear PdL_2, "double-decker" type Pd_3L_4 cage, and "hour-glass" shaped Pd_3L_4 cage, respectively.

5. Single crystal XRD data analysis

Crystallographic Data Collection and Refinement. X-ray data was collected with a Bruker AXS Kappa Apex II CCD diffractometer equipped with graphite monochromated Mo Kα (λ = 0.7107Å) radiation. Crystal fixed at the tip of the glass fiber was mounted on the Goniometer head and was optically centered. The automatic cell determination routine, with 36 frames at three different orientations of the detector was employed to collect reflections and the program APEXII-SAINT (Bruker, 2008) was used for finding the unit cell parameters.[10] A 4-fold redundancy per reflection was utilized for achieving good absorption correction using a multiscan procedure. Besides absorption, Lorentz polarization and decay correction were

applied during data reduction. The program SADABS (Bruker, 2008) was used for absorption correction using the multiscan procedure. The structures were solved by direct methods using SHELXS-97, (Sheldrick, 2008)[11] and refined by full-matrix least squares techniques using SHELXL-97 (Sheldrick, 2014)[12] computer program. All hydrogen atoms were fixed at chemically meaningful positions and riding model refinement was applied. Molecular graphics were generated using Mercury programs.[13] For cage **4a′**, PLATON/SQUEEZE (Spek, 2009)[14] was employed to remove the excess electron density resulting from the disordered sea of solvent molecules, subsequently resulting in improved refinement. ORTEPs were generated using ORTEP-3.[15]

Single crystals of cage, **4a′** suitable for X-ray diffraction studies were obtained by slow diffusion of n-butanol into a solution of cage, **4a′** in DMF solvent. X-ray diffraction data indicated that the cage **4a′** belongs to a triclinic space group $P\bar{1}$. The asymmetric unit consists of the two palladium(II) ions (one palladium(II) with full and other with half occupancies), two ligand strands and three nitrate anions. The suitable single crystals for X-ray diffraction studies were obtained by slow diffusion of n-butanol into DMSO containing the complex, **6a**. The complex crystallized in a triclinic space group $P\bar{1}$. The asymmetric unit consists of the two palladium(II) ions (one palladium(II) with full and other with half occupancies), two ligand strands, two nitrate anions and two DMSO molecules.

Crystal structures of trinuclear Pd_3L_4 type cages. However, NMR and mass spectrometry cannot provide a complete specific configuration of Pd_3L_4 cages due to the presence of possible isomers in solution state. To further investigate the details of supramolecular architecture, single crystal X-ray diffraction was utilized to characterize the specific structural configuration of the corresponding trinuclear cages. The suitable single crystals of the complexes **4a′** and **6a** were obtained from their DMF and DMSO solutions by slow vapour diffusion methods. Three

square planar Pd(II) centres are bridged by four ligands in each cage. The detail descriptions are provided in later paragraphs.

Crystal structure of the cage $[Pd_3(L4)_4](NO_3)_6$, 4a′. The crystal structure of the self-assembled cage shown in Figure S111 unambiguously supports the unique "hour-glass" shaped trinuclear cage configuration in which the two terminal PdN_4 planes of the cage, **4a′**, parallel to each other, are perpendicular to the vertically oriented middle PdN_4 plane. Crystallographic data and structure refinement parameters for the cage **4a′** are summarized in the Table S1. A total of four ligand strands coordinate to three Pd(II) sites in which the terminal pyridines of the each ligand strand coordinated to one Pd(II) centre whereas internal pyridine coordinated to another Pd(II) centre and forming an "hour-glass" shaped Pd_3L_4 cage.

Crystal structure of the cage $[Pd_3(L2)_4](NO_3)_6$, 5b and 5b′. Several attempts to characterize the complex **5b** and **5b′** by single crystal XRD were unsuccessful.

Crystal structure of the cage $[Pd_3(L6)_4](NO_3)_6$, 6a. In crystal structure of cage, **6a** all PdN_4 planes are parallel to each other and oriented vertically one above other to form a double-decker type structural arrangement with two identical compartments and two molecules of DMSO were found within each of the compartments probably by electrostatic interaction of $(O)_{DMSO}$ with metal ions and several CH---O interactions using $(O)_{urea}$ and $(H)_{DMSO}$ to fill the space. The distances between the Pd_1-Pd_2 and Pd_1-Pd_1 were found to be 14.42 and 28.84 Å. All the NH groups of sixteen urea moieties are disposed exohedrally thus making the outside edge of the cage suitable for interaction with anions.

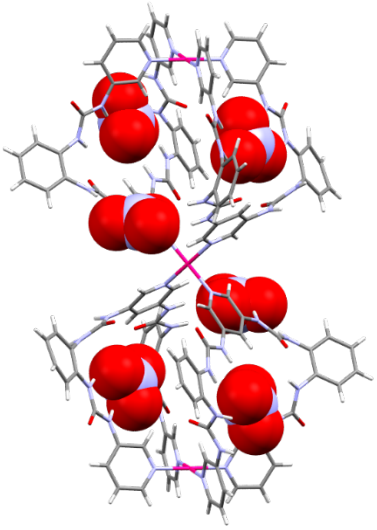

Fig. S84 Crystal structure of the cage $[Pd_3(\mathbf{L4})_4](NO_3)_6$, **4a′** showing dispositions of nitrate anions. Solvent molecules are omitted for clarity.

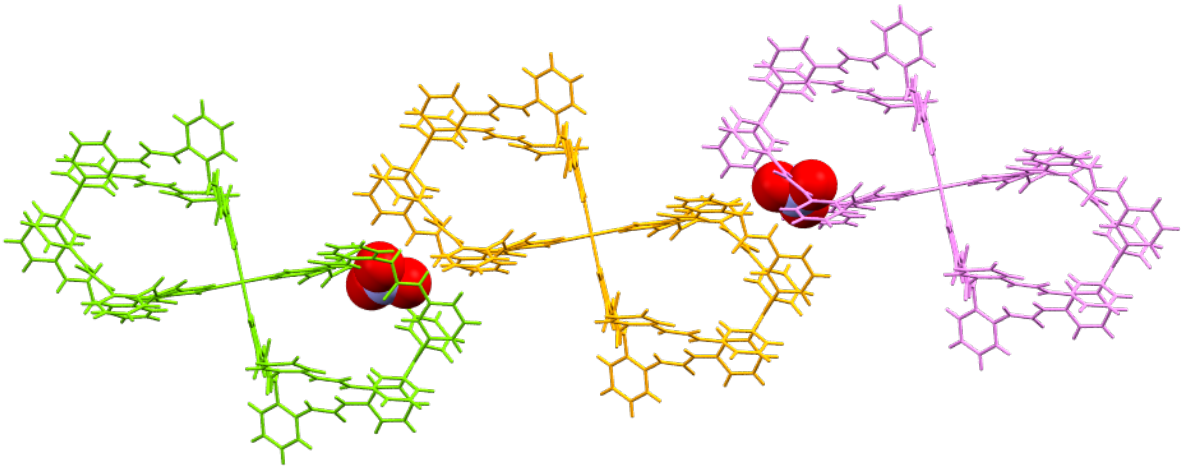

Fig. S85 Packing diagram representing the interactions of one unit of $[Pd_3(\mathbf{L4})_4](NO_3)_6$, **4a′** with two neighboring units. Solvent molecules are omitted for clarity.

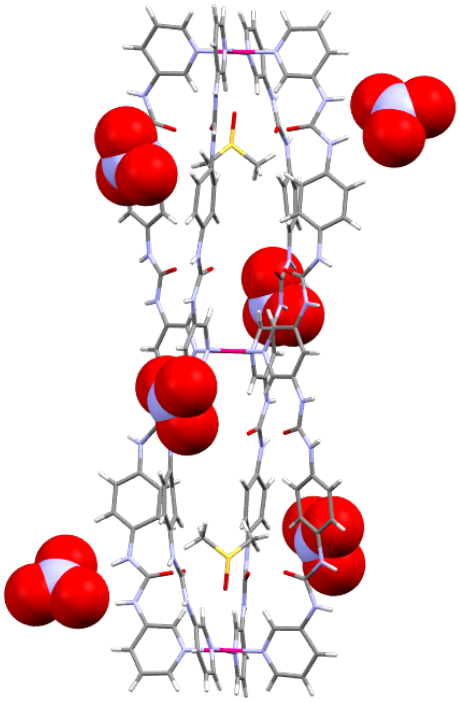

Fig. S86 Crystal structure of the cage $[Pd_3(\mathbf{L6})_4](NO_3)_6$, **6a** showing dispositions of nitrate anions. Solvent molecules are omitted for clarity.

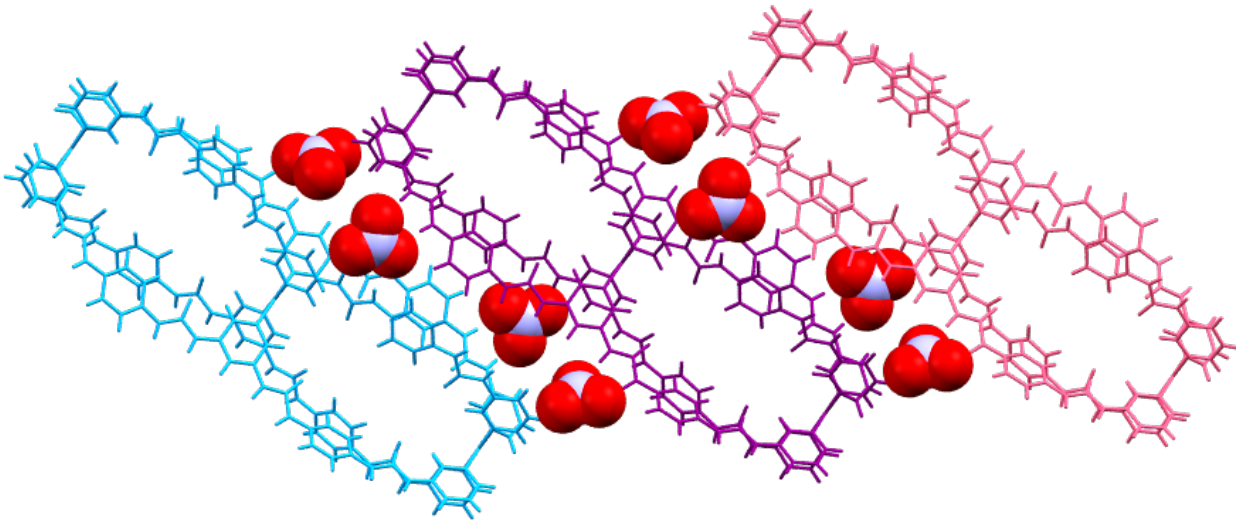

Fig. S87 Packing diagram representing the interactions of one unit of $[Pd_3(\mathbf{L6})_4](NO_3)_6$, **6a** with two neighboring units. Solvent molecules are omitted for clarity.

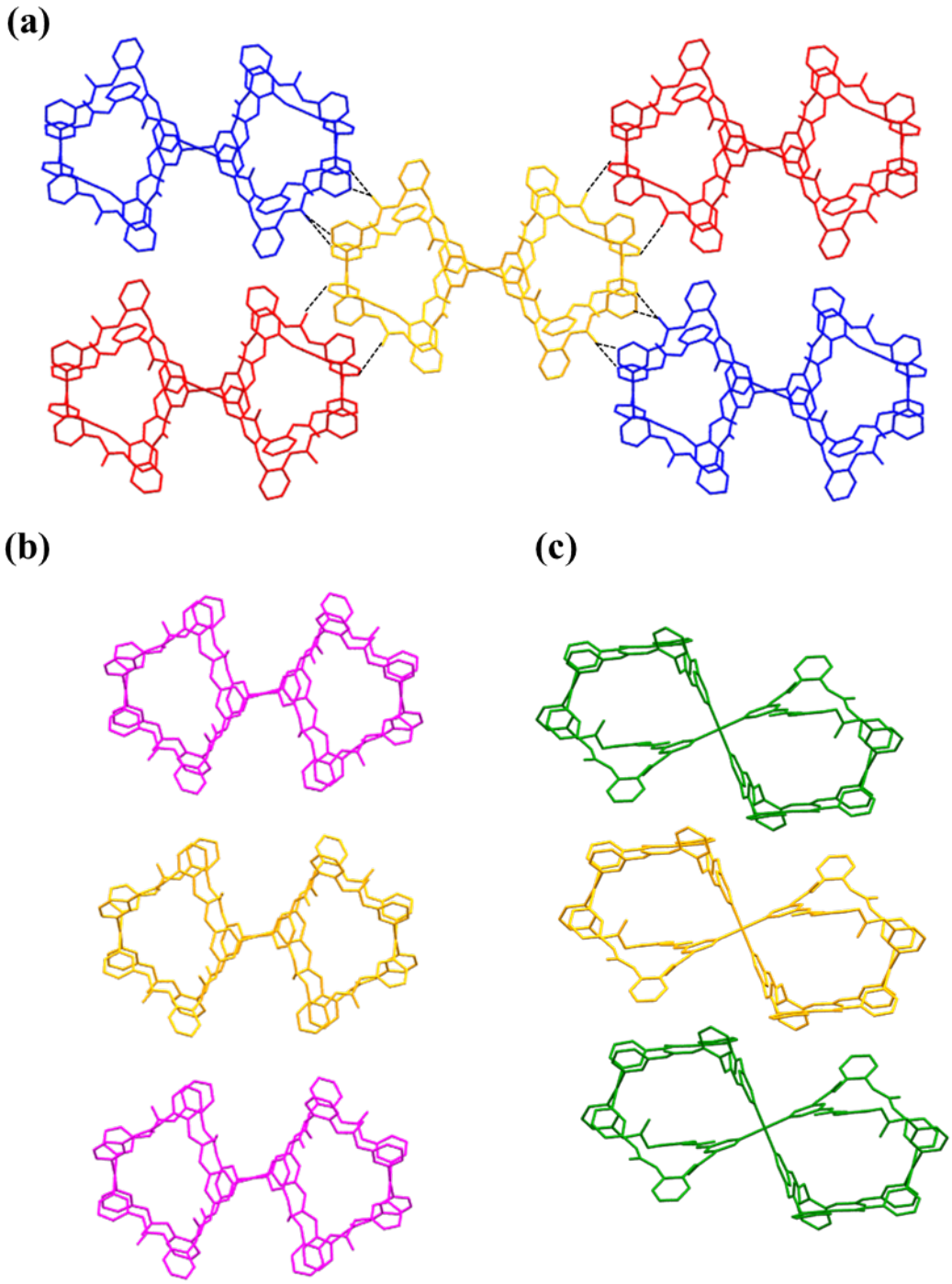

Fig. S88 Packing diagram of $[Pd_3(\mathbf{L4})_4](NO_3)_6$, **4a′** in some other views. Solvent molecules and hydrogen atoms are omitted for clarity.

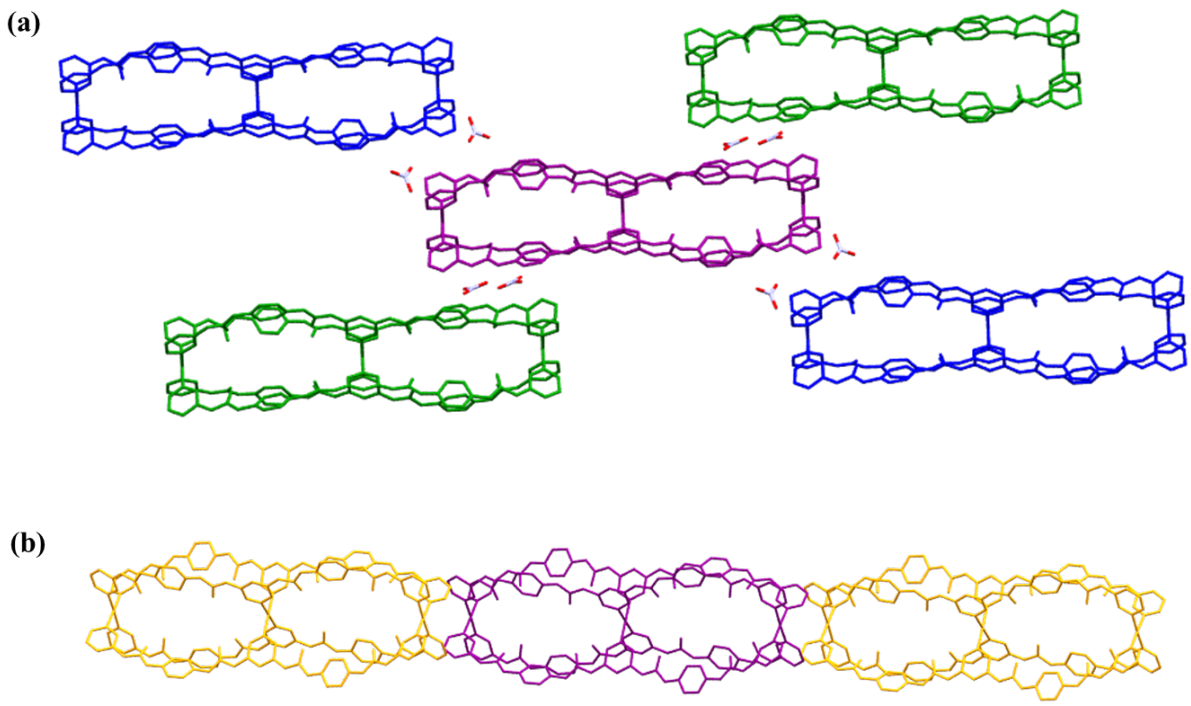

Fig. S89 Packing diagram of $[Pd_3(\mathbf{L6})_4](NO_3)_6$, **6a** in some other views. Solvent molecules and hydrogen atoms are omitted for clarity.

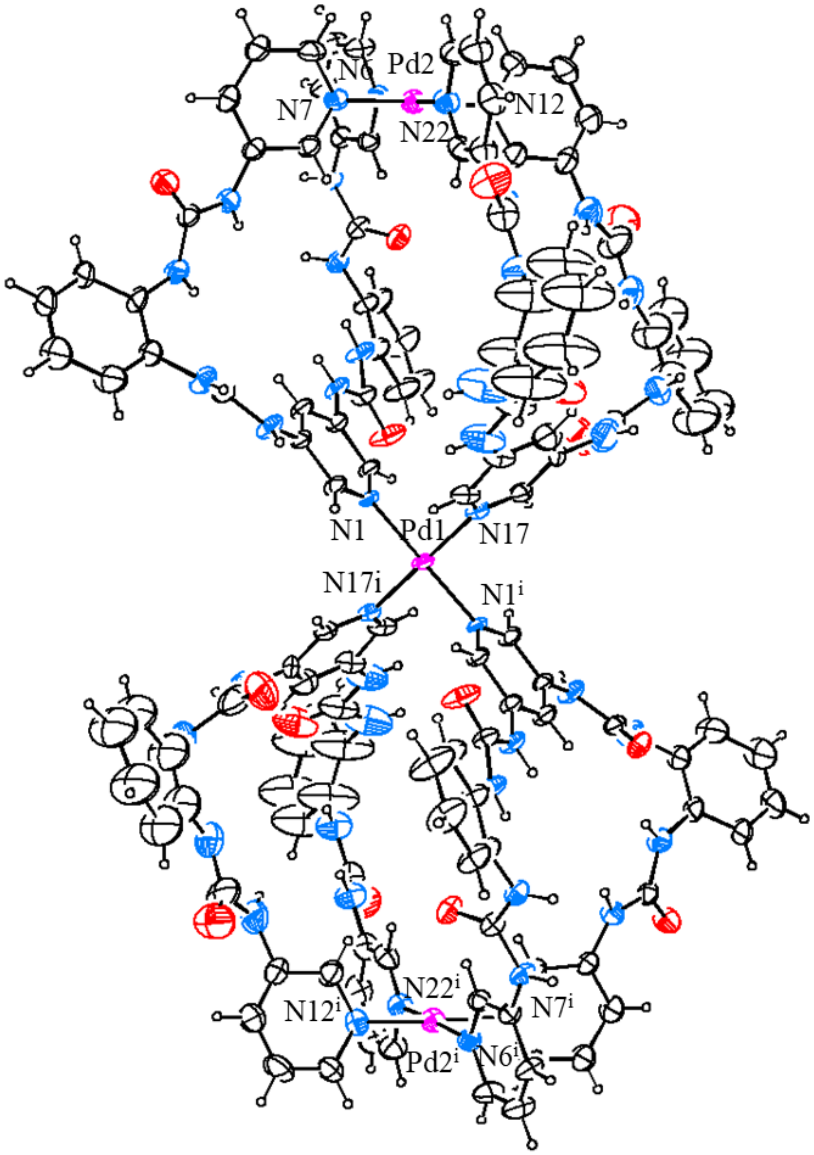

Fig. S90 ORTEP diagram for trinuclear cage $[Pd_3(\mathbf{L4})_4](NO_3)_6$, **4a′** showing labeling of palladium atoms and nitrogen atoms which are coordinated to palladium only. All anions and solvent molecules of crystallization are omitted for clarity. (Thermal ellipsoids are shown in 20% probability).

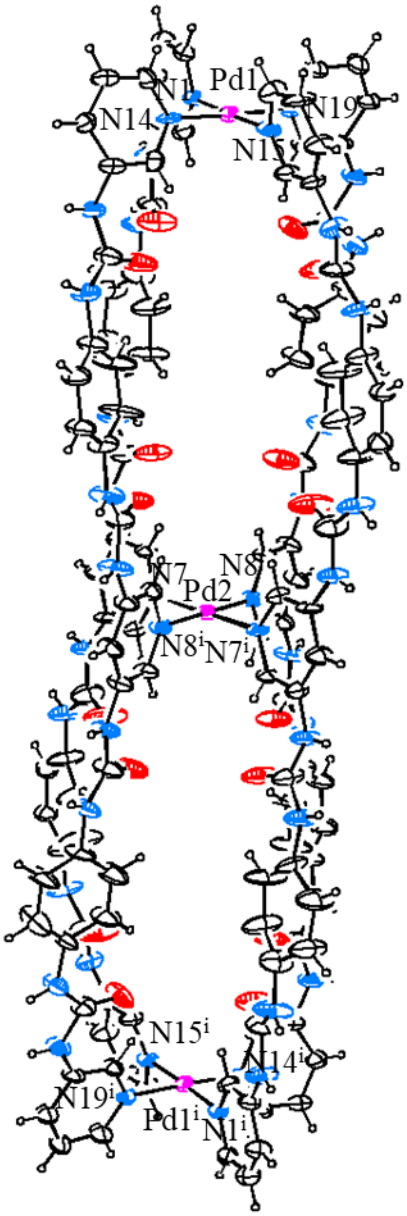

Fig. S91 ORTEP diagram for trinuclear cage $[Pd_3(\mathbf{L6})_4](NO_3)_6$, **6a** showing labeling of palladium atoms and nitrogen atoms which are coordinated to palladium only. All anions and solvent molecules of crystallization are omitted for clarity. (Thermal ellipsoids are shown in 20% probability).

Table S1. Crystallographic data and structure refinement parameters for trinuclear cages **$[Pd_3(L4)_4](NO_3)_6$**, **4a′** and **$[Pd_3(L6)_4](NO_3)_6$**, **6a**.

Parameters	**4a′**	**6a**
CCDC No	**2167195**	**2167196**
Empirical formula	$C_{124}\ H_{108}\ N_{50}\ O_{34}\ Pd_3$	$C_{66}\ H_{66}\ N_{24}\ O_{16}\ Pd_{1.50}\ S_2$
Formula weight	3161.80	1675.14
Crystal size (mm)	0.220 x 0.150 x 0.100	0.250 x 0.220 x 0.100
Temperature (K)	296(2)	296(2)
Wavelength (Å)	0.71073	0.71073
Crystal system	Triclinic	Triclinic
space group	$P\bar{1}$	$P\bar{1}$
a (Å)	14.6119(7)	13.5383(10)
b (Å)	19.5758(9)	19.9005(15)
c (Å)	21.2217(8)	21.4915(16)
α (°)	101.622(2)	84.364(3)
β (°)	95.405(2)	78.149(3)
γ (°)	109.496(2)	87.554(3)
Volume $(Å)^3$	5518.6(4)	5637.9(7)
Z	1	2
D_{calc} (mg/m^3)	0.951	0.987
absorption coefficient (mm^{-1})	0.302	0.333
F(000)	1612	1718
θ min/max (deg)	0.995 to 21.407	1.349 to 19.044
h, *k*, *l* (min, max)	(-14, 14) (-20, 20) (-21, 21)	(-12, 12) (-18, 18) (-19, 19)
Reflections collected / unique	47441 / 12422	34117/9027
R_{int}	0.0693	0.0719
Data / restraints / parameters	12422 / 96 / 941	9027/0/992
Goodness-of-fit on F^2	0.871	0.897
Final R indices [I>2σ(I)]	R1 = 0.0537, wR2 = 0.1296	R1 = 0.0559, wR2 = 0.1403
R indices (all data)	R1 = 0.0878, wR2 = 0.1402	R1 = 0.0826, wR2 = 0.1505
Largest diff peak and hole $(Å)^3$	0.425 and -0.312	0.458 and -0.262

References

1 M. C. Naranthatta, D. Das, D. Tripathy, H. S. Sahoo, V. Ramkumar and D. K. Chand, *Cryst. Growth Des.*, 2012, **12**, 6012-6022.

2 M. -O. M. Piepenbrock, N. Clarke and J. W. Steed, *Soft Matter*, 2011, **7**, 2412-2418.

3 Y. Y. Chu-Farseeva, N. Mustafa, A. Poulsen, E. C. Tan, J. J. Y. Yen, W. J. Chng and B. W. Dymock, *Eur. J. Med. Chem.*, 2018, **158**, 593-619.

4 L. Lee, Y. R. Leroux, P. Hapiot and A. Downard, *Langmuir*, 2015, **31**, 5071-5077.

5 H. Dasary, R. Jagan and D. K. Chand, *Inorg. Chem.*, 2018, **57**, 12222-12231.

6 M. J. Frisch, G. W. Trucks, H. B. Schlegel, G. E. Scuseria, M. A. Robb, J. R. Cheeseman, G. Scalmani, V. Barone, G. A. Petersson, H. Nakatsuji, X. Li, M. Caricato, A. V. Marenich, J. Bloino, B. G. Janesko, R. Gomperts, B. Mennucci, H. P. Hratchian, J. V. Ortiz, A. F. Izmaylov, J. L. Sonnenberg, D. W.-Young, F. Ding, F. Lipparini, F. Egidi, J. Goings, B. Peng, A. Petrone, T. Henderson, D. Ranasinghe, V. G. Zakrzewski, J. Gao, N. Rega, G. Zheng, W. Liang, M. Hada, M. Ehara, K. Toyota, R. Fukuda, J. Hasegawa, M. Ishida, T. Nakajima, Y. Honda, O. Kitao, H. Nakai, T. Vreven, K. Throssell, J. A. Montgomery, J. E. Peralta, F. Ogliaro, M. J. Bearpark, J. J. Heyd, E. Brothers, K. N. Kudin, V. N. Staroverov, T. A. Keith, R. Kobayashi, J. Normand, K. Raghavachari, A. P. Rendell, J. C. Burant, S. S. Iyengar, J. Tomasi, M. Cossi, J. M. Millam, M. Klene, C. Adamo, R. Cammi, J. W. Ochterski, R. L. Martin, K. Morokuma, O. Farkas, J. B. Foresman and D. J. Fox, *Gaussian 16*, Revision A.03; Gaussian, Inc.: Wallingford, CT, 2016.

7 A. D. Becke, *Phys. Rev. A.*, 1988, **38**, 3098-3100.

8 D. A. McMorran and P. Steel, *Supramol. Chem.*, 2002, **14**, 79-85.

9 S. Bandi, A. K. Pal, G. S. Hanan and D. K. Chand, *Chem. - A Eur. J.*, 2014, **20**, 13122-13126.

10 SAINT, version 7.06a; Bruker AXS Inc., Madison, Wisconsin, 2008.

11 G. M. Sheldrick, *Acta Crystallogr. A*, 2008, **64**, 112-122.

12 G. M. Sheldrick, *Acta Crystallogr. C*, 2015, **71**, 3-8.

13 C. F. Macrae, P. R. Edgington, P. McCabe, E. Pidcock, G. P. Shields, R. Taylor, M. Towler and J. van de Streek, *Mercury:* visualization and analysis of crystal structures. *J. Appl. Crystallogr.* 2006, **39**, 453–457.

14 A. L. Speck, *Acta Crystallogr. D*, 2009, **65**, 148-155

15 L. J. Farrugia, *WinGX* and *ORTEP for Windows*: an update. *J. Appl. Crystallogr.* 2012, **45**, 849–854.